Journal of NUCLEAR SCIENCE and TECHNOLOGY, Supplement 5, p. 681–684 (June 2008)

Quantitative Analysis of Meteorological Conditions for a Comparative Risk Estimation of Nuclear Power Plants in Korea

Moon Hee HAN *, Won Tae HWANG, Hyo Joon JEONG, and Eun Han KIM

Korea Atomic Energy Research Institute, Yuseong, Daejeon, Korea

The meteorological conditions of Korean nuclear power plant sites were analyzed by using the integral parameters developed by Allwine and Whiteman. The method of integral parameters was applied to 76 sites in Korea which are evenly distributed. The integral quantities of stagnation and recirculation were calculated at four nuclear power plant (NPP) sites and these values were analyzed with the distribution of the integral quantities estimated with the results of the 76 sites. The comparative study shows that the meteorological conditions of the four NPP sites in Korea are quite good from the meteorological aspects.

KEYWORDS: meteorological data, stagnation, recirculation, nuclear power plant site, radiological risk

I. Introduction

The risk due to the operation of an industrial facility should be managed to be lower than the predetermined levels for public health. The estimation of a radiological risk due to the operation of a nuclear power is complicated and needs lots of information including environmental data. Among the environmental information, the meteorological condition is an influential factor for the estimation of a risk. Therefore, a quantitative analysis of the meteorological characteristics of an industrial site is needed for the management of the risk of industrial facilities.

Dispersion of the pollutants released into the atmosphere is dependent on the meteorological conditions. Several scholars have tried to examine some meteorological aspects in different sites. Lyons and Steedman reported the observations of marked decoupling of the surface layer and sudden nocturnal air temperature variations observed at a desert location in western Australia[1]. Tapp examined some of the meteorological features associated with an extended period of stagnation of the near-surface air mass in Melbourne, during which a severe and prolonged buildup of air pollutants occurred[2]. Katsoulis examined the meteorology of high concentration episodes and an air stagnation index for Athens[3].

Several approaches have been devised to quantitatively analyze these meteorological characteristics. The three terms of stagnation, recirculation and ventilation are useful indicators for characterizing the meteorological condition at a site. Allwine and Whiteman proposed mathematical definitions of integral quantities for characterizing the stagnation, recirculation and ventilation potential of various stations with the wind data measured at single station[4]. These integral quantities provide useful characterizations of the flow at individual measurement points. The obtained integral quantities represent the site-specific meteorological conditions including geographic features. Crescenti analyzed the meteorological conditions of Brownsville and the Lower Rio Grande valley by using the method of an integral parameter (wind run, resultant transport distance and direction, and recirculation factor) developed by Allwine and Whiteman[5]. And Kim *et*. al., estimated the meteorological characteristics of four Korean nuclear power sites by using the integral parameters developed by Allwine and Whiteman[6].

In this study, the integral quantities of stagnation and recirculation were estimated with the meteorological data measured at 76 weather stations which are evenly distributed in Korea. The obtained integral quantities were statistically analyzed and the distributions of the integral quantities were obtained for both stagnation and recirculation. And a comparative study of the integral quantities of the four nuclear power plant sites has been performed using the distribution. The obtained results show that the meteorological conditions of the four nuclear sites are quite good in a meteorological point of view.

II. Methodology

1. Critical Transportation Indices

Allwine and Whiteman defined integral quantities which may be used to identify "stagnation" and "recirculation" conditions during a certain period with only the surface wind data measured at a meteorological station[4]. **Fig. 1** shows the trajectories of the released effluents in a horizontal space. Allwine and Whiteman proposed an approach to study site-specific atmospheric transport and diffusion conditions by means of 'stagnation' and 'recirculation' concepts[4].

In this method, the representative integral quantities for stagnation and recirculation are calculated on the basis of the measured wind speed and direction. The measured horizontal wind vectors are divided into 'east-west', u_i and 'north-south', v_i , components, respectively, as follows:

*Corresponding Author, Tel. +82-42-868-2353, Fax. +82-42-868-2370, E-mail: mhhan@kaeri.re.kr

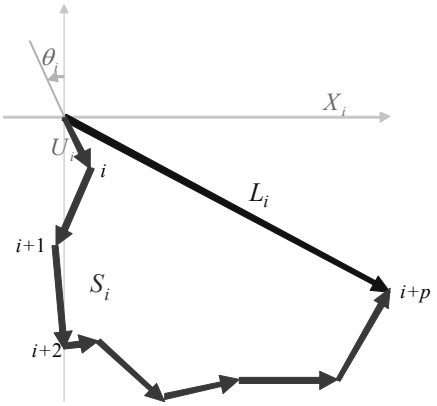

Fig. 1 Wind run and transport distance

$$u_i = U_i \sin(\theta_i - 180) \quad (1)$$

$$v_i = U_i \cos(\theta_i - 180) \quad (2)$$

where U_i is the wind speed and θ_i is the wind direction from which the wind blows, clockwise from the north.

Meteorological phenomena have a general tendency of daily change. Therefore, by summing equations (1) and (2) over 24 hours, we can calculate the transportation distance of the effluents in the directions of 'east-west' and 'north-south', respectively.

$$X_i = \tau \sum_{j=i}^{i+p} u_j \quad (3)$$

$$Y_i = \tau \sum_{j=i}^{i+p} v_j \quad (4)$$

where τ is the sampling intervals and p = 24hr/τ. And the straight-line distance from the release point is calculated, as;.

$$L_i = \sqrt{X_i^2 + Y_i^2} \quad (5)$$

Then the real transport distance so called the 'wind run' S_i is represented by,

$$S_i = \tau \sum_{j=i}^{i+p} U_i \quad (6)$$

And the recirculation factor is computed at each time step t_t by the following equation,

$$R_i = 1 - \frac{L_i}{S_i} \quad (7)$$

In this method, the representative integral quantities for stagnation and recirculation are calculated on the basis of the measured wind speed and direction. Allwine and Whiteman proposed an approach for classifying the atmosphere of different sites, for comparing the mean values of the wind run $\overline{S}$ and of the recirculation factor $\overline{R}$, with predetermined critical values. By analyzing the values of S_t and R_t for a long time, they proposed the following [4];

$\overline{S} \le \overline{S_c}$: site prone to stagnation

$\overline{R} \ge \overline{R_c}$: site prone to recirculation

$\overline{S} \ge \overline{S_{cv}}$ and $\overline{R} \le \overline{R_{cv}}$: site prone to ventilation

where $\overline{S_c}$ and $\overline{R_c}$ are the average daily critical transport indices (CTIs) for stagnation and recirculation, respectively, and $\overline{S_{cv}}$ and $\overline{R_{cv}}$ are the averaged daily CTIs for ventilation. Allwine and Whiteman proposed daily CTIs for Grand Canyon region $\overline{S_c}$ = 170 km (-2 m/s average daily wind speed), $\overline{R_c}$ = 0.4, $\overline{S_{cv}}$ = 250 km (- 3 m/s average daily wind speed), and $\overline{R_{cv}}$ = 0.2 Allwine and Whiteman mentioned that the values of the CTIs used in their study were given solely to demonstrate the ability of the integral quantities and were not intended to be a definitive set of CTIs for the Grand Canyon region, or any region. The values of the CTIs proposed by Allwine and Whiteman were also used in the study conducted on five cities in Argentina by Venegas and Mazzeo[7]. The integral quantities such as S and R represent the site-specific characteristics including geographic features. Therefore, it is possible to estimate the degree of stagnation, recirculation and ventilation potential of a site with the obtained integral quantities.

2. Meteorological Data

For the analysis of meteorological data, the data measured at 76 non-nuclear power plant (NPP) sites and 4 NPP sites were used. The meteorological data was measured for 1 year (2005). **Fig. 2** represents the 76 non-NPP sites and 4 nuclear sites. Fig. 2 also shows the four nuclear power plant sites in Korea. All of them are located at sea coasts. Younggwang nuclear (YGN) site is located at the western coast and the others, Kori (KRN), Uljin(UJN) and Wolsung (WSN) sites are located at the eastern coast. **Fig. 3** shows the wind roses of the four nuclear power plant sites.

III. Application to Different Sites in Korea

1. Non-Nuclear Power Plant Sites

For the analysis of the meteorological data measured at 76 points, the average stagnation, recirculation values were calculated using equations (6) and (7), respectively. The distribution of the logarithm values of averaged stagnation and recirculation are represented in **Fig. 4** and **5**, respectively. **Fig. 4** shows that the distribution of the average

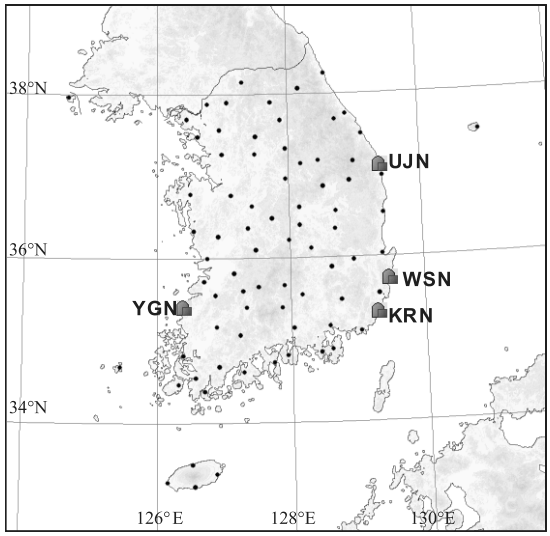

Fig. 2 76 non-nuclear power plant sites and 4 nuclear power plant sites (YGN: Younggwang Nuclear, UJN: Ulchin Nuclear, WSN: Wolsung Nuclear, KRN: Kori Nuclear)

values of stagnation has a normal distribution with an averaged value of 181.9 m and a standard deviation of 1.5 m. **Fig. 5** represents that the distribution of the averaged values of recirculation taken a normal distribution with an averaged value of 0.33 and a standard deviation of 0.08.

2. Nuclear Power Plant Sites

The four NPP sites are represented in **Fig. 2**. Each nuclear power plant site has a meteorological tower with a height of 58 meters. Wind speed, wind direction, temperature and relative humidity are measured at two levels of 10 m and 58 m every 10 seconds. Authors analyzed the meteorological data measured at four NPP sites for a year (2005). Table 1 represents the mean values of the wind run $\overline{S}$, the recirculation factor $\overline{R}$ of the four sites with the values of the Arizona study case. This analysis showed that the mean stagnations of each site are 431 km for the KNR site, 227 km for the UJN site, 257 km for the YGN site and 403 km for the WSN site. And the mean recirculation of each site are

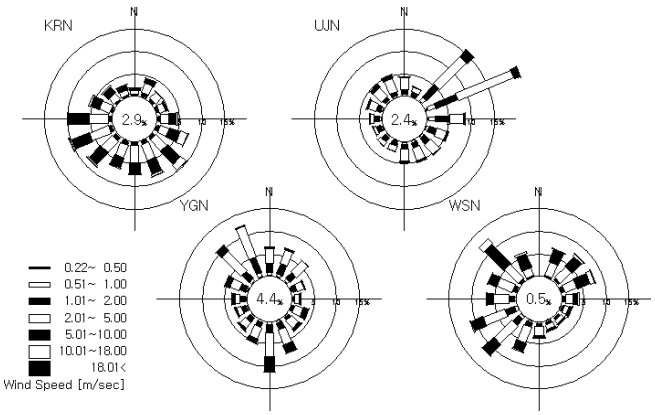

Fig. 3 Wind Roses of four sites in 2005

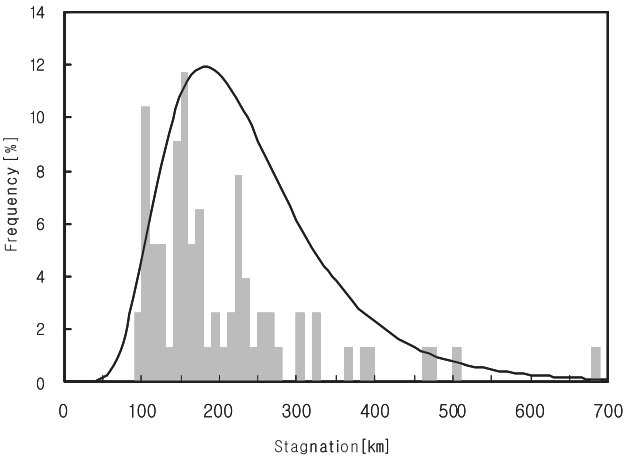

Fig. 4 Distribution of the average stagnation analyzed using the meteorological data measured at 76 non-nuclear power plant sites.

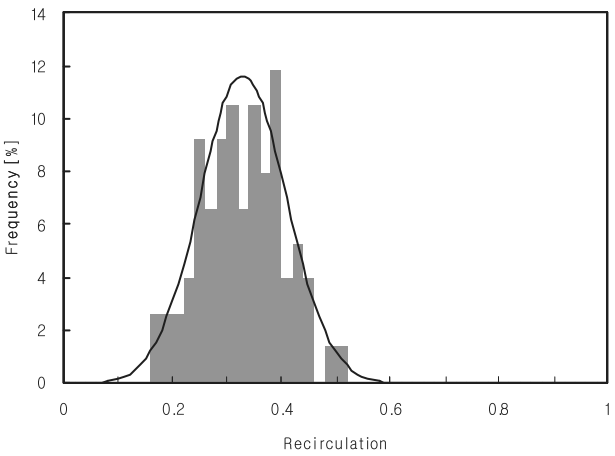

Fig. 5 Distribution of the average recirculation analyzed using the meteorological data measured at 76 non-nuclear power plant sites.

0.23 for the KRN site, 0.31 for the UJN site, 0.24 for the YGN site and 0.31 for the WSN site. Comparing these values with CTIs provided by Allwine and Whiteman, four NPP sites are not prone to stagnation and recirculation.

Table 1 also shows the percentile values representing the comparative position of the sites in the distribution that was obtained with the meteorological data of 76 sites. **Table 1** shows that four NPP sites in Korea have quite good meteorological conditions in view of the meteorological aspects. KRN site has the best ventilation condition with the mean stagnation of 431 km (95 percentile) and the mean recirculation of each site are 0.23 (92 percentile).

Table. 1 The average stagnation and recirculation values at the 4 nuclear sites and its percentile in the distribution of 76 sites

Site		(Percentile)	(Percentile)
USA Arizona	Bulfrog Basin	145 (31 %)	0.49 (1 %)
	Desert View	250 (79 %)	0.18 (99 %)
Korea	KRN	431 (95 %)	0.23 (92 %)
	UJN	227 (71 %)	0.31 (63 %)
	YGN	257 (81 %)	0.24 (91 %)
	WSN	403 (95 %)	0.31 (63 %)

IV. Conclusions

The meteorological data measured at 76 measuring points and four nuclear power plant sites were analyzed using the method of integral quantities provided by Allwine and Whiteman. The average values of the stagnation and recirculation were estimated for each point. And the distribution of the average values of the stagnation and recirculation were obtained by statistically analysis. The averaged values for four NPP sites were compared with the obtained distributions for stagnation and recirculation. The obtained result shows that the flow conditions at the four nuclear power plant sites are quite good comparing to the general distribution of the integral quantities. That means that four NPP sites have good site characteristics from the meteorological aspects. Among four NPP sites, KRN site represents the best condition.

Compared to the corresponding critical value of stagnation $\overline{S_c}$ = 170 km, it is revealed that four power plant sites are not prone to stagnation. And also, compared to the corresponding critical value of recirculation $\overline{R_c}$ = 0.4, it is revealed that four NPP sites are not prone to recirculation. The comparative study shows that the meteorological conditions of four NPP sites in Korea are quite good for a nuclear site from the meteorological aspects

The meteorological condition is an influential factor for determining the compatibility of a site in risk aspects. Using the obtained results, it can be possible to estimate the relative risk of several sites even without any information on the facility itself.

It is needed to determine the CTIs suitable for Korean environmental conditions. For determining a general set of CTIs, it is necessary to calculate integral quantities for numerous stations in many airshed of known dispersion potential. This study is the first approach to analyze the characteristics of the flow at various sites including four NPP sites in Korea. The obtained results might be used for the estimation of relative risk of an industrial site only with meteorological information.

Acknowledgement

This work was performed under the long-term nuclear research and development program sponsored by Ministry of Science and Technology of Korea.

References

1) T.J. Lyons and R.K Steedman, Stagnation and noctural temperature jumps in a. desert region of flow relief, Boundary-Layer Meteorology 21, 369-387, 1981.
2) R.G Tapp, Indications of topographyically-induced eddies in stratified flow during a severe air pollution, Boundary-Layer Meteorology 33, 283-302, 1985.
3) B.D. Katsoulis, Some meteorological aspects of air pollution in Athens, Greece, Meteorol. Atmos. Physics 39, 203-212, 1988.
4) K. Jerry Allwine and C. David Whiteman, Single-station Integral Measures of Atmospheric Stagnation, recirculation and Ventilation, Atmospheric Environment 28, No. 4, p 713-721, 1993.
5) G. H. Crescenti, Meteorological measurements during the Lower Rio Grand Valley environmental study, Environment International 23, No. 5, 629-642, 1997.
6) E. H. Kim, K.S. Suh, H. J. Jeong, W.T. Hwang, M. H. Han and J.I. Moon, " Analysis of the site characteristics of Korean nuclear power sites from the meteorological aspects", Annals of Nuclear Energy, In press, 2007.
7) L.E. Venegas and N.A. Mazzeo, Atmospheric stagnation, recirculation and ventilation potential of several sites in Argentina, Atmospheric Research 52, 43-57, 1999.

Journal of NUCLEAR SCIENCE and TECHNOLOGY, Supplement 5, p. 685–689 (June 2008)

Program of Asian Long Range Tracer Experiment

YAO Rentai[1*], XU Xiangjun[1], XUAN Yiren[1], YANG Yanqiu[2], and CHEN Hui[3]

[1]*China Institute for Radiation Protection, P.O.Box 120, Taiyuan, Shanxi 030006, China*
[2]*Institute of Nuclear Physics and Chemistry, China Academy of Engineering Physics, Chengdu, China*
[3]*China Academy of Meteorological Science, Beijing 100081, China*

Increased concern over regional and international aspects of air pollution, acid deposition and accidental releases has created a need for air pollution dispersion model development and evaluation. Under the framework of the US-China Peaceful Uses of Nuclear Technologies (PUNT) Agreement, a program to carry out an Asian tracer experiment was proposed. In this paper, the long range tracer experiments conducted internationally and evaluation of long range dispersion models were reviewed and a preliminary planning on the former several aspects was analyzed and discussed.

KEY WORDS: long range, tracer experiment, Asia, trajectory modeling

I. Introduction

In 2002, more than 90 US and Chinese government officials, scientists and researchers participated in the first US-China Workshop on Nuclear Technology Cooperation under the framework of the US-China Peaceful Uses of Nuclear Technologies (PUNT) Agreement signed in 1998 between the US Department of Energy (DOE) and China's State Development Planning Commission (SDPC). One of the most promising technical areas for initial cooperation is sensitivity analysis of air dispersion models for emergency planning. During 2004~2005, the first cooperation, i.e. a small scale tracer experiment conducted at Qinshan Nuclear Power Plant and validation of models, was carried out. In early 2006, a program to carry out an Asian tracer experiment was proposed in order to further enhance the Sino-US nuclear technology cooperation. It is designed to test the readiness of relevant services to respond in the case of an emergency, to organize the tracer release and compile a data set of measured air concentrations and to investigate the performance of long range atmospheric transport and dispersion models using that data set. In this paper, the long range tracer experiments conducted internationally and evaluation of long range dispersion models were reviewed and a preliminary planning on the former several aspects was analyzed and discussed.

II. Long Range Tracer Experiment and Model Evaluation

Increased concern over regional and international impacts of air pollution, acid deposition and accidental releases has created a need for air pollution model development and evaluation as far as 1000 km from pollutant sources. One of the more traditional methods for evaluation and verification of models is field experiments, in which a known amount of an inert tracer is released from a source and concurrent measurements of its air concentration are made at various downwind distances and locations. During 1980s of last century, 3 long range tracer experiments, named ACURATE[1], CAPTEX[2] and ANATEX[3] respectively, were conducted in US to test the tracer technology for application to 1000-km-scale studies, to provide data to evaluate and improve computer models of pollutant dispersion, and to provide insight into the mechanisms involved in long-range transport and dispersion.

After the Chernobyl accident in April 1986, the joint IAEA/WMO Atmospheric Transport Model Evaluation Study (ATMES)[4] was initiated in November 1986 in order to compare the evolution of the radioactive cloud (^{131}I and ^{137}Cs) with the evolution predicted by mathematical models for atmospheric dispersion, using as input only the estimated source term and the meteorological data for the days following the accident. Considering that the limited information on Chernobyl source strength, height, and vertical distribution of material caused a consistent uncertainty in model results, a long range tracer experiment named ETEX[5] was conducted in Europe in 1994 in conditions as close as possible to those which could be found in a real emergency case, with the advantage of complete knowledge of the source term. Almost two years after the ETEX releases, the ATMES-II modeling exercise[6] was launched. Contrary to ETEX, in ATMES-II exercise the differences between field measured concentration and modeled one can be more directly related to the dispersion simulation, owing to the use of the same wind field. However, even in this case, discrepancies are not only due to the calculation of dispersion, but also to a different usage of meteorological information. ETEX created widespread interest and resulted in considerable dispersion model development as well as the reinforcement of communication and collaboration between national institutes and international organizations.

*Corresponding author, Tel. +86-351-2202230, Fax. +86-351-7020407, E-Mail: yaorentai001@vip.sina.com

III. Preliminary Design and Planning of Tracer Experiment

As for such a large experiment planning, many aspects of the experiment preparation should be taken into account as follows: (a) definition of suitable meteorological condition, (b) choice of release site, (c) choice of tracer and establishment and validation of analytical procedures, (d) choice, construction, validation and deployment of samplers, (e) choice of ground-level sampling sites, (f) meteorological observation network, (g) establishment of data management protocols, (h) co-ordination of the release, sampling and modeling efforts, and (i) collation, dissemination and archiving of the resultant database. In this paper, the preliminary planning on the former several aspects was analyzed and discussed.

1. The Potential Release Site and Opportunity

It is very important to choose the suitable release site and experiment opportunity to maximize the probability of identifying in advance meteorological situations which will ensure the dispersion of the tracer being within the area covered by the ground sampling network. In order to conduct a tracer experiment cover a distance of up to 2000 km in the Eastern Asia, the perfect release site will be some area lying in the southwest and northwest of China with a release occurring in meteorological conditions with a prevailing westerly or northwesterly air flow. Five potential release sites are selected, involving Chengdu, Xian, Pingliang, Baiyin and Yinchuan, as shown in Fig 1.

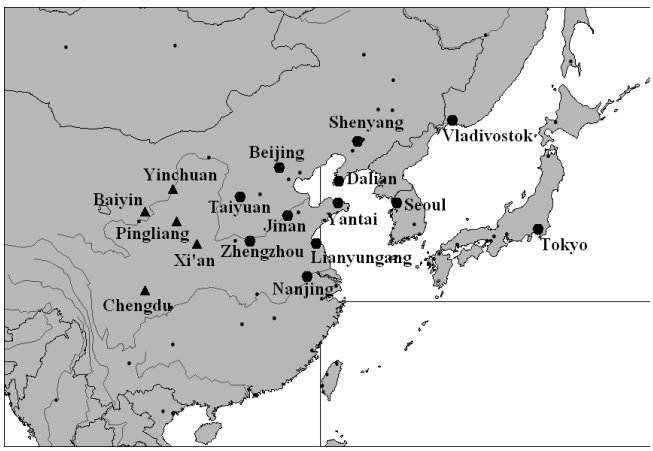

Fig. 1 The potential source sites and geographical domain of experiment.
Triangle: the potential release sites; Circle: the concerned points and areas**.**

The trajectory model[7, 8] has been used for the climatological trajectory analysis to determine the best time of year and the best tracer release location for the experiment. All forward 3D trajectories from the potential release sites regions were computed 8 times per day (at 00, 03, 06, 09, 12, 15, 18 and 21 UTC) for a period of 4 years, 2001-2005. The meteorological data is from the Dataset DS083.2 - NCEP global tropospheric analysis dataset[9] – with the resolution of 1° x 1°, latitude vs. longitude. The release height of the trajectories is 50 m. Considering uncertainties in the trajectory calculations after 5 days and the relative proximity of the analyzed release site impact geographical regions to the sites of interest, all selected trajectories for further statistical analysis were terminated at the end of 5 days.

In order to know the characteristics of climatological trajectories released from the potential tracer release locations, a set of statistical methods[8] including analysis of atmospheric transport pathway using cluster analysis, analysis of transport of tracer to potential concerned regions and analysis of airflow transport probability field, was used for analysis of results from trajectory modeling.

We analyzed all forward trajectories that originated over the five potential release locations to investigate the likelihood that the release sites would impact on many distant geographical regions representing the potential sampling points or areas. It wound be assumed that any trajectory, which crosses into the boundaries of the chosen geographical region, might bring air parcels containing tracer. Therefore, only trajectories crossing boundaries of these regions were used in the further analysis.

Considering the potential release sites and westerly air flow, the points selected lie some cities with an area of 2° × 2°, involving Taiyuan, Zhengzhou, Beijing, Jinan, Shenyang, Dalian, Yantai, Lianyungang and Nanjing (as shown in **Fig. 1**). As for the distant sampling, the regions are selected as South Korea (125-130°E vs. 34-38°N), North Japan (140-145°E vs. 38-45°N), Central Japan (136-142°E vs. 33-38°N) and South Japan (130-136°E vs. 30-36°N).

Table 1 shows the frequencies of trajectories from the five potential release locations pointing to concerned points and areas by statistics of direction of transport. The monthly variations in the percentage (%) of trajectories reached the concerned points and areas from those five locations were shown in **Fig. 2**, where the results for Zhengzgou, Yantai, South Korea and Central Japan were shown as an example.

Table 1 Seasonal variability of contribution (%) of atmospheric transport pathways in the direction of pointing to concerned points and areas

Potential release locations	Frequencies (%)			
	Spring	Summer	Fall	Winter
Chendu	18.3	12.7	22.6	20.6
Xian	46.5	28.7	50.5	41.3
Pingliang	45.9	26.9	55.6	54.1
Baiyin	54.9	41.3	62.8	57.7
Yinchuan	50.5	31.4	67.1	62.4

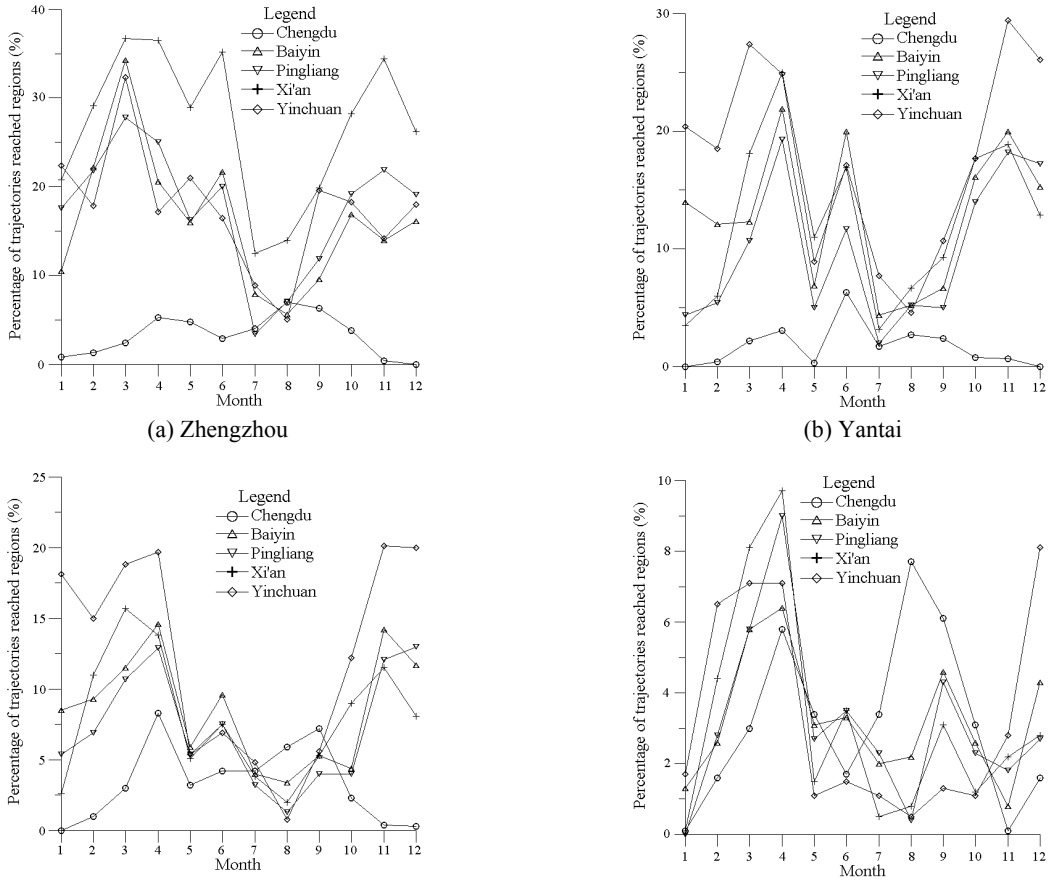

(a) Zhengzhou (b) Yantai

(c) South Korea (d) Central Japan

Fig. 2 Monthly variations in the percentage (%) of trajectories from different release locations reaching concerned regions during 2001-2005.

As shown from the above results, in general, there are two high frequency periods of time for Xian, Pingliang, Baiyin and Yinchuan to be propitious to carry out tracer experiment, i.e. from March to April and from October to November. The frequencies of trajectories reaching the concerned points and areas from Yinchuan are higher than from other locations. As a consequence, the best tracer release location is at Yinchuan and the best time for the experiment is during March - April, or October – November. As an example, **Fig. 3** shows all trajectories and atmospheric transport pathways (cluster mean trajectories) released from Yinchuan in November.

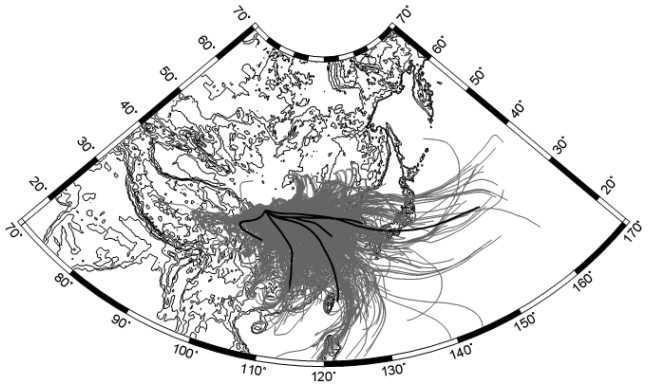

Fig. 3 All trajectories and atmospheric transport pathways (cluster mean trajectories) relesed from Yinchuan in November.

2. Atmospheric Tracers and Analysis Techniques of Tracers

Atmospheric tracers must be safe for humans and the environment. They must be stable in air (non-depositing, non-scavenged, non-reactive), with a low background and detectable with a high sensitivity. Also, they must have a reasonably low cost. Perfluorocarbon compounds (PFCs) will be used as the tracers during the tracer experiment. There are at least seven PFCs that are used for tracer experiments. They are PDCB, PMCP, o-PDCH, PECH, i-PPCH, PTCH and PMCH. There are several advantages to releasing more than one kind of PFCs. Thus, considering the present analysis technique, it is viable to use three kinds of PFC, i.e. PMCH, PMCP and PDCB.

The PFCs can be collected as whole air samples using conventional means such as bags, bottles, syringes, etc. Another tracer sampling method is called as adsorption sampling, using active sampler or passive sampler. In ETEX campaigns, only active samplers were used. A known air-volume is passed through and adsorbed in a column of activated charcoal packed into a tube that quantitatively removes all PFC material from the air.

In this experiment, there are more than 7200 samples from 180 sampling sits scattered in northern China, South Korea and Japan. It is a very hard work to transport so many

samples to the tracer's analyzing laboratory. In order to reduce the volume of samples and to transport easily, active samplers should be recommended.

The analytical method to determine tracer concentration is based on the laboratory gas chromatograph system for PFCs. The tracer concentration of every sample subtracted by the background is the concentration increment due to the release.

3. Sampling Network

More than 150 ground level samplers should be required for a successful experiment. The preliminary proposal is to use the existing various national meteorological observing stations network as the air sample collection sites. Considering the release location (Yinchuan) and the meteorological conditions to tracer experiment and combining the simulations of the downwind concentration field of the tracer material (as shown in **Fig.4** for one instance out of many), the plan of sampling network consisting of 170~180 ground level collection sites is designed as follows and shown in **Fig.5**:

(a) 130~135 sites in China,

(b) 7 sites in South Korea,

(c) 13 sites in Japan, and

(d) 20~25 standby sites.

In addition, there are 5 sites near lying along plume axis for upper-air sampling using captive balloon. As shown in **Fig. 5**, these ground sampling sites have a representative distribution in space and near six arcs at different distance from the source are formed. 20~25 standby sites are set in case of having denser sampling sites for short distance from the source, the effect of wind-meander, some sites lying over the sea and on the islands, etc.

Each sampling site is designed to sample over a period of 120 consecutive hours (40 three-hour samples), with sampling starting time progressively delayed from West to East. The sites closest to the release location will start sampling 3 hours before the release start; the most distant stations will end sampling 150 hours after the release start. Overall some 7200 samples will be successfully collected in the one experiment.

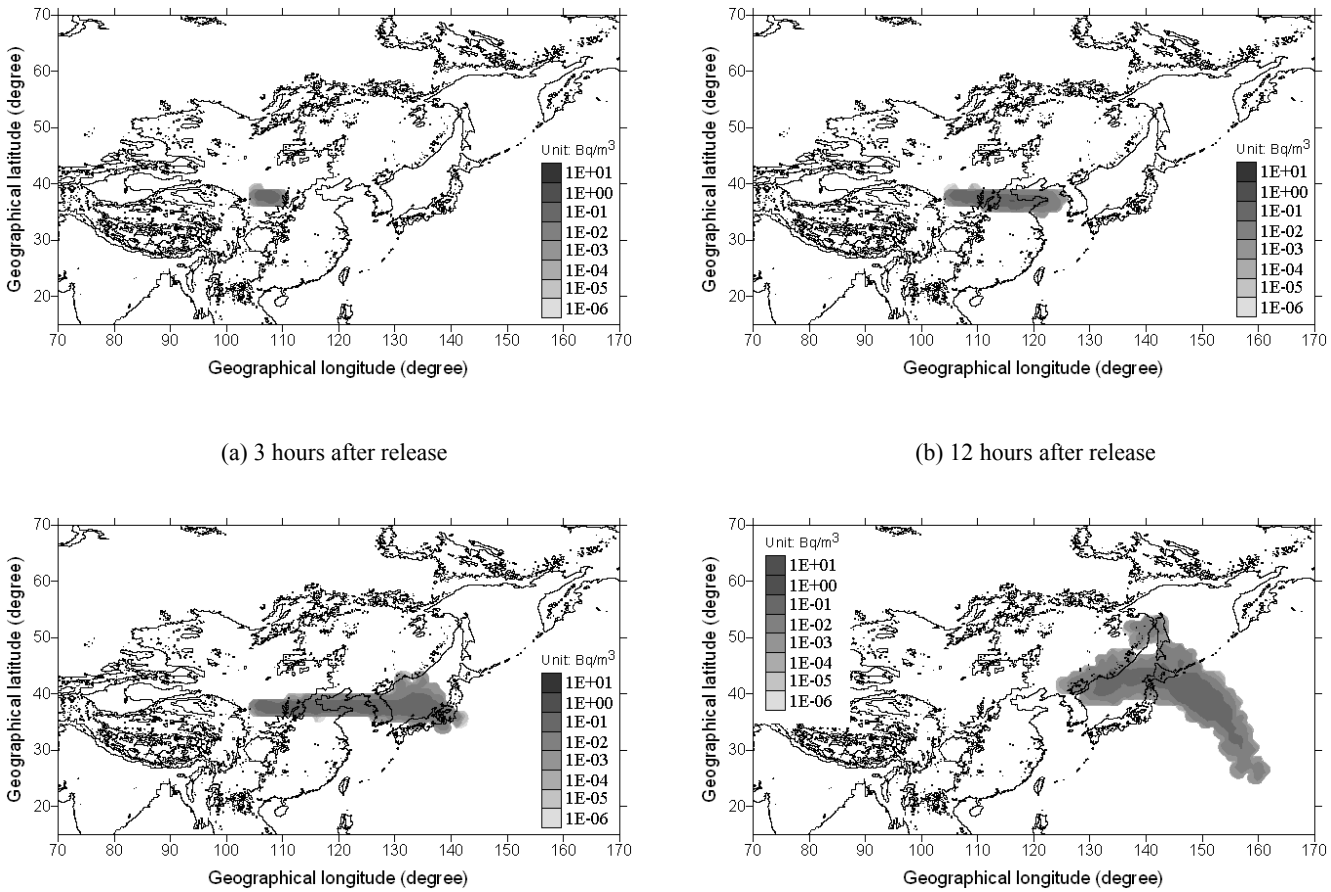

(a) 3 hours after release

(b) 12 hours after release

(c) 24 hours after release

(d) 42 hours after release

Fig. 4 Simulations of the downwind concentration of the tracer material for March 15, 2004.

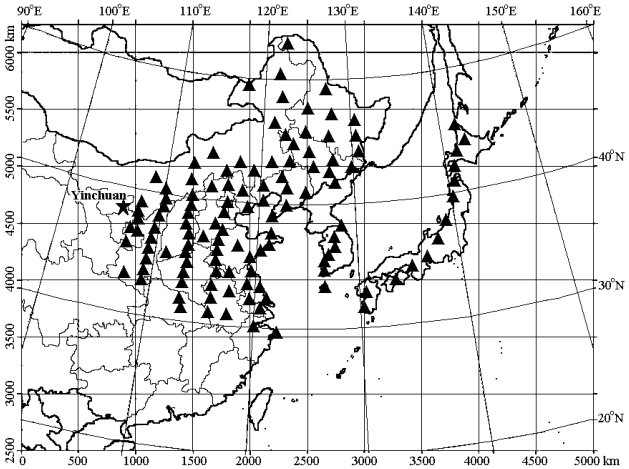

Fig. 5 Tracer release location and ground samplers.
Star: the release site; Triangle: the locations of ground samplers.

4. Meteorological Observations and Information

(1) Ground observations

At the release site a sonic anemometer will be mounted to measure the small scale wind and temperature fluctuations during the period of the release.

During the whole tracer experiment, routine synoptic weather observations will be collected from all 170~180 stations. Additional observations will also be collected from those stations in South Korea and in Japan.

(2) Upper air data

i) At the release location

During the each release, the use of constant-volume balloons (CVB) will be planned to monitor the meteorological characteristics of the air masses responsible for the plume transport. Furthermore the use of the balloons could provide real time information on the trajectory of the plume for more than a hundred kilometres downwind.

In addition, a SODAR (sound detection and ranging instrument) will be mounted at the tracer release location. The radiosonde data from the release location will be provided by Yinchuan Weather Bureau.

ii) At other stations

The data from near 90 operational meteorological observing stations in China equipped with SODARs and/or with routine radiosoundings will be collected for the periods of the tracer experiment.

(3) Other meteorological information

Wind data from numerical weather prediction products such as the NWP products from China Meteorological Center, the Dataset DS083.2 - NCEP Global Tropospheric Analyses, and the ECMWF analysed data archive.

IV. Concluding Remarks

Such a large and complex experiment will require a detailed and exercisable experiment design and planning involving technique, organizing, arrangement, quality assurance and quality control, etc. Up to now, 5 sponsoring organizations, China Institute for Radiation Protection, Lawrence Livermore National Laboratory, Japan Atomic Energy Agency, Korean Atomic Energy Research Institute and Korean Institute for Nuclear Safety have been involved in this project. Each side will designate a project leader for their respective group and topical area.

Quality assurance for a successful experiment is essential. It is very important for a successful experiment to implement quality assurance/quality control of all procedures, especially for air sample collection site selection, tracer sampling, air sample collection and laboratory analysis procedures including analysis of background concentrations of PFCs.

On the other hand, we will profit from technique progress of modern society. Since the accident in Chernobyl and ETEX experiment, we have made enormous progress in communication and computer technology, so that we are now capable of providing swiftly the information and predictions so desperately needed at that time.

References

1) J. L. Heffter and J. F. Schubert, “Atlantic Coast Unique Regional Atmospheric Tracer Experiment (ACURATE),” NOAA Technical Memorandum ERL ARL-130 (1984).
2) G. J. Ferber, J. L. Heffter, R. R. Draxler, et al., “Cross-Appalachian Tracer Experiment (CAPTEX’ 83) Final Report,” NOAA Technical Memorandum ERL ARL-142 (1984).
3) R. R. Draxler and J. L. Heffter, “Across North America Tracer Experiment (ANATEX) Volume I: Description, Ground-Level Sampling at Primary Sites, and Meteorology,” NOAA Technical Memorandum ERL ARL-167 (1989).
4) W. Klug, G. Graziani, G. Grippa, et al. (Eds), “Evaluation of Long Range Atmospheric Transport Models Using Environmental Radioactivity Data from Chernobyl Accident: the ATMES report”, Elsevier Applied Science (1992).
5) Van Dop H, Addis R, Fraser G, et al., “A European Tracer Experiment: Observations, Dispersion Modelling and Emergency Response”, Atmospheric Environment, 32, 4089 (1998).
6) S. Mosca, R. Bianconi, R. Bellasio, et al., “ATMES II - Evaluation of long range dispersion modes using data of the 1st ETEX release”, EUR 17756 EN, Luxembourg (1998).
7) R. Yao and W. Gao, “Simulations of Transboundary Atmospheric Transport of Radioactivity Released from Nuclear Risk Sites at the Far East”, Journal of Nuclear Science and Technology, Supplement 4, 491-494 (2004).
8) R. Yao, X. Xu, H. Hao, et al., “Simulations of Long-Range Transport of Airborned Radioactivity Released from Nuclear Risk Sites at the Far East”, Radiation Protection, 25,193 (2005) (in Chinese).
9) NCEP, http://dss.ucar.edu/datasets/ds083.2/.

Journal of NUCLEAR SCIENCE and TECHNOLOGY, Supplement 5, p. 690–693 (June 2008)

Radiological Dose Assessment for Clearance of Biological Shield Concrete from KRR-2

Sang Bum HONG*, Gye Hong KIM, Hee Reyoung KIM, Mun Ja KANG, and Un Soo CHUNG

Korea Atomic Energy Research Institute, 150 Deokijn-dong, Yuseong, Deajuon, 305-353, Korea

A large amount of radioactive concrete waste was generated during the decommissioning work of the Korean Research Reactor #2 (KRR-2). More than 85% of the dismantled concrete waste will be disposed of by a recycling or landfill by the application of a clearance principle. Currently, the Korean Atomic Energy Act and relevant regulation comply with the international recommendation of the sources/practices meeting an individual dose criterion 10 μSv/y and a collective dose criterion of less than 1 man.Sv/y. A variety of radionuclides was generated in the biological shield concrete by a neutron reaction during the operation of a reactor. The specific activities of these radionuclides were measured by using the developed methods and procedures. For the evaluation of a radiological dose, seven scenarios were selected which encompassed a realistic situation of a recycling such as a road construction and landfill disposal route. The external and internal exposure doses of each scenario were calculated by using the MCNP4C code and a mathematical model respectively. The dose assessment regarding the residents and industrial workers was evaluated by using the RESRAD code for the landfill disposal scenario. The maximum individual dose rate was 7.21 μSv/y and the maximum collective dose was 0.05 man . Sv/yr for the landfill disposal scenario.

KEYWORDS: clearance, radiological dose assessment, activated concrete, decommissioning

I. Introduction

A large amount of radioactively contaminated and activated materials is generated from the decommissioning and decontamination of nuclear facilities, most of which may be slightly contaminated or activated. The generation of a decommissioning waste can be significantly reduced through the implementation of a proper clearance principal. Clearance is defined as the removal of radioactive materials or radioactive objects within authorized practices from any further regulatory control by a regulatory body[1]. The Korean Atomic Energy Act and relevant regulation for clearance criteria are defined as an individual dose of less than 10 μSv/y and a collective dose of less than 1 man.Sv/y [2].

The dismantling work of the biological shield concrete of the Korean Research Reactor #2 (KRR-2) was successfully completed at the end of 2006. All the solid waste from the decommissioning project was categorized into three groups based on their radioactivity; radioactive, restricted releasable and not-contaminated waste. The radioactive waste, which has a higher radioactivity than 0.4 Bq/g for beta/gamma emitting nuclides, was packed into drums of 200 liters or a container of 4 m^3 according to its physical properties. It will be temporally stored in the reactor building of the KRR-2 and will be sent to the national LILW disposal site which is being constructed by KHNP (Korea Hydro and Nuclear Power Company) to start operation at the end of 2008. The restricted releasable waste will be treated according to a pre-determined route. In the near future, a study on a local disposal or long term storage of this waste at the KAERI site will be carried out. The radioactivity level of the not-contaminated waste is less than MDA, which was calculated as 0.013 Bq/g for the beta/gamma emitting nuclides. It will be treated as a general industrial waste by applying a clearance principle. In order to apply a clearance concept to the not-contaminated concrete waste, it should be proven that the calculated potential radiological dose would be lower than the clearance criteria for the release of the waste and the route to final destination should be observed.

In this study, the results of radiological dose assessment for a recycling or a landfill disposal of selected scenarios were discussed for radionuclides in the activated concrete. The specific activities of these radionuclides were measured by using developed methods and procedures.

II. Measurement and Dose Assessment Method

1. Measurement

The characterization of a physical property and a radiological survey were carried out before dismantling the biological shield concrete of KRR2. The structure of KRR-2 is shown in **Fig. 1**. The size of the structure is 9.7 m (W), 17.4 m (L) and 7.8 m (H) and the estimated volume is 650 m^3. It was composed of normal concrete of 2.4 g/cm^3 and heavy concrete of 3.0 ~ 3.2 g/cm^3. The radiological survey was initiated to determine the boundary between the area of the activated and non-activated part. A sample was taken to measure the radioactivity distribution of the inside and the depth of the concrete by using the HPGe detector. According to this result, non-activated or not-contaminated concrete waste was dismantled by a core boring and a diamond wire cutting. The activated (radioactive waste) concrete was applied to a hydraulic breaker in a green house. Total of 1,913 tons was generated during the dismantling work and more than 85 % of the concrete was classified as not-

* Corresponding Author, Tel No: +82-42-868-2745, Fax No: +82-42-868-2499, E-Mail; sbhong@kaeri.re.kr

contaminated waste.

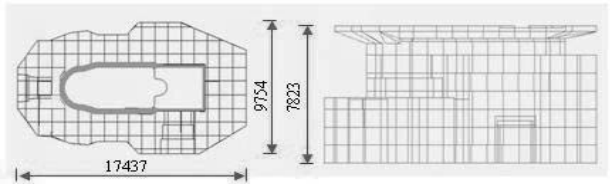

Fig. 1 The schematic diagram of the structure of KRR-2

Firstly, about 800 tons of the concrete will be disposed of conventionally by recycling or landfill disposal after approval of the clearance plan by the regulatory authority. A considerable number of methods and instruments are available for determining a radioactivity which can be used for checking on a compliance with a clearance level. The characterization procedures to apply a clearance principle to concrete have been set up and applied. The surface dose rate and the gross alpha and beta contaminations of a surface were measured by using a GM (Geiger-Muller) type survey meter and a low background alpha/beta counter respectively. A gamma spectrometry was used to define the isotropic composition by using the HPGe detector. To ensure the homogeneity, a sample was taken from each surface of a concrete block at regular intervals. However, a variety of radionuclides had been generated in the biological shield concrete by a neutron reaction during the operation of the reactor [3-4], including ^{3}H, ^{14}C, ^{55}Fe, ^{60}Co, ^{63}Ni, ^{134}Cs, ^{137}Cs, ^{152}Eu and ^{154}Eu. The radioactivities of ^{3}H and ^{14}C were determined by a commercially available tube furnace and a liquid scintillation counter, and ^{55}Fe and ^{63}Ni by a combined method of an extraction chromatography and a liquid scintillation analysis. Most of the measured results of the specific activities of these radionuclides were less than MDA, but a high-level of activity was detected in a highly activated part of the biological shielding concrete. The results are presented in **Table 1**.

Table 1 Results of the specific activities in not-contaminated or activated concrete waste from KRR-2

Nuclide	Half-life (y)	Results (Bq/g)	Nuclide	Half-life (y)	Results (Bq/g)
^{3}H	12.3	1.080 a)	^{134}Cs	2.1	0.013
^{14}C	5730	0.032	^{137}Cs	30.1	0.013
^{55}Fe	2.7	0.200	^{152}Eu	13.3	0.013
^{60}Co	5.3	0.013	^{154}Eu	8.8	0.013
^{63}Ni	96	0.250			

a) MDA level of ^{3}H is 0.048 which was calculated MDA equation [5].

2. Selection of the Scenarios and Assumptions

The general flow of a cleared concrete was divided into a processing, transportation, road construction and a landfill disposal. For the calculation of a radiological dose, seven scenarios were selected which encompassed a realistic situation of the recycling industry in Korea. The selected scenarios were composed of exposure pathways, which contained specific exposure conditions. There are three main exposure pathways; an external, inhalation and ingestion exposure. An external exposure is caused by the photons penetrating the human body from gamma emitting radionuclides. Inhalation of contaminated dust and inadvertent ingestion of a contaminated material can occur in many exposure situations. The detail information of the exposure pathway of each scenario is shown in **Table 2**.

Table 2 The concrete recycling and disposal scenarios and the exposure pathways

Scenario	Exposure duration (h)	Exposure pathway Ext. / Inh. / Ing.
Handling and Processing		
SC1 : Processor	2000	O / O / O
SC2 : Truck driver	4	O / X / X
SC3 : Loader/Unloaded	100	O / O / O
Product use		
SC4 : Construction worker	2000	O / O / O
SC5 : Driver on road	20	O / X / X
Landfill disposal		
SC6 : Disposal worker	2000	O / O / O
SC7 : Resident	4380	O / O / O

On the basis of a calculation that follows, it is conservatively assumed that 1,000 tons of the concrete is recycled or disposed at a general landfill site during a year. A large dilution could be occurred during the construction a road, but no dilution is assumed for this analysis. The exposure duration of each scenario in the Safety Series of the IAEA is adopted and calculated based on the distance, working efficiency and speed of a car.

3. Dose Assessment Method

The study on a combination of the radiation exposure pathways of each scenario used to conceptually model the potential future conditions, that could result in radiation exposures to individuals or group is processed. The individual dose and collective dose for each scenario were evaluated by using an appropriate mathematical modeling of the NUREG-1640, MCNP4C and RESRAD codes.[7-9] A basis of a selection for an input parameter was conservatively chosen for each scenario by reflecting the industrial conditions in Korea and comparing them with other countries as a reference.

(1) External exposure

The external exposure to a stream of a residually radioactive material is assessed as follows:

$$D_{ix} = C_{ij} F_{ix} t_{xy} U_x e^{-\lambda i\, ts} \quad (1)$$

D_{ix} = dose from external exposure to radionuclide *i* during assessment period (μSv)

C_{ij} = average activity concentration of radionuclide *i* in medium *j* (Bq/g)

F_{ix} = dose coefficient for external exposure to radionuclides *i* (μSv/h per Bq/g)

t_{xy} = exposure duration during assessment period (h)

λi = radioactivity decay constant of radionuclide *i* (d^{-1})

t_s = interval from time concrete is cleared until scenario being

The relation between an external dose and a radioactivity is complicated, depending not only on the radioactivity but also on the geometry in which the radioactivity distribution, on the shielding effects, on the self-absorption effects, and on the distance to the source. The suitable dose coefficients for each nuclide and scenario are calculated by using the MCNP code. The geometry of each scenario was modeled as follows:

Processor scenario: the source is modeled as 1,000 tons of concrete pile by using cone geometry with a length of 8 m and a radius of 8 m. The average distance between the workers to the source is 2 m.

Truck driver scenario and load scenario – the truck load source is modeled as a 25 tons load by using a box geometry with a length of 14.9 m, a height of 2.9 m and a width of 2.6 m. The average distance between the truck driver and the source and between the load/unload worker and the source is 1m and 2 m respectively.

Construction worker and drive on the road scenario – the road construction source is modeled as 1,000 tons by using the box geometry of 3 m (W), 800 m (L) and 0.2 m (H), the average distance between the surface of road and the source is 0.5 m. Drive on a road scenario is the same geometry as the road construction scenario, but the driver is shielded by a 5 cm frame of the car.

The effective dose rate was calculated for each geometry of the scenarios, by applying conversion coefficients in the ICRP74.[10)]

(2) Inhalation exposure

The dose from an inhalation exposure is calculated as follows:

$$D_{ih} = C_{ij} F_{ih} R_h t_{iy} \chi_d e^{-\lambda i\, ts} \quad (2)$$

D_{ih} = dose from inhalation exposure to radionuclide *i* during assessment period (μSv)
F_{ix} = dose coefficient for inhalation of radionuclide *i* (μSv/Bq)
R_h = inhalation rate (m^3/h)
t_{iy} = exposure duration during assessment period (h)
χ_d = airborne concentration of dust (mass loading) (g/m^3)

Inhalation rate for a light activity has a time weighed average of 1.2 m^3/h in the ICRP 1994. This parameter was assigned to an inhalation exposure. The exposure of a worker to an inhalation of concrete dust is subject to the eight hours work limit of 14 mg/m^3. This parameter is more conservative than the notice of the Minister of Labor in Korea. The committed effective dose coefficient for calculating the dose coefficient for a worker used in this study was taken as 5μm of AMAD (activity median aerodynamic diameter) from the ICRP68.[11)]

(3) Inadvertent ingestion exposure

The dose from an ingestion exposure is calculated as follows:

$$D_{ig} = C_i F_{ig} I_s t_{iy} e^{-\lambda i\, ts} \quad (3)$$

D_{ig} = dose from ingestion of radionuclides *i* during assessment periods (μSv)
F_{ig} = dose coefficient for ingestion of radionuclide *i* (μSv/Bq)
I_s = secondary ingestion rate (g/h)

The parameter of a secondary ingestion rate of 30 mg/h was selected from NUREG-1640, this value was used for the dose calculation for an ingestion pathway. The committed effective dose coefficient for calculating the dose coefficient used in this study was taken from the ICRP 68.

The dose assessments of the residents and industrial workers for the landfill disposal scenario were evaluated by using RESRAD code. RESRAD is a computer model to estimate a radiation dose and risks from residual radioactive materials. An external gamma dose, dust inhalation dose, soil ingestion dose, food (plant, meat and milk) ingestion dose and drinking water for the residents and industrial workers were considered. RESRAD used a committed effective dose equivalent dose conversion coefficient for an inhalation and ingestion from the Federal Guidance Report. The modified dose conversion coefficients based on the IAEA Safety Series 115 [12)] were used in this study.

III. Results and Discussion

For the evaluation of a radiological dose, seven scenarios were selected which encompassed a realistic situation of a recycling from a road construction and a landfill disposal route. The results of this study are based on the generic exposure scenario and pathway analyses using the measured results of 9 radionuclides from dismantling the biological shielding concrete from KRR-2. Totally 7 individual exposure pathways were considered for each scenario, and the results are shown in **Fig. 2**. All individual exposure doses are under the does based criteria of 10 μSv/y. The exposure dose rate of the workers who are responsible for a landfill disposal scenario (SC6) shows the maximum dose rate which is 7.21 μSv/y. The main exposure pathway is an external exposure and the most dominant radionuclide is ^{60}Co which takes charge of 37 % of the total individual dose of the landfill disposal scenario. The clearance levels were calculated based on the dose based results and compared with the NUREG-1640 and IAEA report. For example, the calculated clearance level of ^{60}Co is 0.1 Bq/g which is the same value as the IAEA report, but the NUREG-1640 suggests 0.04 Bq/g conservatively. For the other radionuclides, they showed the same trends for the clearance levels.

The collective dose was estimated both on the basis of an individual dose and the number of people exposed on the basis of generic exposure scenarios. The number of people was conservatively estimated from the average population of

the disposal site in this study. The collective dose of residents after closed the site scenario (SC7) shows a maximum value of 0.05 man.Sv/y, which is also well below the collective dose criterion of 1 man.Sv/y. The detailed results for each scenario are presented in **Fig. 3**.

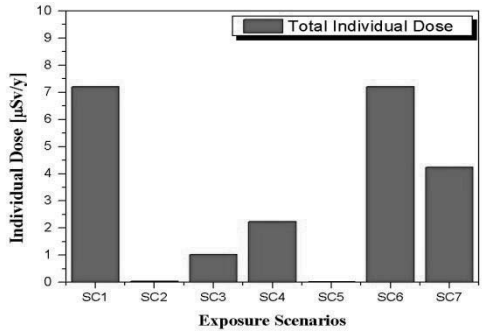

Fig. 2 The results of individual dose for scenario.

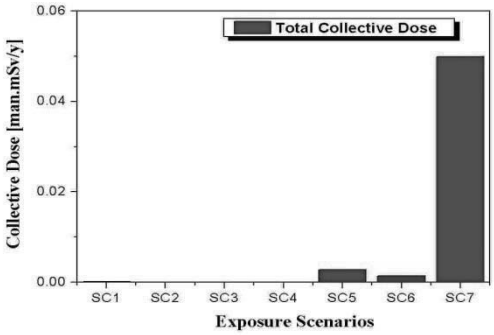

Fig. 3 The results of collective dose for scenario.

IV. Conclusions

In this study, the assessment of a potential radiation exposure in the case of a concrete recycling and a landfill disposal was evaluated. This study suggests a radiological dose assessment method for a concrete waste based on a realistic industrial situation. The measurement methods and procedures were established for a sampling and analysis of the gamma and beta emitting nuclides in an activated concrete. They could be a technical basis for the application of a clearance principal.

Acknowledgement

This work was performed under the nuclear research and development program sponsored by Ministry of Science and Technology of Korea.

References

1) IAEA, "Application of the Concepts of Exclusion, Exemption and Clearance," IAEA Safety Standards Series. No, RS-G-1.7, IAEA, Vienna, (2004).
2) S. B. Hong, J. H. Park, "Waste Management in Decommissioning Projects at KAERI," Proc. of Int. Sym. on Radiation Safety Management, Daejeon, Korea, Nov. 2-4, 2005, p.167-176(2005).
3) T. M. Sullivan, 'Assessment of Release Rates for Radionuclides in Activated Concrete,' BNL-71537, (2003).
4) Xiaolin Hou, 'Rapid analysis of ^{14}C and ^{3}C in graphite and concrete for decommissioning of nuclear reactor,' Applied Radiation and Isotopes, 62, 871 (2005).
5) L. Curie, 'Limits for qualitative determination and Quantitative determination,' anal. Chem., **40**[3]586 (1968).
6) R. Anigstein et al, 'Radiological Assessments for Clearance of Materials from Nuclear Facilities,' NUREG-1640, (2003).
7) IAEA, 'Application of Exemption of Exemption Principles to the Recycle and Reuse of Materials from Nuclear Facilities,' IAEA Safety Series No. 111-P-1.1, IAEA, Vienna, (1992).
8) J. F. Briesmeister, Ed., 'MCNP-A General Monte Carlo N-Particle Transport Code Version 4C.' LA-13709-M, Los Alamos National Laboratory, (2000).
9) C. Yu et al, 'User's Manual for RESRAD version 6,' ANL/EAD-4, (2001).
10) International Commission on Radiological Protection, 'Conversion Coefficients for use in Radiological Protection against External Radiation,' ICRP Publication 74, Annals of the ICRP 26(3/4), Tarrytown, NY : Elsevier Science Inc, (1996).
11) International Commission on Radiological Protection, 'Conversion Coefficients for Intakes of Radionuclides by Workers,' ICRP Publication 68, Annals of the ICRP 24(4), Tarrytown, NY : Elsevier Science Inc, (1994).
12) IAEA, 'International Basic Safety Standards for Protection against Ionizing Radiation and for the Safety of Radiation Source,' IAEA Safety Series No. 115, Vienna, (1996).

Journal of NUCLEAR SCIENCE and TECHNOLOGY, Supplement 5, p. 694–697 (June 2008)

2D Monte Carlo Analysis of Radiological Risk Assessment for the Food Intake In Korea

Han Ki JANG,*, Joo Yeon KIM, and Jai Ki LEE

Hanyang University, 17, Haengdang-dong, Seongdong-ku, Seoul, Korea

Most public health risk assessments assume and combine a series of average, conservative and worst-case values to derive an acceptable point estimate of risk. To improve quality of risk information, insight of uncertainty in the assessments is needed and more emphasis is put on the probabilistic risk assessment. Probabilistic risk assessment studies use probability distributions for one or more variables of the risk equation in order to quantitatively characterize variability and uncertainty. In this study, an advanced technique called the two-dimensional Monte Carlo analysis (2D MCA) is applied to estimation of internal doses from intake of radionuclides in foodstuffs and drinking water in Korea. The variables of the risk model along with the parameters of these variables are described in terms of probability density functions (PDFs). In addition, sensitivity analyses were performed to identify important factors to the radiation doses.

KEYWORDS: 2D MCA, variability, uncertainty, probabilistic risk assessment, sensitivity analysis

I. Introduction

In 2005, the radioactivity in foodstuffs consumed by Korean population, obtained from the National Environmental Radiation Monitoring Network operated by the Korea Institute of Nuclear Safety (KINS), was used together with the dietary data to estimate the internal doses due to ingestion of the foodstuffs[1)]. The United States Environmental Protection Agency (U.S. EPA) recommends the use of the one-sided 95% upper confidence limit of the arithmetic mean based on either a normal or lognormal distribution for the exposure factor in the Superfund risk assessment process[2)]. It is, therefore, required that the individual exposure or risk to be presented as a specific distribution resulting from an iterative simulation. Since the previous estimation was based on the radioactivities in foodstuffs and food consumption rates measured as a point estimate or representative value, revaluation of the committed effective dose is attempted by applying a probabilistic risk analysis.

Probabilistic risk assessment (PRA) studied use probability distributions for one or more variables of the risk models in order to quantitatively characterize the variability and uncertainty. The use of PRA to size variability and uncertainty in risks gets increased popularity as recommended by the National Research Council addressing science and judgment in the risk assessment[3)]. Both variability and uncertainty may be quantified using probability distributions.

However, the interpretation of the distributions differs in the two case. Kaplan and Garrick[4)] suggest that uncertainty regarding variability may be viewed in terms of probability regarding frequencies. The International Atomic Energy Agency (IAEA) interprets distributions for variable quantities as representing the relative frequency of values from a specified interval, and distributions for uncertain quantities as representing the degree of belief, or subjective probability, that a known value is within a specified interval[5)]. Morgan and Henrion[6)] suggest that variability is described by frequency distributions, and that uncertainty in general, including sampling error, measurement error, and estimates based upon judgment, is described by probability distributions. To distinguish between stochastic variability (Type-V) and lack of knowledge uncertainty about fixed values (Type-U), Monte Carlo simulation should be applied for two stages.

Perhaps the most widely used method in PRA is Monte Carlo Analysis (MCA), which is a means of quantifying uncertainty or variability in a probabilistic framework using computer simulation. One of the advanced modeling approaches that may be used to conduct PRA studies is two-dimensional Monte Carlo analysis (2D MCA). A 2D MCA is a term used to describe a model that simulates both uncertainty and variability in one or more input variables. A detail of conducting a 2D MCA is explained elsewhere [7,8)].

In this paper the 2D MCA approaches were applied in the assessment of internal doses and public health risk due to radioactivities in the foodstuffs consumed by Korean population.

II. Methodology

1. Data Collection and Exposure Model

The data used in this analysis were collected from two sources. The radioactivity concentrations in foodstuffs consumed by Korean population were obtained from the Korea Institute of Nuclear Safety who operates the National Environmental Radiation Monitoring Network. The radioactivities of 10 naturally occurring radionuclides and ^{137}Cs in 59 kinds of foodstuffs and drinking water were evaluated. The dietary data of various foodstuffs were

* Corresponding Author, Tel No: +82-2-2220-0571, Fax No:. 82-2-2296-3690, E-Mail; hkjang@rrl.hanyang.ac.kr

extracted from the results of dietary surveys carried out by the Ministry of Health and Welfare in 2001 and 2002.

The collected data were evaluated and processed to construct the probability distribution. Data outlying from the 90% confidence interval were excluded from the analysis and new means and standard deviations were produced for those data within the stated interval. This process aims at reducing risk of unacceptably scattered outcomes by excluding the raw data either obtained from the areas with temporally extreme values resulted from a variation of the environment or having probable systematic measurement errors. The results of dietary surveys were combined with the radioactivity content data after some adjustment in grouping the foodstuffs to calculate effective doses due to ingestion.

Dose coefficients per unit intake radionuclides are provided by the ICRP[9] and calculated for the committed effective doses to age 70 years based on recent metabolic data and models. The age categories are infants (1-2 years), children (>7 to 12years) and adult (>18years). The committed effective dose from the ingestion of foodstuffs was calculated as follows:

$$D = \sum_{N}^{i} \sum_{j}^{k} DC_N \times C_{jN} \times U_i \quad (1)$$

where D is committed effective dose [mSv y^{-1}], DC_N is ingestion dose conversion coefficients for nuclide N [mSv Bq^{-1}], C_{jN} is concentration of nuclide N in food j [Bq kg^{-1}] and U_j is consumption of foods and water drinking [kg y^{-1}].

2. 2D Monte Carlo Analysis

The 2D MCA is a procedure characterizing both uncertainty and variability on one or more variables. All probability density functions (PDFs) used to describe the variability in the model have some certain degree of uncertainties. For example, variability in the radioactivity concentration can be presented by using a normal PDF with a mean and a standard deviation. Uncertainty in a second order variable can be treated in 2D MCA by representing its parameters in terms of PDFs. In this paper, we used lognormal, normal and uniform PDFs to describe random variables. **Table 1** provides information required to estimate 2D MCA.

In 2D MCA, these distributions representing variability and uncertainty are derived from nested computational loops. That is, the inner loop simulates variability by repeatedly sampling values for each variable from the specific probability density functions whose parameters are selected in the outer loop. **Fig. 1** shows 2D MCA procedure as presented in reference[10].

For radioactivity concentration and food intake, these inputs are modeled as second order random variables. The lognormal, normal and uniform PDFs used for the parameters of the random variable are provided in Table 1. In this study, the outer loop iterates 250 times, while the inner loop iterates 10000 times. The total number of simulations required is equal to the number of outer loop iterations times that of inner loop iterations. A total of 250 cumulative distribution functions (CDFs) are then generated and it takes the total of MCA is computationally intensive since the two nested loops with large sampling within each loop are used.

The primary purpose of probabilistic risk estimation is to analyze uncertainty and its sources as they associate with the risk estimates. The probabilistic analysis may be performed using software packages such as the Crystal Ball or @RISK[11] and the former was used in this study.

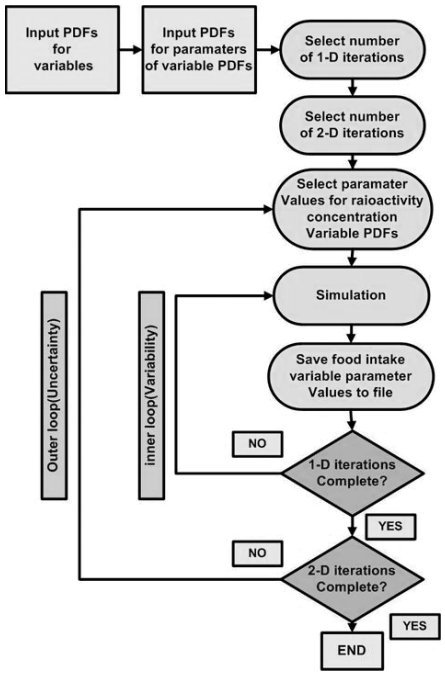

Fig. 1 2D MCA procedure (adapted from Maclntosh et al., 1995)

Table 1 The variability (Type-V) and uncertainty (type-U) of the model parameters

Parameter		[1]C_{jN} [Bq kg^{-1}]	[2]U_j [kg y^{-1}]
Type-V	Dist.	Normal (m_{rc}, s_{rc})	lognormal (m_{fi}, s_{fi})
Type-U	Dist.	m_{rc} ~ normal s_{rc} ~ uniform	m_{fi} ~ lognormal s_{fi} ~ uniform)

[1]C_{jN} is radioactivity concentration of 11 nuclides contained in 60 kinds of foodstuffs.
[2]Uj is the food j ingested mainly by Korean population.

3. Sensitivity Analysis

Generally, the objectives of an uncertainty analysis are: (1) to evaluate the output uncertainty and (2) to find the relative contribution of each model variable to the output uncertainty. The second objective is commonly referred as a sensitivity analysis[12]. For the purpose of sensitivity analysis, variables estimated from models reflecting observed data and alternative or assumed data should be segregated in the probabilistic analysis.

To obtain credible outputs, significant correlation among the input variables must be taken into account in the Monte

Carlo simulation. The Spearman's Rank correlation coefficients (RHO) are calculated for each pair of input variables to determine if a significant correlation exists. Selected significant correlation coefficients are then specified in the simulations.

III. Results and Discussion

1. The Distinction between Variability and Uncertainty

If the end point of the derived distributions is fixed as quantity such as the risk to a specific individual, a maximally exposed individual or specific individual of a specific population subgroup, it is suggested that the true quantity be within the specific limit from the uncertainty analysis. The probability distribution obtained from uncertainty analyses using MC simulation represents a range of degrees of belief that the true but unknown value is equal to or less than any value selected from the distribution. This statement of confidence accounts for multiple sources of uncertainty, including uncertainty associated with the model structure and the presence, variability, and representativeness of data. When the assessment end point is fixed as any quantity, distributions of values obtained from repeated observations represent uncertainty of Type-U because the true value is still an unknown quantity. The summaries of the statistical variability are presented for committed effective dose of infant in 2D MCA in **Fig. 2** and **Table 2**.

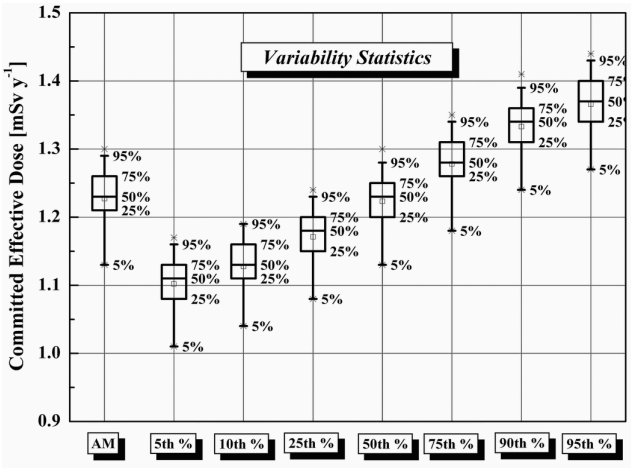

Fig. 2 The statistics for variability of committed effective dose of infant. Output from a 2D MCA showing the estimated internal dose and 90% confidence interval for the arithmetic mean(AM) and selected percentiles of the dose distribution.

2. Results of 2D Monte Carlo Analysis

The output of 2D MCA analysis is a collection of CDFs for each simulation of the outer loop. The food intake rate and radioactivity concentration are modeled as a normally distributed random variable with various mean and standard deviation combinations selected from normal, lognormal and uniform distributions. 250 different mean and standard deviation combinations which were determined from outer loop were generated for the food intake rate and radioactivity concentration in this study. For each mean and standard deviation combination, Monte Carlo simulations of 10000 are conducted to generate one CDF. CDFs of 250 were then produced for committed effective doses for the infant and adult based on 2D MCA.

The 90% confidence intervals were calculated for the quantities such as 5, 10, 25, 50, 75, 90 and 95 percentiles of the dose distribution for infant as presented as an example in **Fig. 2**. It is noted that the dose consistent in the 95th percentile is below 1.43 and 0.27 mSv y^{-1} infant and adult under the probability of 95%, respectively. The 90% confidence interval for the median is the envelope covering the area between CDFs corresponding to the 5th percentile and the 95th percentile. 250 CDFs generated through 2D MCA for infant and adult are used to plot the 90% confidence interval for the median and are given in **Fig. 3**. The results derived from this study can be used as guidance for the decision-making in estimating the internal doses

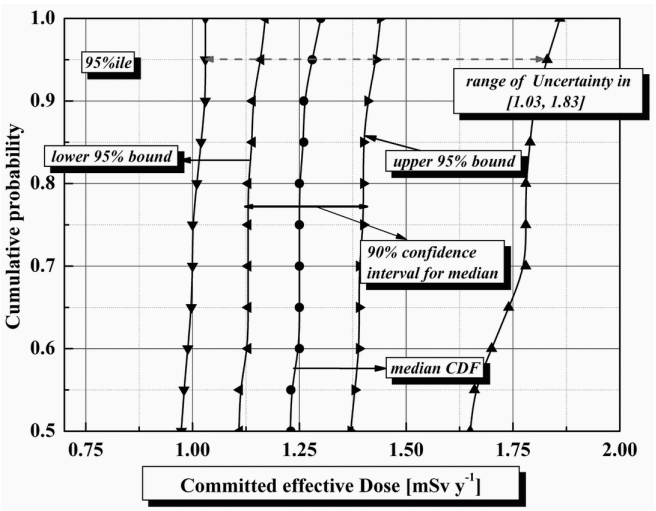

(a) Infant

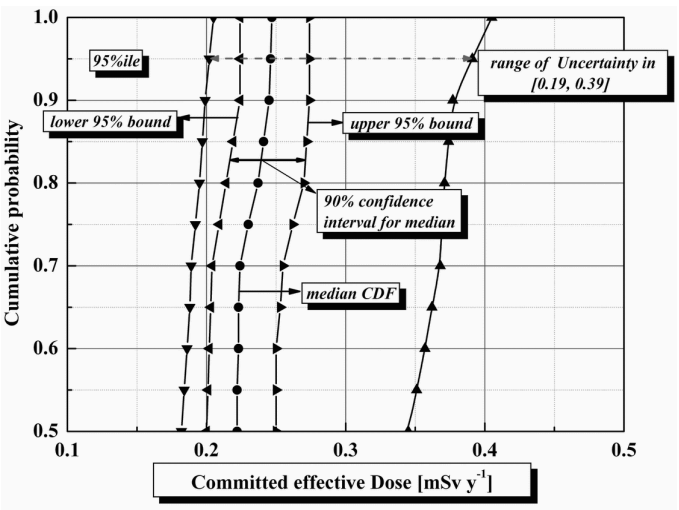

(b) Adult

Fig. 3 90% Confidence interval for the median of the committed effective doses of infant and adult

due to ingestion of foodstuffs in Korea. That is, if the estimation consistent with 95th percentile is below some recommendation of the ingestion, it is very likely that the recommendation may be not exceeded.

In addition, sensitivity analysis was performed on each of the input variables to determine the factors having highest effect on the doses. RHOs were to be 0.67, 0.46, 0.28 and 0.21 for bean, powdered milk, milk and grapes, et al. in order in case of infant. While RHOs were to be 0.68, 0.28, 0.26 and 0.22 for bean, potato, mandarin and persimmon, et al. in order in case of adult.

IV. Conclusions

A radiological dose assessment for Korean population was performed by reflecting the radioactivity data in foodstuffs and food consumption rates based on 2D MCA. According to the sensitivity analysis, ^{40}K in foodstuffs (i e. grain and root vegetables and fruits) was confirmed dominant factor in the result to be contributed to the public health risk. The variability and uncertainty for infant were higher than those for adult due to the deviations of the dose conversion factors and amount of ingestion by age. The committed effective doses based on the 2D MCA of 95th percentile were varied within 10% as compared with the deterministic values for adult and infant. The importance of explicitly including consideration of variability and uncertainty in risk assessments arises directly from their ramifications in risk management. Although the concepts of variability and uncertainty may be easily confused, they remain distinct concepts within a decision-making context. The production of probabilistic risk assessment results that represented a paradigm shift away from the use of point estimates created new challenges for risk managers.

Acknowledgement

This work was performed under the long-term nuclear research and development program sponsored by Ministry of Science and Technology of Korea, and supported by the Innovative Technology Center for Radiation Safety (iTRS), Hanyang University.

References

1) KINS, Design and construction of a radiation dose database for Korean population, KINS/HR-673, (2005).
2) U.S. EPA, Supplemental Guidance to RAGS: Calculating the Concentration Term (office of Solid Waste and Emergency Response, U. S. Environmental Protection Agency, (1992).
3) Kimberly M. Thompson, "Variability and Uncertainty Meet Risk Management and Risk Communication," Risk Analysis 22(3),p647-654, (2002).
4) Kaplan, S. and Garrick, B.J., "On the Quantitative Definition of Risk," Risk Aanlysis 1(1), 11-27, (1981).
5) International Atomic Energy Agency, Evaluating the Reliability of Predictions Using Environmental Transfer Models, Safety Practice Publications of the IAEA, IAEA Safety Series No.100, (1989).
6) Morgan, M.W. and Henrion, M., Uncertainty: A Guide to Dealing with Uncertainty in Quantitative Risk and Policy Analysis, Cambridge University press, New York, (1990).
7) Alison C. Cullen and H. Christopher Frey, Probabilistic Techniques in Exposure Assessment: a handbook for dealing with variability and uncertainty in models and inputs, New York and London, (1998).
8) U.S. EPA, Risk Assessment Guidance for Superfund: Volume 3-part A, Process for Conducting Probabilistic Risk Assessment, U. S. Environment Protection Agency, (2001).
9) ICRP, Age-depent Doses to Members of the Public from Intake of Radionuclides: Part 5 Complication of ingestion and inhalation does coefficients, ICRP Publication 72, (1996).
10) MacIntosh DL, Xue J, Ozkaynak H, Spengler JD, Ryan PB, "A Population based exposure model for benzene," JEAEE, 5(3), p375-403, (1995).
11) NCRP, A Guide for Uncertainty analysis in Dose and Risk Assessments Related to Environmental Contamination, NCRP commentary No. 14, (1996).
12) D.J. Moschandreas, S. Karuchit, "Scenario-model-parameter: a new method of cumulative risk uncertainty analysis," Environment International 28, p247-261, (2002).

Table 2 The summary of 2D MCA for the committed effective doses of infant and adult [mSv y^{-1}]

Age group	percentile	2D MCA						Deterministic
		Min	5%	Mean	Median	95%	Max.	Mean
Infant	5th	8.86E-01	1.01E+00	1.13E+00	1.13E+00	1.27E+00	1.54E+00	1.23E+00
	50th	9.74E-01	1.11E+00	1.23E+00	1.23E+00	1.37E+00	1.65E+00	
	95th	1.03E+00	1.16E+00	1.29E+00	1.28E+00	1.43E+00	1.83E+00	
Adult	5th	1.72E-01	1.87E-01	2.10E-01	2.09E-01	2.37E-01	2.75E-01	2.32E-01
	50th	1.82E-01	2.00E-01	2.24E-01	2.22E-01	2.50E-01	3.45E-01	
	95th	2.02E-01	2.24E-01	2.47E-01	2.46E-01	2.74E-01	3.91E-01	

Journal of NUCLEAR SCIENCE and TECHNOLOGY, Supplement 5, p. 698–701 (June 2008)

Investigation of Gasification Rate for Several Radionuclides Dissolved in HANARO Pool Water

Myong-Seop KIM*, Young-Chil KIM, Ji-Uk KIM and Sang-Jun PARK

Korea Atomic Energy Research Institute
1045 Daedeokdaero(150 Dukjin-Dong), Yuseong, Daejeon, 305-353, Korea

The gasification rates of several radionuclides dissolved in HANARO pool water were investigated in order to produce the basic data related to the potential release of radioactivity from the reactor pool water to the atmospheric environment. The primary coolant water was collected during 30 MW operation of HANARO. The variation of activity concentrations of several radionuclides in the water with the cooling time were continually measured using the HPGe detection system. The nuclides of interest were Ar-41, Xe-133 and iodine nuclides. The effective half-life of Ar-41 in the water sample was measured to be 0.65±0.02 hours, and its elimination half-life due to the gasification and surface exchange coefficient were determined to be 1.01 hours and 6.89×10^{-4} cm s^{-1}, respectively. For Xe-133, the elimination half-life due to the gasification and surface exchange coefficient were determined to be 1.44 days and 2.27×10^{-5} cm s^{-1}, respectively. For iodine nuclides, the measured effective half-lives were similar to their radioactive half-lives. Therefore, it is confirmed that the gasification of the iodine nuclide from the pool water is negligible unless the evaporation of water occurs. Above data for the gasification of several nuclides will be very useful for the assessment of the research reactor safety.

KEYWORDS: gasification rate, HANARO pool water, Ar-41, Xe-133, iodine nuclide, surface exchange coefficient, assessment of research reactor safety

I. Introduction

The coolant water of HANARO, a 30 MW research reactor, contains various radionuclides due to several origins such as the fission of the contaminated uranium on the fuel surface and the activation of the reactor structure material or air. Among them, the radionuclide with a short half-life decays out when passing through the hot water layer formed to delay the convection flow of the reactor pool water near the pool surface. However, the nuclide with a relatively long half-life can reach the surface of the reactor pool. The volatile radionuclides such as radioactive noble gases and iodine can be gasified from the water surface of the reactor pool, and released to the environment through the ventilation system of the reactor building since HANARO is an open pool type reactor. These nuclides are released through the reactor pool surface in a gaseous or aerosol form.[1] Therefore, the gasification rates of these radionuclides are very important for assessing the radiological effect of the research reactor with open pool.

In this paper, the gasification rates of several radionuclides dissolved in HANARO pool water were measured using the typical HPGe gamma-ray spectroscopy system. And, the surface exchange coefficient of each nuclide, which is an important parameter to determine the material diffusion through a surface, was deduced in order to produce the basic data related to the safe operation of HANARO.

* Corresponding Author, Tel No: +82-42-868-8666, Fax No: +82-42-868-8341, E-Mail; mskim@kaeri.re.kr

II. Experimental Method

The primary coolant water was collected during 30 MW operation of HANARO. The coolant was taken from the primary coolant purification system, and the volume of collected water sample was 80 cm^3 for the Ar-41 measurement, and 160 cm^3 for the long-lived nuclide measurement. By using the gamma-ray spectroscopy, the species and concentrations of the radionuclides in the primary coolant water were analyzed. The calibration of the full-energy peak efficiency as a function of the photon energy for the HPGe detector was performed using the volume standard source and proper fitting function. The activity concentrations of Na-24, Mg-27 and Al-28 were much higher than those of other nuclides. Their origins were radiative reactions of aluminium used as the structure materials and cladding of the nuclear fuel. The small amount of fission fragment such as I-132 and Xe-138 was also detected in the coolant water. The source of the fission fragments found in the normal operation of the reactor is the surface contamination of the nuclear fuel by uranium in the fabrication process.[2]

After confirming the radionuclides in the coolant water, the variation of the activity concentrations of several radionuclides in the coolant water with the cooling time were continually measured using the HPGe gamma-ray detection system. The nuclides of interest were Ar-41, Xe-133 and iodine nuclides. The reproducibility of the measuring condition was confirmed using the measurement of the half-life for a non-volatile nuclide like Na-24. The activity concentrations of above nuclides, measured in the HANARO

coolant water during 30 MW normal operation, are represented in **Table 1**.

Table 1 The activity concentrations of several nuclides measured in the HANARO coolant water during 30 MW operation

Nuclide	Activity Concentration in the Coolant Water of HANARO (Bq liter^{-1})
Ar-41	3.22×10^{5}
Xe-133	5.27×10^{3}
I-131	4.90×10^{2}
I-133	2.46×10^{3}
Na-24	1.65×10^{6}

At first, the relative activity of Ar-41 as a function of the cooling time was measured after evacuating the gas gathered over the water surface into a sample bottle using ventilating fume hood for a suitable time interval. And then, xenon and iodine activities were measured with the cooling time in the same manner as the argon case. The experimental conditions are shown in **Table 2**.

Table 2 The experimental conditions for measuring the activity concentrations of the radionuclides in the reactor coolant water as a function of the cooling time

	Objective of measurement	
	Ar-41	Xe and I
Diameter of bottle (cm)	4.5	6.0
Area of water surface (cm^2)	15.9	28.3
Surface-to-volume ratio (cm^{-1})	0.199	0.177
Counting time (sec)	300	2200,3600,7200

The counting time of the HPGe detection system was varied for the Xe and I measurements due to counting statistics. The distance from the bottom of the sample bottle to the surface of the aluminum cover of the detector crystal was 5.0 cm. The ambient temperature was maintained at 23~24 ºC. The effect of the temperature variation on the measurements can be neglected.[3)]

The detector used in this work is a closed-ended coaxial HPGe detector with a detection efficiency of 15% of the 3″×3″ NaI(Tl) detector. The shaping time of the amplifier was set at 6 μsec. The dead time of the detection system was less than 5%. In the analysis for the gamma-ray peak area, a straight-line shaped background was assumed and subtracted.

III. Surface Exchange Coefficient

Since the flux of particles at a surface is described by the surface exchange coefficient, the release of radionuclide from the pool water surface into the reactor hall atmosphere is dependent on this coefficient and the concentration of the nuclide in the water. Since the elimination rate of a volatile material due to the gasification is constant for the case with constant surface exchange coefficient, we can introduce an elimination half-life due to the gasification, and it is described by the radioactive half-life T_R and effective half-life T_E by

$$T_G = \frac{T_R \times T_E}{T_R - T_E}. \quad (1)$$

Then, the surface exchange coefficient is given by

$$k = \frac{1}{2 \times T_G \times \frac{a}{V}}, \quad (2)$$

where, (a/V) is the surface-to-volume ratio.[4,5)]

IV. Results and Discussions

1. Ar-41

Ar-41 is not a fission product but an activation product of a dissolved argon in the reactor pool water. However, it is the biggest source of the gaseous radionuclide released from the research reactor operated in a normal state. **Fig. 1** shows the variation of the measured count rate of 1294 keV gamma-rays from Ar-41 in the coolant water as a function of the cooling time.

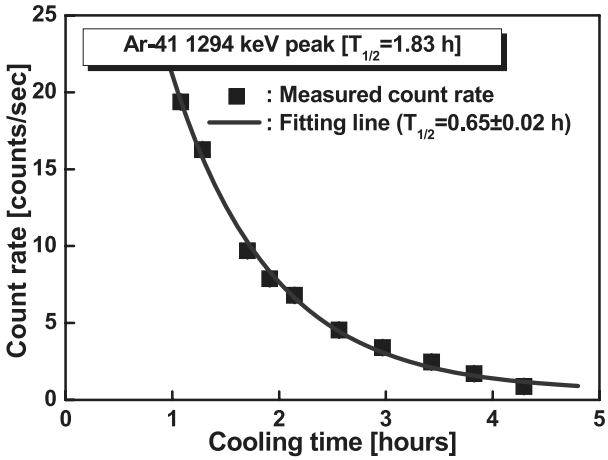

Fig. 1 Variation of the measured count rate of 1294 keV gamma-rays from Ar-41 in the coolant water sample as a function of the cooling time

Measured data show a decreasing trend according to the exponential function, and from the semi-log plot, the linearity between the count rate and the cooling time was confirmed. The solid line in the figure is the fitting line of the measurements with the exponential decay function. In the fitting procedure, the counting uncertainty was utilized as a weighting factor. From the measurements, the effective half-life of the Ar-41 in the water sample was measured to be 0.65±0.02 hours. And then, the gasification half-life and surface exchange coefficient for Ar-41 can be deduced to be 1.01 hours and 6.89×10^{-4} cm s^{-1}, respectively.

2. Xe-133

Xe-133 is an important gaseous radionuclide in assessment of a failure or defect of a research reactor fuel. Since it is a noble gas with a relatively long half-life (5.29 days), it can reach the pool water surface without substantial

reductions. It can be directly generated from the fission process and also by the decay of parent fission products. The half-life of the I-133, its parent nuclide, is 20.9 hours and the cumulative fission yield is quite big.6) Therefore, if the reduction of I-133 from the water surface is neglected, the specific activity of Xe-133 at a time after collecting the coolant water is given by

$$A_{Xe}(t) = \frac{\lambda_{Xe}}{\lambda_{Xe} - \lambda_I}(e^{-\lambda_I t} - e^{-\lambda_{Xe} t})A_I^0 + A_{Xe}^0 e^{-\lambda_{Xe} t}, \quad (3)$$

where, λ_{Xe} and λ_I are the radioactive decay constants of Xe-133 and I-133, and A_{Xe}^0 and A_I^0 are the initial activities of Xe-133 and I-133 at t=0. We calculated the relative Xe-133 specific activity in the coolant water including the effect of I-133 decay. From the calculation result, it was confirmed that the radioactive decay half-life of Xe-133 was prolonged to be 5.77 days. We used this value to deduce the elimination half-life due to the gasification.

Fig. 2 shows the variation of the measured count rate of 81 keV gamma-rays from Xe-133 in the coolant water as a function of the cooling time. From the measurements, effective half-life of the Xe-133 in the coolant water sample was measured to be 1.15±0.04 days. And then, the gasification half-life and surface exchange coefficient for Xe-133 can be deduced to be 1.44 days and 2.27×10^{-5} cm s^{-1}, respectively.

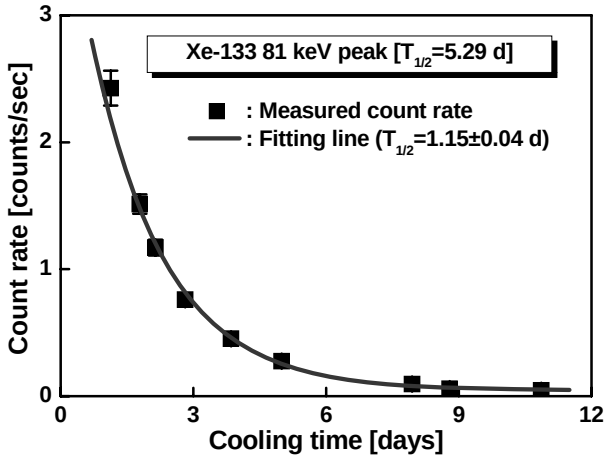

Fig. 2 Variation of the measured count rate of 81 keV gamma-rays from Xe-133 in the coolant water sample as a function of the cooling time

3. Iodine nuclides

In the normal operation of HANARO, several iodine radionuclides, generated in the fission process, are observed. A significant environmental concern associated with the risk of radioactive iodine from the accident of the power reactor is I-129 because of its very long half-life. However, in consideration of the radiological effect for the HANARO, I-131 and I-133 are the two main radioactive iodine nuclides. Although a larger amount of I-132 can be measured than I-131 and I-133 in the coolant water, it decays out through the hot water layer due to its short half-life.

Fig. 3 shows the measured count rates of the gamma-ray peaks from I-131 and I-133. From these measurements, effective half-lives of the I-131 and I-133 in the coolant water were measured to be 8.31±2.23 and 0.94±0.18 days, respectively. The uncertainties in the measurements are much bigger than those in the other nuclide measurements because of poor counting statistics. Nevertheless, for the I-131 and I-133, it can be concluded that the measured effective half-lives are similar to their radioactive half-lives.

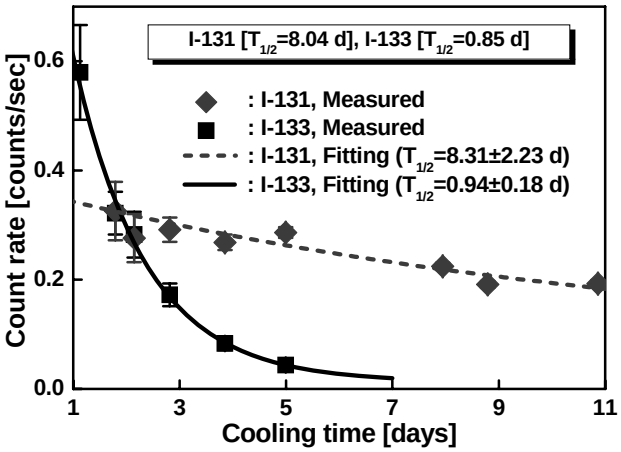

Fig. 3 Variation of the measured count rates of gamma-ray peaks from two iodine nuclides as a function of the cooling time

Since, in most aqueous environments, iodine is present in the –1 valence state as the iodine ion, I^{-1}, it can be assumed that the primary form of the iodine released from the reactor is aerosol particles, not gaseous elemental iodine.[7] Therefore, it is confirmed that the gasification of the iodine nuclide from the pool water of HANARO is negligible unless the evaporation of water occurs.

Fig. 4 shows the variation of the count rates of 1369 keV gamma-ray peak from Na-24 measured in the coolant water simultaneously with the xenon and iodine measurements.

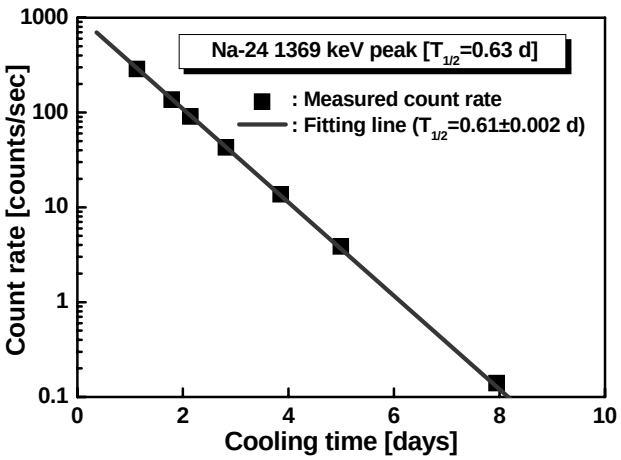

Fig. 4 Variation of the measured count rates of 1369 keV gamma-ray peak from Na-24 in the coolant water

Na-24 is the biggest radiation source of the coolant water of the research reactor. The measured count rate of the Na-24 is much bigger than those of the fission fragments. The figure is represented in a semi-log plot, and it shows a good linearity between the cooling time and the measured count rate. The measured effective half-life is very similar to its radioactive half-life. Since the Na-24 is non-volatile nuclide, the reproducibility of the measuring condition for the above effective half-lives of several nuclides is confirmed by using the measurement of the half-life for Na-24.

V. Conclusions

The gasification rates of radioactive argon, xenon and iodine nuclides in HANARO pool water were investigated. The elimination half-lives due to the gasification and surface exchange coefficients were determined for Ar-41 and Xe-133 nuclides. It is confirmed that the gasification of the iodine nuclide from the pool water of HANARO is negligible unless the evaporation of water occurs. The obtained data for the gasification of several nuclides which are important in the coolant of the research reactor will be very useful for the assessment of the research reactor safety.

References

1) A. T. Wassel, A. F. Mills, D. C. Bugby and R. N. Oehlberg, "Analysis of radionuclide retention in water pools," Nucl. Eng. Des., 90, 87-104 (1985).
2) M. S. Kim, B. C. Lee, S, J. Park and B. J. Jun, "Sensitivity of fuel failure detection by the delayed neutron measurement in the primary cooling circuit of HANARO," Ann. Nucl. Energ., 33, 1134-1140 (2006).
3) H. L. Clever, Solubility Data Series Volume 2 Krypton, Xenon and Radon - Gas Solubilities, Pergamon Press, Oxford, 134 (1979).
4) M. Imamura and K. Une, "High temperature steam oxidation of UO_2 fuel pellets," J. Nucl. Mater., 247, 131-137 (1997).
5) M. Schulz, H. Fritze, H. L. Tuller and H. Seh, "Diffusion-related implications for langasite resonator operation," IEEE Trans. on Ultrasonics, Ferroelectrics, and Frequency Control, 51[11], 1381 (2004).
6) T. R. England and B. F. Rider, Fission Product Yields per 100 Fissions for ^{235}U Thermal Neutron Induced Fission Decay, LA-UR-94-3106, ENDF-349 (1993).
7) W. Um, R. J. Serne and K. M. Krupka, "Linearity and reversibility of iodide adsorption on sediments from Hanford, Washington under water saturated conditions," Water Res., 38, 2009-2016 (2004).

Journal of NUCLEAR SCIENCE and TECHNOLOGY, Supplement 5, p. 702–705 (June 2008)

Comparative Analysis of a Fission Product Behavior during Severe Accidents for a Typical PLWR and PHWR

Soo Yong PARK* and Yong Mann SONG

Korea Atomic Energy Research Institute, Daejeon, Korea

The fission product behaviors of a severe accident sequence were analyzed for the typical pressurized light water reactor (PLWR) and heavy water reactor (PHWR) operated in Korea. The OPR-1000 and the Wolsong-2 plant were selected as reference plants. The obtained results are for:(1) the fission product release from the core, (2) the fission product distributions in a reactor coolant system, a molten corium, a reactor vessel, or a containment building, (3) the fission product release from the containment. The thermal hydraulic, severe accident phenomenological, and radiological analyses for their evaluation have been performed by using the MAAP(Modular Accident Analysis Program) and ISAAC (Integrated Severe Accident Analysis Code for CANDU Plant) computer program. Based on the ISAAC and MAAP calculation, the results show that the accident progression, including the fission product transportation, of the CANDU-6 type reactor is much more delayed than the typical PLWR, however, the possibility of a fission product release to the environment can be earlier due to the lower reactor building design pressure.

KEYWORDS: fission product behavior, severe accident, MAAP code, ISAAC code

I. Introduction

Severe accident source term analysis is a very important research area for an accident management and an emergency planning. Especially, a fission product behavior, i.e. (1) a release from the core, (2) a distribution between a reactor coolant system and containment, or (3) release into an environment, during a severe accident should be obtained to develop accident management strategies. On the other hand, the fission product behavior of a heavy water reactor (PHWR) is very different from a pressurized light water reactor (PLWR). Accordingly, a comparative analysis of the severe accident scenarios has been performed during a developing process of the CANDU-6 accident management strategies. The purpose of the analysis was to investigate the comparative characteristics of a severe accident progression and a fission product release or distribution between the CANDU-6 plant and the typical 1000 MW(electric) PLWR.

II. Methodology

The OPR-1000(Optimized Power Reactor) and the Wolsong-2 plant were selected as reference plants of a typical PLWR and PHWR, respectively.

A small loss of coolant is simulated as an initiating event of the OPR-1000 severe accident sequence. The break size considered is about a two inches diameter in the cold leg. All the emergency core cooling (ECC) systems, auxiliary feedwater system, and the containment spray are assumed to be inoperable to simulate the severe core damage scenario.

A small out-of-core break in the piping of the primary heat transport system (PHTS) is selected as an accident sequence of the Wolsong-2 plant. The scenario is a small loss of coolant accident without any recovery action by an operator. The break size considered is a 2.5% reactor inlet header with a discharge rate of about 460 kg/s. All the emergency core cooling systems, the moderator cooling system, the end-shield cooling system, and the dousing spray/local air cooler are assumed to be inoperable to simulate the severe core damage case

The thermal hydraulic, severe accident phenomenological, or radiological analyses for the evaluation have been performed by using the MAAP[1)](Modular Accident Analysis Program) 4.06 for the OPR-1000 and the ISSAC[2)](Integrated Severe Accident Analysis Code for the CANDU Plants) 2.02 for the Wolsong-2 plant. The ISAAC program has been developed based on MAAP. Therefore, most of basic thermal hydraulic or radiological models of those two computer codes are similar. Only the plant specific system models are different from each other.

There are several models available for fission product release from fuel in the MAAP and ISAAC code. The steam oxidation model of Cubicciotti[3)] has been selected to calculate the release rate of the volatile fission products from the fuel. For non-volatile fission products, Kelly's correlations[4)] have been used to calculate the release rate. No fission products are released until the cladding fails.

In this paper, the important design parameters of the two plants are compared, and then the characteristics of a severe accident progression are analyzed, and the fission product behaviors are evaluated afterwards.

III. Thermal Hydraulic and Severe Accident Phenomenological Analysis

1. Comparison of Design Parameter between Wolsong-2 and OPR-1000

The design parameters of the Wolsong-2 and OPR-1000 are summarized in the **Table 1**. The core thermal out of the

* Corresponding Author, Tel. No: +82-42-868-8298, Fax No:. +82-42-868-8256, E-Mail; sypark@kaeri.re.kr

OPR-1000 is 2,815MWt. The coolant inventory of RCS, SG, and safety injection tank (passive ECCS) are $2.30x10^5$ kg, $1.34x10^5$ kg, and $2.08x10^5$ kg, respectively. And the reactor cavity condition is always dry during normal operation. Therefore, the in-vessel retention through a external vessel cooling might be not feasible without active ECCS systems (i.e. high pressure or low pressure safety injection system). Some of the major different design features of the Wolsong-2 plant from the other light water reactors, in terms of a severe accident, are that the plant adopts a duel primary heat transport system and has an additional amount of cooling water in the calandria vessel and the calandria vault. Another feature is that the calandria vessel is always submerged in the water because the calandria vault is flooded during a normal operation. Furthermore, the molten corium in the bottom of the calandria vessel has a lower volumetric decay heat power because of the natural uranium, and it has a very large heat transfer area to the outside water of the calandria vault through the vessel wall. The maximum decay heat power density and the heat transfer area of the relocated corium at the calandria bottom for a typical LOCA scenario in the Wolsong-2 is about 0.62 MW/m^3 and 38.8 m^2, whereas it is about 1.63 MW/m^3 and 24.8 m^2 in the OPR-1000 (**Table 1**). Meanwhile the reactor building failure pressure of the Wolsong-2 plant is 0.417 MPa(g) which is considerably lower than that of the OPR-1000(1.175 MPa(g)).

Table 1 Design Parameters of the Wolsong-2 Plant and the OPR-1000

Design Parameter		Wolsong-2	OPR-1000
Plant Type		PHWR	PLWR
Power (MW_{th})		2,140	2,815
Coolant Inventory (10^3 kg)	Steam Generators	151	134
	PHTS (RCS)	120	230
	ECC Tanks (SIT)	214	208
	Calandria	216	N/A
	Calandria Vault	500	N/A
Core Material (10^3 kg)	UO_2	99 (Natural)	86 (Enriched)
	Zircaloy	43	20
Corium Material in Lower Head Vessel (*)	Decay Heat Power Density (MW/m^3)	0.62	1.63
	Vessel Wall Area Covered by Corium (m^2)	38.8 (**)	24.8
Containment Failure Pressure ($10^6Pa_{(g)}$)		0.417	1.175

(*) The values are calculated by ISAAC, MAAP and hand calculation for the maximum amount of corium in the lower head vessel during a typical LOCA scenario.

(**) The value includes calandria tube sheet area through which the decay heat transfer to the end-shielding.

2. Comparative Severe Accident Progression Analysis

The selected scenarios are a typical small loss of coolant sequence without any recovery action, where the ISAAC and the MAAP computer programs have been used in the calculations for Wolsong-2 and OPR-1000, respectively. All the emergency core cooling systems and the feedwater systems of the two plants are unavailable. Furthermore, the make-up cooling water is assumed as not being supplied to the moderator and the calandria vault in the case for the Wolsong-2 plant.

Following the loss of coolant accident with a 2.5% reactor inlet header break (Wolsong-2), or with two inch cold break (OPR-1000) the core is uncovered after steam generators have dried out. Since there is no recovery action after accident initiation, the fuel channel rupture (3.2 – 3.5 hours), the corium relocation (3.6 hours), the water dryout in the calandria (7.9 hours), the reactor building (R/B) failure (22.3 hours) and the calandria vessel failure (35.8 hours) are occur in the case of Wolsong-2 plant. There is an assumption that the molten corium on the calandria bottom would be coolable in the Wolsong-2 plant because the in-vessel corium retention, so-called, by an external calandria vessel might be very feasible.[5] In the likely manner, the core melt start (1.3 hours), the corium relocation (2.0 hours), the water dryout in the reactor vessel (RV) (2.2 hours), and the reactor vessel failure (3.1 hours) are occur in the OPR-1000. A containment has not failed until the calculation time of 72 hours in the OPR-1000.

The calculation results are summarized in **Table 2**. The results show that the initiation times for the corium relocation, the calandria water depletion and the calandria failure for the Wolsong-2 plant are considerably more delayed than those for the OPR-1000. These result from the design differences between the two plants. The delayed accident progression of the Wolsong-2 plant is due to the additional cooling water in the calandria and the calandria vault, and the lower volumetric decay heat power of the molten corium on the calandria vessel bottom. In the case of the loss of coolant accident, the steam generator inventory of an intact loop can serve as a heat sink in the Wolsong-2 plant which adopts a duel primary heat transport system. Another advantage, in terms of a calandria integrity for the Wolsong-2 plant, is that the system always maintains a low pressure at the time of a calandria vessel failure since the rupture disks are opened during a moderator evaporation. In contrast, the calculation results show that the reactor building failure of the Wolsong-2 plant occurs considerably earlier than that of the OPR-1000 due to the lower failure pressure of the building. Based on these calculations, the Wolsong-2 plant has an advantage in maintaining its calandria integrity but a disadvantage for its reactor building integrity during a severe accident situation.

Table 2 Comparison of the Accident Progression of the Wolsong Plant with OPR-1000 for a S-LOCA

Event	Wolsong-2 (hours)		OPR-1000 (hours)
	LOOP 1 (Ruptured)	LOOP 2 (Intact)	
SG dryout	2.8	0.9	0.8

LRV(or PSV) open	N/A	1.8	N/A
Core uncovery start	0.5	2.3	0.8
Loop 1&2 fuel channel rupture (WS-2) or Core melt start(OPR-1000)	3.5	3.2	1.3
Corium relocation start	3.6		2.0
Calandria vessel (or RV) dryout	7.9		2.2
Calandria vessel (or RV) failure	35.8		3.1
R/B (or Containment) failure	22.3		> 72

IV. Fission Product Behavior

In this paper, an analysis is focused on the fission product (FP) release from a core, the FP distribution inside a plant, and the FP release from a containment building into an environment. The fission product behavior during an accident is strongly dependent on the thermal hydraulic or severe accident phenomenological conditions which were discussed previously. On the other hand, fission product elements are grouped into twelve fission product species in MAAP and ISAAC code. Among these fission products group, noble gas and cesium iodine group are considered as more volatile. The noble gas, which is chemically inert materials, pose a considerably lesser danger to human health. Instead, the iodine is one of the elements vital to the proper functioning of the human body. Iodine exits from damaged fuel rods predominantly as cesium iodine (CsI) rather than as molecular iodine (I_2). Therefore, the CsI is selected as representative fission products. The CsI behavior is illustrated in **Fig. 1** for the Wolsong-2 plant. The CsI release into the primary heat transport system (PHTS) was initiated as the cladding damage occurs. Since a reactor inlet header has a break hole and a liquid relief valve (LRV) at loop 2 is open after 1.8 hour (Table 2) of an accident initiation, CsI can be transported to the containment. Moreover, when a molten fuel relocation started at 3.6 hours (Table 2), the CsI is included in the molten corium. About 20%, 30% and 50% of the initial CsI mass are distributed in the corium, PHTS and containment, respectively. Even if a fuel channel fails, some of fuel rods are relocated into lower head as a particulated debris bed without oxidation because the fuel channel is structured horizontally in Wolsong-2. Therefore, 20% of CsI can be located in the corium. The CsI in the corium is released into the containment only after the molten corium-concrete interaction had started. The molten corium-concrete interaction initiated when the calandria vessel had failed at 35.8 hours (Table 2) and the water of the calandria vault had dried out. The fission product release to the environment started from a reactor building failure time (22.3 hours) and the CsI release fraction reached about 2% of the initial inventory.

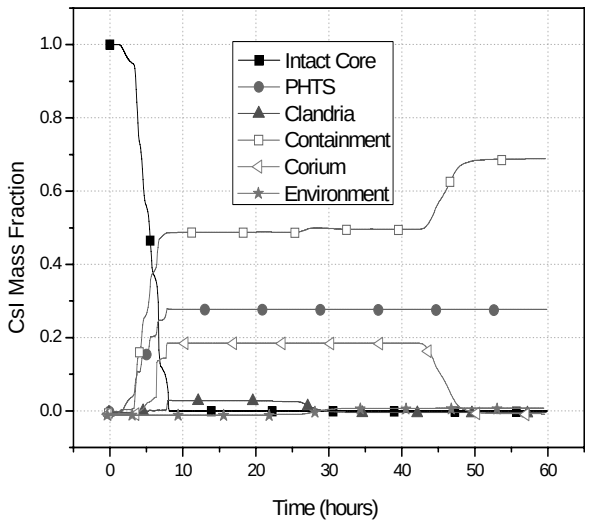

Fig. 1 Fission Product(CsI) Distribution in Wolsong-Plant for Small-LOCA Scenario

The CsI behavior as a representative fission product is illustrated in **Fig 2** for the OPR-1000. The CsI release into the reactor coolant system (RCS) was initiated when the cladding damage occurred at 1.2 hours. The fission product is transported to a containment through a ruptured hole of the cold leg. About 40% and 60% of the initial CsI inventory are distributed in the RCS and containment, respectively. During a melting process of the OPR-1000, the vertical fuel rods have an enough chance to be oxidized with high temperature. Accordingly, all the CsI were released to the RCS primarily from the core, and then moved to the containment partially. There is no fission product release to the environment for the OPR-1000, because the containment building had not failed during 72 hours of the calculation time

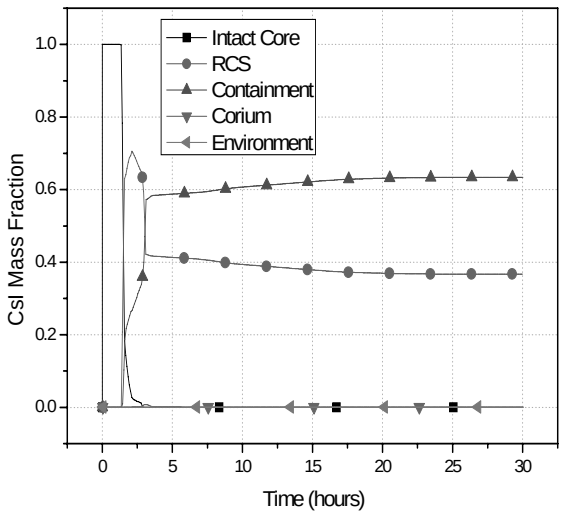

Fig. 2 Fission Product(CsI) Distribution in OPR-1000 for Small-LOCA Scenario

V. Conclusions

In this study a comparative analysis was performed for the typical CANDU-6 and Light Water Reactor operated in Korea. The study includes the major design differences that would impact on accident progressions, the thermal hydraulic and severe accident phenomenological analysis, and fission product distribution during a small loss of coolant initiated severe accident. Furthermore, the analysis includes the fission product behavior that should be considered in severe accident management strategies. Based on the ISAAC and MAAP calculation, the results show that the accident progression, including the fission product transportation, of the CANDU-6 type reactor is much more delayed than the typical PLWR, however, the possibility of a fission product release to the environment can be earlier due to the lower reactor building design pressure.

Acknowledgement

This work was performed under the long-term nuclear research and development program sponsored by Ministry of Science and Technology of Korea.

References

1) Fauske and Associate Inc, “Modular Accident Analysis Program,”.1994.
2) KAERI, ”Development of Computer Code for Level 2 PSA of CANDU Plant,” *KAERI/RR-1573/95*, 1995.
3) ”Analysis of In-Vessel Core Melt Progression,” IDCOR Report 15.1B, Industry Degraded Core Rulemaking Program, 1983.
4) J.L.Kelly,A.B.Reynolds,and M.E.McGown, ”Temperature Dependence of Fission Product Release Rates,” Nuclear Science and Engineering, 88, 184 (1984)
5) S.Y.Park et al, “An Investigation of an In-vessel Corium Retention Strategy for the Wolsong Pressurized Heavy water Reactor,” Nuclear Technology, 158, 109 (2007).

Journal of NUCLEAR SCIENCE and TECHNOLOGY, Supplement 5, p. 706–709 (June 2008)

A Study on an Accident Diagnosis Methodology Using Influence Diagrams

Kyung-Min KANG and Moosung JAE*

Department of Nuclear Engineering, Hanyang University
17 Haengdang-Dong, Sungdong-Gu, Seoul, 133-791, Korea

In nuclear power plants, operators are allowed to follow EOPs (Emergency Operating Procedures) when reactor tripped because of accidents. But, it's very difficult to diagnose accidents and find out appropriate procedures to mitigate current accidents in a given short time. Even if they diagnose accidents quickly, it also has possibility to misdiagnose. Methodology using Influence Diagrams has been developed and applied for representing the dependency behaviors and uncertain behaviors of complex systems. An example to diagnose the accidents such as SLOCA and SGTR with similar symptoms has been introduced. From the constructed model, operators could diagnose accidents at any states of accidents. Also, The integrated design of Thermal Hydraulics Online Monitoring Advisory System(THOMAS) is introduced in this paper. THOMAS, for improved Korea Standard Nuclear Power Plant, is an advisory monitoring system that uses the digital engineering technology such as virtual reality, and database. It is believed that the new design will improve the operability and maintainability and simplify design process of the monitoring and diagnosis system of the nuclear power plant. And this model can offer the information about accidents with given symptoms. This model might help operators to diagnose correctly and rapidly. It might be very useful to support operators for reducing human error.

KEYWORDS: accident diagnosis, emergency operating procedures, influence diagrams, bayesian theorem

I. Introductio[n]

For nuclear power plants, EOPs help operators to diagnose, control and mitigate accidents. But, it is very difficult that operators follow appropriate EOPs for accidents with similar symptoms in a given short time. Also EOPs are very complicated to follow and have many procedures to do. Therefore, if operators couldn't diagnose correctly, the accident would become severe. In process of diagnostic action, it depends on decisions of operators. So, the methodology that can diagnose accidents quickly and help operators to follow appropriate procedures should be developed. And it is very important to reduce human errors during diagnostic actions. In this study, the accident diagnosis model has been constructed and this is based on EOPs, accident symptoms and component reliabilities to minimize human errors. For construction of model, Influence Diagrams have been applied. This decision-making tool is consisted of nodes and arcs. It is applicable to complicated situations, such as those required for developing strategies for managing severe accidents in nuclear power plants. And quantification of model has performed with total probability and Bayesian theorem. Through this quantification, the results might help operators to diagnose confusing accidents. In this paper the methodology is demonstrated with application to a USN3&4.

II. Modeling Methods

1. Emergency Operating Procedures

EOPs give operators procedures to mitigate accidents occurred with reactor trip. The emergency states are classified according to the emergency operating states and consequences of accidents. And if reactor trip occurred automatically or manually, the states are concerned as sufficiently severe states. Emergency states are classified into 2 types as follow. First, it is the state that operators could analyze accidents with components, related symptoms, knowledge and current operating history. In this case, it is possible to follow optimal recovery procedures. Second is that operators couldn't diagnose accidents or misdiagnose. EOPs compose of 4 types of procedures: SPTA (Standard Post Trip Actions), Diagnostic Actions, Optimal recovery procedure and Functional recovery procedure. SPTA offered operators the procedures that should be performed in the first place. Diagnostic actions are logical processes for offering operators exact diagnosis for given accidents[2)]. This part has been modeled using Influence Diagrams by collecting relevant parameters and evaluating them. Optimal recovery procedures involve procedures of each accident such as LOCA, SGTR, etc. In other abnormal states that are unable to diagnose and other accidents except accidents mentioned on optimal recovery procedure, functional recovery procedures are taken and performed.

2. Influence Diagrams

Influence Diagrams are networks consisting of nodes and two of directed arcs (conditional and informational) that represent the conditional dependence between the random quantities and the timing of information and decision. Nodes

*Corresponding Author, Tel No: +81-2-2290-1346, Fax No: +81-2-2293-7014, E-mail: jae@hanyang.ac.kr

are of four types: decision, chance, deterministic, and value nodes. According to convention, decision nodes (representing decision points) have a square or rectangular shape; chance nodes (representing uncertain quantities) are circular; deterministic nodes (representing functions of the values of predecessor nodes) have a double circle shape. The shape of the value node is not standardized; it may be a diamond shape or a rectangle with rounded corners, depending on the analyst[3]. In general, once constructed, Influence Diagrams can be quantified and solved in order to evaluate decision strategies. Solving the Influence Diagrams means to compute the expected values associated with the attributes of the value node, given the possible decisions. Computation of probabilities in the Influence Diagrams is straightforward, although it is sometimes inefficient. Inefficiency of computation results from evidence variables, which represents one of two kinds of chance variables (parameter variables being the other). A parameter variable in any model corresponds to a random variable denoted by a chance node, while an evidence variable (which may be represented by a shaded node for convenience) is relevant to observed or experimental evidence. This evidence introduces minor complications in the evaluation. The basic operations for evaluating Influence Diagrams containing these two kinds of chance variables have been applied and are summarized as follows:[4-7] Quantification of Influence Diagrams is performed with total probability theorem and Bayesian Theorem.

3. THOMAS

Digital-based thermal hydraulics online monitoring advisory system of nuclear power plant, as called THOMAS, which is can be developed economically compared with existing monitoring system is used for the decision making tool in the accident condition. We selected the Ulchin 3&4 units which is the type of Korea Standard Nuclear Power Plant(KSNP) as reference plant. THOMAS has a characteristics as compared with existing monitoring systems. It is three - dimensional visualization to support operator using Virtual Reality(VR) technology. VR describes an environment that is simulated by a computer. In the VR space, using mapping, component color is changed with linked value of safety variable. Therefore operator can easily recognize the plant condition. This is related with human factor engineering. The final goal of this system is, in the accident situation, to present the success path to the operator for the recovery of system. The table 01 are summarized the comparison of design concept between THOMAS and existing digital monitoring systems. At present developing level, database is supply the signal to THOMAS. In the other words, the various nuclear system analysis codes are provide the safety value to the database, and after the values are inputted to THOMAS from database with the network.

III. Data Analysis

In this study, Ulchin Unit 3&4 has been chosen as a reference plant. And the purpose of the modeling is to discriminate between SLOCA and SGTR. The reason of this selection is that these accidents have very similar symptoms at an early stage. The chance node and deterministic node have introduced for construction of accident diagnosis model. And nodes for modeling Influence Diagrams have selected from Diagnostic Actions and procedures of each accident (SLOCA and SGTR). In this selection of nodes, parameters of SPTA have been ignored. Because entry condition of Diagnostic Actions has already contained SPTA which is performed. Thus, the focus of this study is on discrimination between SLOCA and SGTR. The model has been constructed with one accident diagnosis node, 13 symptom nodes and 13 detection nodes. The accident diagnosis node has 3 states: ①Normal Operation, ②SLOCA and ③SGTR. Symptom nodes have 3 states: ①No Change, ②Increase and ③Decrease. And Detection nodes have 4 states: ①Normal, ②Fail High, ③Stuck at Steady State and ④Fail Low.

Arcs are connected from accident diagnosis node and detection nodes to symptom nodes. Because symptoms are related with the type of accidents and the status of detection components. Also, the dependency between nodes has been considered in this model. For example, if containment moisture increases, it could cause RDT level to increase. Data of accident diagnosis node are based on PSA report of reference plant, and yields of selected accidents in terms of frequencies have been applied as probabilities. In constructed model, it can be possible that the changes of these yields represent increase or decrease of the probabilities. Also, assumed that only 2 types of accident exist in this model and others are included in Normal Operation for simplification. EOPs are mainly applied to obtain symptom node data. In EOPs, each accident has their symptoms. From these symptoms and EOPs, data have been chosen. Also, probabilities of symptom nodes are know, because it is clearly shown that the types of accidents have significant symptoms. And it is possible that symptom node data has only two probability of 1.0 or 0.0 in relevant accidents. RDT pressure increases at SLOCA when detector is operating normally. At SGTR, it has no change. And at other states of detector, data are fixed; state of “Fail High” always has value of 1.0 at “Increase” state. “Stuck at Steady State” has 1.0 at “No Change” state, and “Fail Low” has 1.0 at “Decrease” state. These are identically applied to all nodes. Data of RDT pressure node are listed in Table 6 as an example. Dependencies of nodes have been concerned. For example, in case of SGTR, RDT level has practically no change. But, if containment moisture increases, it influences RDT level, because all drained water is collected in RDT. Thus, even if accident is SGTR, the probability of RDT level increase is 1.0. The total probability and Bayesian theory is used for the quantity calculation of the influence diagram. Firstly, measurement node is absorbed into the symptom node by calculating total probability theory using given data of sensor. And then, Bayesian theory is used to reverse the direction of arc such as **Fig. 1**. Lastly, total probability theory is used once more to determine the accident which coincides with given symptom.

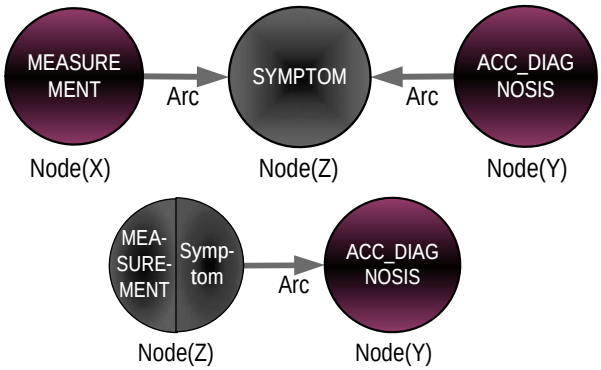

Fig. 1 Probability and Bayesian Theory

At present, user can only select 3 types of symptom which are increase, decrease, changeless state about given safety parameters. However, it is difficult to apply this method for real nuclear power plant because each symptom of accident is able to very rapidly change during short time. For example, during SGTR, the steam generator pressure is perturbed. Therefore it is important to choose the base line for type of symptom. In this research, it is selected by result of nuclear thermal hydraulics system codes such as RELAP and RETRAN. And the advices of experts are also one of method for choosing the base line.

We show the procedure to perform the reference calculations of Steam Generator Tube Rupture (SGTR) with SG tube ruptured for validation. In addition, the thermal-hydraulic response of the reactor coolant system (RCS) was studied in detail. For the thermal-hydraulic output graph and input model delivered from USN train center was used. Then the trends of SGTR parameters are shown below.(**Fig.2**)

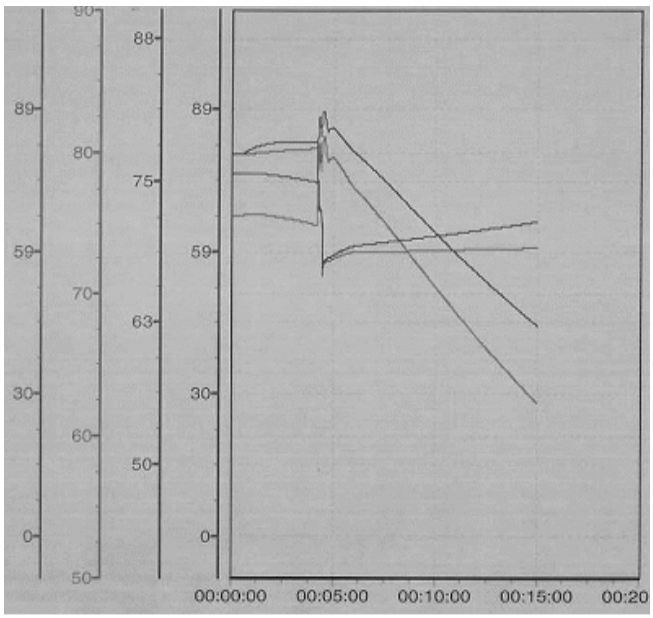

Fig. 2 The trends of SGTR parameters

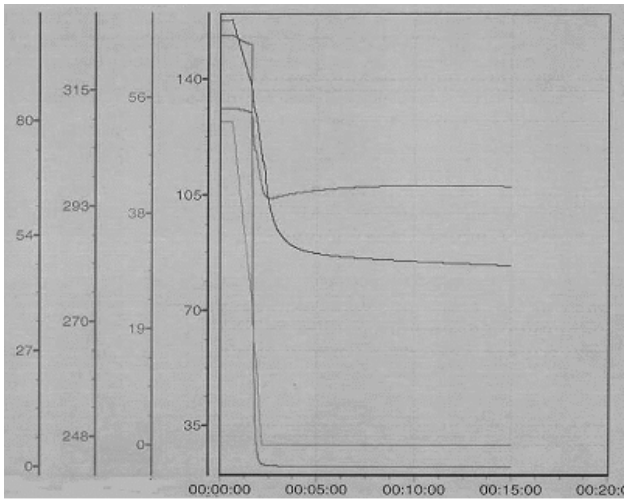

Fig. 3 The trends of SLOCA parameters

And, we show the procedure to perform the reference calculations of SLOCA for validation. For the thermal-hydraulic trend graph delivered from USN train center was used. Then the trends of SLOCA parameters are shown in **Fig 3**.

IV. Results

Bayesian Theorem has been mainly used for quantification of this model. Also, in this study, some evidences have been applied for quantification. That is, if symptoms are given, the changes of probabilities caused by symptoms could be calculated by quantification of this model. Before application of given evidence, the probability of each accidents are: “Normal Operation”: 94%, “SLOCA”: 2.4% and “SGTR”: 3.6% (**Fig.4**). As an example, some of symptoms have been applied. Then the results are shown below. In this case 1, situation which has pressurizer level and pressure decrease, and containment radiation increase has been applied and quantified by this model. After application, these values have been changed as shown in **Fig. 5.** For this case, operators could diagnose this accident occurred currently as SLOCA.

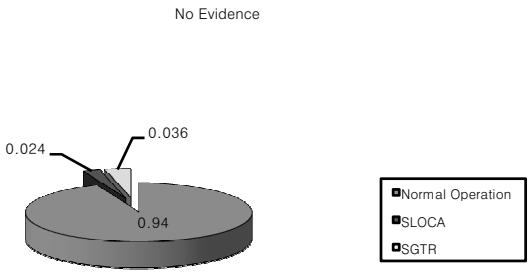

Fig. 4 Probabilities of No Evidence

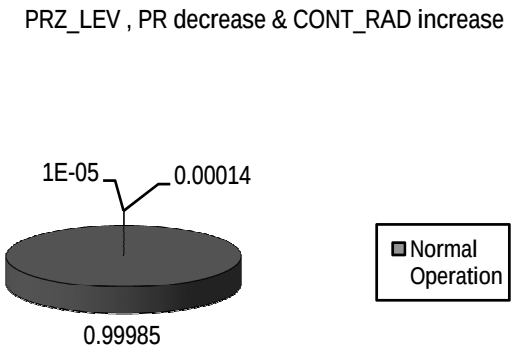

Fig. 5 Probabilities of Case I

In this case 2, situation which has pressurizer level and pressure decrease, and steam generator radiation increase has been applied and quantified by this model. After application, accident diagnosis node values have been changed as shown in **Fig. 6** and operators could diagnose this accident occurred currently as SGTR. For quantification, some of representative symptoms are applied above. Also, it is verified that evidences are given more, the result is clearer. As results, this model could help operators to diagnose accidents that have similar symptoms. Some accidents such as SLOCA and SGTR applied in this study have similar symptoms and it is very important to diagnose them correctly. This methodology using Influence Diagrams could be quantified with any combinations of symptoms.

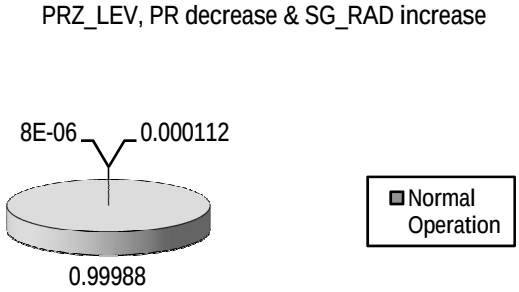

Fig. 6 Probabilities of Case II

V. Conclusions

Operators are allowed to follow EOPs when reactor tripped because of accidents. But, it is very difficult to diagnose accidents and find out appropriate procedures to mitigate current accidents in a given short time. Even if they diagnose accidents, it also has possibility to misdiagnose. TMI accident is a good example of operators errors. Thus, the methodology to support operators to diagnose correctly and rapidly should be developed. In this study, accident diagnosis methodology has been developed. This model based on EOPs, symptoms of accidents and components reliabilities to reduce human error. To construct and quantify the model, Influence Diagrams have been introduced. Influence Diagrams are powerful tool for decision-making. This tool is also easy to modify and quantify the model. From the constructed model, operators could diagnose accidents at any states of accidents. This model can offer the information about accidents with given symptoms. This model might help operators to diagnose correctly and rapidly. It might be very useful to support operators for reduce human error. Also, from this study, it is applicable to other accidents with similar symptoms and to analyze causes of reactor trip.

Acknowledgement

This research was supported by iTRS (Innovative Technology Center for Radiation Safety), and Hanyang University

References

1) Korea Electric Power Corporation, "Ulchin Unit 3&4 Emergency Procedure Guideline" (1995).
2) R. M. Oliver, J. Q. Smith, Influence Diagrams, Belief Nets and Decision Analysis, John Wile and Sons (1990).
3) M. Jae, G. E. Apostolakis, "The Use of Influence Diagrams for Evaluating Severe Accident Management Strategies," Nuclear Technology, 99[2], 142-157 (1992).
4) US. Electric Power Research Institute, ALWR URD.
5) A. Manrique, J. Carlos Valdivia, A.Jimenez, "Human Factor Engineering Applied to Nuclear Power Plant Design," 2003 International Congress on Advances in Nuclear Power Plants, Cordoba, Spain, 2003.

Journal of NUCLEAR SCIENCE and TECHNOLOGY, Supplement 5, p. 710–713 (June 2008)

The Robust Bayesian Analysis Due to a Variation of Effective Height in the Atmospheric Dispersion

Joo Yeon KIM*, Han Ki JANG, and Jai Ki LEE
Hanyang University, 17, Haengdang-dong, Seongdong-ku, Seoul, Korea

The robust Bayesian analysis was suggested to estimate the sector-averaged concentrations expected through the atmospheric dispersion of the airborne nuclides. The sector-averaged concentrations due to variation of effective height under F-stability were calculated by applying the plausible and contaminated priors according to the CSA model for Ulchin nuclear power units 3 and 4 of Korea. The median of the sector-averaged concentrations considerably agreed with the deterministic concentrations and was then suitable as the representative quantile of their distributions. Additionally, the medians of the concentrations reflecting the symmetric unimodal priors nearly agreed with those of the concentrations reflecting the plausible ones within 10% by downwind distance and the Bayesian inferences were, therefore, found to be sufficiently robust to reasonable variations in priors. From sensitivity analysis, horizontal dispersion coefficient was the highest effect in the atmospheric dispersion model due to the fanning condition under F-stability. In addition, the atmospheric dispersion model was less sensitive to all inputs, as the downwind distance increases to 5 km.

KEYWORDS: atmospheric dispersion, robust Bayesian analysis, sensitivity analysis, contaminated priors

I. Introduction

The Gaussian plume model is the atmospheric dispersion model most widely used for estimating airborne radionuclide exposures in that it produces results similar to any other model when comparisons are made between model predictions and experimental data. Since the inputs in the stated model are taken from the site-specific data such as meteorological and topographical data, it is expected to have a parametric variability of the inputs in the model. However, (χ / Q) concentrations have been resulted to be conservative by applying the deterministic values of inputs in the model in Korea. A probabilistic approach will be, therefore, reasonable for analyzing the atmospheric dispersion.

According to Turner, the concentrations should be correct within a factor of three and it is expected to have the uncertainties for inputs of dispersion coefficients, wind speed and effective height[1]. We, therefore, try estimating the uncertainty and sensitivity of the Gaussian plume model by applying the robust Bayesian analysis. The stated inputs are updated by the Bayes' theorem and then applied to the model. The sector-averaged concentrations for sixteen cardinal wind directions and the sensitivity due to variation of effective height are analyzed.

The robust Bayesian analysis is performed by considering the contaminated prior based on the class of ε-contamination for the inputs in the model[2, 3]. The symmetric unimodal (SU) prior is defined as the contaminated one for estimating the atmospheric dispersion and their results reflecting the plausible and contaminated priors are compared and analyzed. A program for calculating the sector-averaged concentration was written by using WinBUGS 1.4.1 based on the Markov Chain Monte Carlo method[4]. Ulchin nuclear power plants (NPP) 3 and 4 of Korea are selected as reference unit in this study.

* Corresponding Author, Tel. +82-2-2220-0571, Fax. +82-2-2296-3690, E-Mail; jykim@ rrl.hanyang.ac.kr

II. Materials and Method

1. Gaussian Plume Model

The Gaussian plume model suggested in the Canadian Standard Association was used for analyzing the atmospheric dispersion to parametric variability of the inputs[5]. The sector-averaged concentrations at the centerline ($y = 0$) of the plume due to the release in effective heights of 0, 10 and 20m were calculated for the short-term release of radionuclide and the sensitivities due to variability of the effective heights also analyzed for dispersion coefficients and wind speed. For correcting the dispersion coefficients by the building wake effect, cross-sectional area of the nearby building normal to the wind direction was then assumed to be 400m^2 in this study. F-stability, which is generally expected to be maximum concentration in the CSA model, was only assumed as the atmospheric stability class.

According to U.S. NRC, the exposure due to atmospheric dispersion of radionuclides should be estimated within a distance of 50 mile (80km) from the release point[6]. However, since the impacts in EAB and outer LPZ have been predicted to be low doses for the hypothetic severe accidents presented in Final Safety Analysis Report of reference unit, the sector-averaged concentrations were calculated for the downwind distances within 5km in this study[7].

2. Robust Bayesian Analysis

From the Bayes' theorem of Eq. (1), we take prior beliefs about various possible hypotheses and then modify these prior beliefs in the light of relevant data which we have collected in order to arrive at posterior beliefs.

$$(posterior) \propto (prior) \times (likelihood) \quad (1)$$

However, any real application of the Bayesian analysis must acknowledge that both prior and likelihood have only been specified as more or less convenient approximations to whatever the analyzer's true beliefs might be. If the inferences from the Bayesian analysis are to be trusted, it is important to determine that they are robust to such variations of prior and likelihood as might also be consistent with the analyzer's stated beliefs. The variation due to type or parametric variability of the prior and likelihood is defined as "contamination" in the robust Bayesian analysis. The prior tends to be more contaminated than the likelihood in the robust analysis, because the former is quantified by the subjective knowledge of the analyzer, while the latter is constructed through the evidence[3]. The priors for horizontal and vertical dispersion coefficients and wind speed are, therefore, only assumed to be contaminated in this study.

A class of "ε-contamination" of prior based on the SU one taking uniform type, which is defined as non-informative prior in the Bayesian analysis, was applied to analyzing a robustness and was defined by Eq. (2) [2, 3]. ε determines the amount of probabilistic deviation from the plausible prior π_0 that is allowed and $0 < \varepsilon < 1$ reflects how "close" is π to π_0. Q is a class of possible contaminations.

$$\Gamma_{su} = \{\pi = (1-\varepsilon)\pi_0 + \varepsilon q, q \in Q \quad and\ q\ is\ U[\mu - k, \mu + k]\ for\ some\ k > 0\} \quad (2)$$

where μ is the mean of plausible priors and k is the lower or upper range consistent with the standard deviations of the contaminated priors. By setting ε as 10%, k was assumed to be more contaminated by 10% of them in addition to the standard deviations of the plausible ones in this study.

The distributions of all inputs were assumed as log-normal ones for the prior and the likelihood by Hamby[8]. The means of the priors of two dispersion coefficients were assumed as the values calculated from the equations of the dispersion coefficients recommended in CSA model. Their standard deviations were assumed as 10% of the midpoint values determined by logarithmic interpolation between the Pasquill curves of E and F-stabilities at a given downwind distance in this study.

The uncertainties for each input are expected to be within a factor of 2 for vertical dispersion coefficient, a factor of 0.5 to 0.6 for horizontal dispersion coefficient according to Turner, if the uncertainty for the ground level centerline concentration is divided by the inputs in the model[1]. From the stated information of uncertainties of the inputs, the standard deviations of the likelihoods of horizontal and vertical dispersion coefficients were set as 50% and 200% of the midpoints of dispersion coefficients at a given downwind distance calculated in CSA model, respectively.

While the prior and the likelihood for wind speed were constructed by examining the data measured in real-time in the reference unit during 2004 to 2005 year. The data were then sorted by stability class and sector. Since the data of wind speed were classified into A to G-stability by U.S. NRC, the data of wind speed consistent with G-stability were added to the data of F-stability for applying to the CSA model in this study[9]. The data measured in 2004 and 2005 years were assumed as the prior and the likelihood of wind speed, respectively.

The priors and likelihoods of all inputs were then transformed to normal distributions by taking natural logarithm for writing a program for calculating the sector-averaged concentrations by WinBUGS 1.4.1. Iterative simulations of 5500 were performed for calculating the concentrations with the addition of the burn-in of 500. In **Table 1** and **Table 2**, the summaries of the priors and likelihoods are presented for dispersion coefficients and wind speed, respectively.

Table 1 The priors and likelihoods of dispersion coefficients

Dist. (m)	Input	Distribution		
		Plausible prior	SU prior	[1]Likelihood
1000	Σ_y	N(3.63, 0.12^2)	U[3.50, 3.77]	N(p, 0.57^2)
	Σ_z	N(2.69, 0.14^2)	U[2.54, 2.84]	N(p, 1.47^2)
2000	Σ_y	N(4.28, 0.12^2)	U[4.15, 4.42]	N(p, 0.57^2)
	Σ_z	N(3.13, 0.14^2)	U[2.98, 3.29]	N(p, 1.49^2)
3000	Σ_y	N(4.65, 0.12^2)	U[4.51, 4.78]	N(p, 0.57^2)
	Σ_z	N(3.38, 0.14^2)	U[3.22, 3.53]	N(p, 1.49^2)
4000	Σ_y	N(4.90, 0.12^2)	U[4.77, 5.03]	N(p, 0.57^2)
	Σ_z	N(3.54, 0.15^2)	U[3.39, 3.70]	N(p, 1.50^2)
5000	Σ_y	N(5.09, 0.12^2)	U[4.95, 5.22]	N(p, 0.57^2)
	Σ_z	N(3.67, 0.15^2)	U[3.51, 3.83]	N(p, 1.50^2)

[1]Values sampled from the priors of each input are applied to 'p' of the likelihoods and specific posterior distributions are then derived through the Bayes' theorem. The distributions of the updated inputs are applied to the Gaussian plume model.

Table 2 The priors and likelihoods of wind speed

Sector	Distribution		
	Plausible prior	SU prior	[2]Likelihood
N	N(-0.86, 0.42^2)	U[-1.32, -0.40]	N(p, 0.96^2)
NNE	N(-1.05, 0.48^2)	U[-1.58, -0.52]	N(p, 0.85^2)
NE	N(-1.00, 0.31^2)	U[-1.34, -0.66]	N(p, 0.76^2)
ENE	N(-1.29, 0.60^2)	U[-1.95, -0.62]	N(p, 0.76^2)
E	N(-0.51, 0.41^2)	U[-0.96, -0.06]	N(p, 0.87^2)
ESE	N(-0.58, 0.47^2)	U[-1.10, -0.06]	N(p, 0.89^2)
SE	N(-0.93, 0.55^2)	U[-1.53, -0.32]	N(p, 0.54^2)
SSE	N(-1.11, 0.54^2)	U[-1.70, -0.52]	N(p, 0.64^2)
S	N(-0.72, 0.68^2)	U[-1.47, 0.03]	N(p, 0.56^2)
SSW	N(-0.78, 0.67^2)	U[-1.52, -0.03]	N(p, 0.56^2)
SW	N(-0.46, 0.55^2)	U[-1.06, 0.15]	N(p, 0.52^2)
WSW	N(-0.44, 0.48^2)	U[-0.96, 0.08]	N(p, 0.48^2)
W	N(-0.17, 0.36^2)	U[-0.57, 0.23]	N(p, 0.46^2)
WNW	N(-0.04, 0.34^2)	U[-0.42, 0.33]	N(p, 0.57^2)
NW	N(-0.31, 0.40^2)	U[-0.75, 0.13]	N(p, 0.79^2)
NNW	N(-0.63, 0.38^2)	U[-1.04, -0.21]	N(p, 0.83^2)

[2]The likelihoods are applied the same as those of Table 1 are.

III. Results and Discussion

The sector-averaged concentrations, which were calculated by reflecting the plausible and symmetric unimodal priors, in effective height of 0m and downwind distance of 1000m were presented as an example in **Fig. 1**. The distribution resembled log-normal one and its median considerably agreed with the deterministic value of the concentration. The median was, thus, defined as the representative quantile of the distribution. Though ε was assumed as 10% in this study, the median of the distribution reflecting the SU prior was varied about 6.0% for given downwind distance as compared with that of the distribution reflecting the plausible one.

The medians reflecting the plausible priors were compared with those reflecting the SU ones by downwind distance for effective height of 0m in **Fig. 2**. The medians based on the SU priors were varied about 1.3 to 9.7% as compared with those based on the plausible ones by given downwind distance. It was then noted that the Bayesian inferences applying the plausible priors were found to be sufficiently robust to reasonable variations in priors, and the reliable inferences for the concentrations were drawn in this study. The stated inferences are applied the same for the concentrations considering effective heights of 10 and 20m.

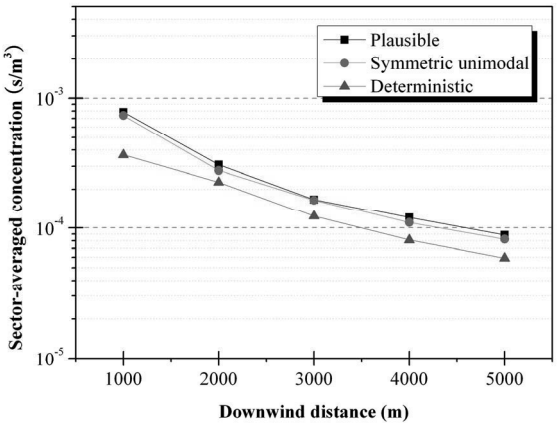

Fig. 2 Medians of sector-averaged concentrations based on two priors; Effective height of 0m

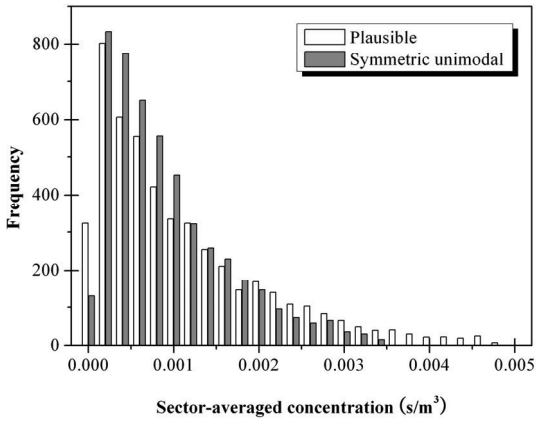

Fig. 1 Distributions of sector-averaged concentrations; Effective height of 0m and downwind distance of 1000m

The statistical summaries of the sector-averaged concentrations for all effective heights were presented by the type of prior in **Table 3**. The medians of the distributions reflecting the SU priors were varied about 3.9 to 8.3% by given downwind distance as compared with those of the distributions reflecting the plausible one in effective height of 10m, while those of the distributions reflecting the SU ones varied about 2.8 to 5.6% by given downwind distance in effective height of 20m. It is also noted that the results of the concentrations are reliable regardless of variation of the priors. Additionally, as the effective height increases to 20m, the sector-averaged concentrations were more robust due to

Table 3 Statistical summaries of the sector-averaged concentrations for all effective heights (s/m^3)

Height (m)	Quantile	Downwind distance (m)									
		Plausible prior					Symmetric unimodal prior				
		1000	2000	3000	4000	5000	1000	2000	3000	4000	5000
0	2.5%	4.64E-5	1.69E-5	7.41E-6	4.85E-6	3.80E-6	9.86E-5	3.53E-5	1.95E-5	1.23E-5	9.06E-6
	Median	7.84E-4	3.09E-4	1.67E-4	1.20E-4	8.85E-5	7.37E-4	2.79E-4	1.65E-4	1.10E-4	8.23E-5
	Mean	1.19E-3	5.02E-4	3.06E-4	2.31E-4	1.71E-4	9.73E-4	3.99E-4	2.47E-4	1.74E-4	1.30E-4
	97.5%	4.55E-3	2.06E-3	1.41E-3	1.04E-3	8.07E-4	3.22E-3	1.43E-3	9.01E-4	6.77E-4	5.20E-4
	SD	1.21E-3	5.78E-4	4.04E-4	2.97E-4	2.40E-4	8.38E-4	3.87E-4	2.49E-4	1.84E-4	1.38E-4
	Deterministic	3.67E-4	2.27E-4	1.23E-4	8.10E-5	5.92E-5	3.67E-4	2.27E-4	1.23E-4	8.10E-5	5.92E-5
10	2.5%	4.51E-5	1.45E-5	7.15E-6	5.12E-6	3.71E-6	1.05E-4	3.36E-5	1.80E-5	1.12E-5	8.83E-6
	Median	5.79E-4	2.46E-6	1.45E-4	1.04E-4	7.73E-5	5.34E-4	2.34E-4	1.39E-4	9.70E-5	7.10E-5
	Mean	7.95E-4	3.63E-4	2.30E-4	1.68E-4	1.28E-4	6.75E-7	3.16E-4	1.93E-4	1.39E-4	1.05E-4
	97.5%	2.91E-3	1.40E-3	9.64E-4	7.03E-4	5.58E-4	2.07E-3	1.05E-3	6.66E-4	5.13E-4	3.91E-4
	SD	7.81E-4	3.97E-4	2.70E-4	2.03E-4	1.58E-4	5.25E-4	2.83E-4	1.78E-4	1.36E-4	1.03E-4
	Deterministic	3.08E-4	2.07E-4	1.16E-4	7.78E-5	5.74E-5	3.08E-4	2.07E-4	1.16E-4	7.78E-5	5.74E-5
20	2.5%	5.98E-6	3.62E-6	2.67E-6	2.43E-6	1.82E-6	1.29E-5	9.78E-6	8.60E-6	6.22E-6	5.07E-6
	Median	1.67E-4	8.50E-5	5.63E-5	4.28E-5	3.35E-5	1.75E-4	8.98E-5	5.95E-5	4.46E-5	3.45E-5
	Mean	2.47E-4	1.26E-4	8.53E-5	6.54E-5	5.16E-5	2.22E-4	1.19E-4	7.88E-5	5.94E-5	4.77E-5
	97.5%	9.41E-4	5.01E-4	3.34E-4	2.65E-4	2.19E-4	6.99E-4	3.97E-4	2.58E-4	2.03E-4	1.66E-4
	SD	2.61E-4	1.38E-4	9.71E-5	7.35E-5	5.92E-5	1.84E-4	1.06E-4	6.89E-5	5.22E-5	4.24E-5
	Deterministic	1.82E-4	1.56E-4	9.80E-5	6.88E-5	5.21E-5	1.82E-4	1.56E-4	9.80E-5	6.88E-5	5.21E-5

Table 4 Summary of sensitivity analysis

Height (m)	Input	Downwind distance (m)				
		1000	2000	3000	4000	5000
0	Σ_y	-0.42	-0.36	-0.35	-0.36	-0.31
	Σ_z	-0.25	-0.23	-0.22	-0.27	-0.24
	Wind speed	-0.29	-0.27	-0.24	-0.25	-0.24
10	Σ_y	-0.44	-0.40	-0.39	-0.36	-0.36
	Σ_z	-0.29	-0.20	-0.13	-0.26	-0.24
	Wind speed	-0.31	-0.29	-0.27	-0.27	-0.26
20	Σ_y	-0.40	-0.39	-0.40	-0.38	-0.39
	Σ_z	-0.18	-0.16	-0.11	-0.23	-0.22
	Wind speed	-0.30	-0.30	-0.28	-0.28	-0.28

the decreases of the differences of two medians from the results of robust inferences. From all inferences, we conclude that the plausible priors for all inputs have been reasonably quantified for estimating the sector-averaged concentrations in this study.

The sensitivities due to the variations of downwind distance and effective height were summarized in **Table 4**. The distributions of concentrations by downwind distance were taken as log-normal ones characterized by the high density at lower region as presented in Figure 1, since all of correlation coefficients were resulted to be negative. Horizontal dispersion coefficient was the highest effect in the atmospheric dispersion model because of the fanning condition. It is the atmospheric characteristic of F-stability taking moderately stable condition and the airborne radionuclides are horizontally and flat dispersed as "v-type" under the fanning condition. And, the wind speed and vertical dispersion coefficient contributed to the concentration in order.

The larger the downwind distance is, the less the horizontal dispersion coefficient and wind speed are sensitive. That is, as the downwind distance increases to 5km, the atmospheric dispersion model is less sensitive to the stated inputs. For the vertical dispersion coefficient, as the downwind distance increases to 3km, the atmospheric dispersion model is also less sensitive to the stated input. However, its sensitivity tends to increase in 4km more or less and again to decrease in 5km. It is also expected that the atmospheric dispersion model is generally speaking less sensitive to the stated input by downwind distance. From the sensitivity analysis, we conclude that as the downwind distance increases to 5km, the atmospheric dispersion model is less sensitive to all inputs.

IV. Conclusions

This study aims at suggesting the robust Bayesian analysis for estimating the sector-averaged concentrations due to the atmospheric dispersion of the airborne nuclides. The concentrations due to the variations of downwind distance and effective height under F-stability were calculated by applying the plausible and contaminated priors of inputs according to the CSA model in Ulchin nuclear power units 3 and 4 of Korea. Dispersion coefficients and wind speed were updated by the Bayes' theorem based on their priors and likelihoods and then the updated distributions applied the model. The medians of the concentrations considerably agreed with the deterministic values by downwind distance for all effective heights. The medians of the concentrations reflecting the contaminated priors nearly agreed with those of the concentrations reflecting the plausible ones within 10% by downwind distance. From the robust inferences, it is suggested that the plausible priors for all inputs have been reasonably quantified for estimating the atmospheric dispersion.

Horizontal dispersion coefficient was the highest effect in the Gaussian plume model due to the fanning condition under F-stability. As the downwind distance increases to 5km, the model was less sensitive to all inputs. The robust Bayesian and sensitivity analyses suggested in this study will contribute to a decision-making under an emergency due to the atmosphere dispersion of airborne nuclides under a severe accident in NPP.

Acknowledgement

The authors thank for the support of the Innovative Technology Center for Radiation Safety of Korea.

References

1) D. B. Turner, Workbook of Atmospheric Dispersion Estimates:
2) An Introduction to Dispersion Modeling, Lewis Publishers, Boca Raton, 2-13 (1994).
3) S. Sivaganesan, J. O. Berger, "Ranges of posterior measures for priors with unimodal contaminations," Ann. Stat., 17[2], 868 (1989).
4) J. O. Berger, Statistical Decision Theory and Bayesian Analysis, Springer-Verlag New York, Inc., New York, 206 (1985).
5) D. Gamerman, Markov Chain Monte Carlo: Stochastic Simulation for Bayesian Inference, Chapman & Hall/CRC, Boca Raton, 93 (2002).
6) The Canadian Standards Association, Guidelines for Calculating Radiation Doses to the Public from Release of Airborne Radioactive Material under Hypothetical Accident Conditions in Nuclear Reactors, CAN/CSA-N288.2-M91, CSA, (1991).
7) U.S. Nuclear Regulatory Commission, Methods for Estimating Atmospheric Transport and Dispersion of Gaseous Effluents in Routine Releases from Light-Water Cooled Reactors, Regulatory Guide 1.111, rev. 1, U.S. NRC, (1977).
8) Korean Electric Power Corporation, Final Safety Analysis Report of Ulchin Nuclear Power Units 3 & 4, Amendment 1, KOPEC, (1998).
9) D. M. Hamby, "The Gaussian atmospheric transport model and its sensitivity to the joint frequency distribution and parametric variability," Health Phys., 82[1], 64 (2002).
10) U.S. Nuclear Regulatory Commission, Onsite Meteorological Programs, Regulatory Guide 1.23, U.S. NRC, (1972).

Journal of NUCLEAR SCIENCE and TECHNOLOGY, Supplement 5, p. 714–717 (June 2008)

Study on the Intervention and Return Criteria for Relocation Using PSA method

Shogo TAKAHARA*, Masanori KIMURA, Takeshi MATSUBARA, and Toshimitsu HOMMA

Nuclear Safety Research Center, Japan Atomic Energy Agency, Tokai-mura, Japan

Relocation is one of the long-term protective actions for a nuclear and radiological emergency. The objective of relocation should be taken into account the concepts of "safe living condition" and "return to normality", and prepare the strategy adopted these concepts. In order to prepare the strategy, we have examined the model using Return Level which is basis on these concepts. We have investigated the dependence of number of people to be relocated, relocation time, avertable collective dose and avertable per caput dose per year to criteria, i.e. Intervention Level and Return Level. From these results, it would be impossible to justify the strategy in terms of cost-benefit analysis. Therefore, to justify the strategies which are taken into account "safe living condition" and "return to normality", we have to consider the other factor such as social physiological aspects.

KEYWORDS: relocation, intervention level, return level, level 3 PSA, safe living condition, return to normality

I. Introduction

Relocation is one of the nuclear and radiological emergency protective actions, to remove people from contaminated areas to avoid prolonged exposures. The objectives of off-site response such as relocation are described as follows: (a) preventing the occurrence of severe deterministic health effects among the public, (b) avoiding, to the extent practicable, the occurrence of stochastic health effects in the public and (c) preparing, to the extent practicable, for resumption of normal social and economic conditions. The protective actions forming a program of intervention, which always have disadvantages, should be justified, and their form, scale and duration should be optimized so as to maximize the net benefit for achieving the above objectives (a) to (c).

In general consideration of relocation decisions[1-4], some studies have derived that Intervention Level (IL) at which relocation is optimized is about 10 mSv per month from a simple cost-benefit analysis. About 10 mSv per month is obtained from an example of generic optimization for relocation on the basis of two variables that are the cost of continuing relocation and the cost assign to the radiological detriment avoided. In addition, this level is postulated that the points of objective (a) and (b) are satisfied.

On the other hand, we should take into account the point of (c) in consideration of the strategy of protective actions. The ICRP 82 recommendation proposes that existing annual dose of about 10 mSv for the public under prolonged exposure situations is the criteria for intervention which is unlikely to be justifiable. This value would be valid because the existing exposure attributed to natural radiation sources is similar to this order. Hedemann explains the concept of "safe living condition" and "return to normality", and existing annual dose of about 10 mSv should be used as a target to achieve these concepts[5].

* Corresponding Author, Tel No: +81-29-282-6139, Fax No.: +81-29-282-6147, E-mail: takahara.shogo@jaea.go.jp

So far, the introduction and lifting of intervention have been judged from the point of views (a) and (b) mainly. In this study, we have examined the criteria for lifting relocation defined by return-level (RL) from the aspect of (c). Using RL which aims to achieve the objective (c), we have investigated the dependence of the quantities associated with relocation on both IL and RL. Moreover, we have also investigated the time dependence of the quantities associated with relocation.

II. The Probabilistic Accident Consequence Assessment

The approach adopted in this study is to consider the variation in predicted consequences for the range of dose levels at which relocation might be implemented in the probabilistic framework. The probability distributions of consequences such as the number of people to be relocated, the period of relocation and the avertable collective dose have been evaluated. We have used, for calculating these values, the level 3 PSA Code OSCAAR which was developed by Japan Atomic Energy Research Institute (JAERI).

Using OSCAAR, we have calculated prolonged exposures from radioactive material deposited on the ground. The exposure pathways are considered for external dose from deposited radionuclides on the ground and inhalation dose from radionuclides resuspended in the air. We have calculated the dose rates for every ten years.

The analyses have been made of a postulated sever accident and the inventory of radionuclides for 1100 MWe BWR with source terms derived from a generic Level 2 PSA by JAERI[6]. The release fractions for each radionuclide group considered are given in **Table 1** for the accident scenario assumed. In this scenario, the time of release and the height of release are 27 hours and 40 m respectively.

Population distribution data is used for Tokai site compiled from the 1990 census in Japan. The consequence

analysis has been made for the 248 meteorological sequences derived from the total of 8760 meteorological sequences, if the accident is assumed to occurred for every an hour, by bin meteorological sampling method.

We have considered only relocation for protective action in our calculations. Calculations have been carried out for the combinations of IL and RL (IL = 10, 25, 50, 100 and 150 mSv per year, and RL = 1, 5 and 10 mSv per year).

1. The Relationship of the Quantities Associated with Relocation to IL and RL

The expectation values of the number of people to be relocated and the avertable collective dose are shown in **Fig.1** and **Fig.2** respectively. In generic studies, the continuing relocation cost will be proportional to the number of people to be relocated and the period of relocation, and the benefit equivalent to avertable healthy detriments attributed to implement relocation will be proportional to the collective avertable dose[7]. Therefore, the evaluations of these quantities are important in developing numerical guidance on criteria for implementing relocation.

The number of people to be relocated depends on IL, and if RL is constant, it decreases with IL. It should be noted that these values in **Fig.1** represent the relocated people at the time of the introduction of relocation. As the time increases, the dose rate decreases, and the number of people to be relocated decreases with time (see **Fig.5**).

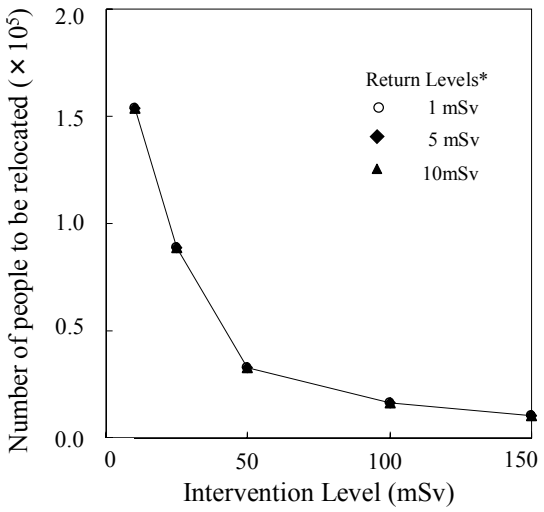

Fig.1 Expectation values of number of people to be relocated for Intervention Level. (*The data derive from each RL are the same values.)

As shown in **Fig.2**, the avertable collective dose attributed to relocation depends on IL, and if RL is constant, it decreases with IL. Both the number of people to be relocated and the avertable collective dose decrease with IL, but the number of people to be relocated strongly varies with IL. In addition, the avertable collective dose strongly depends on RL. Because the avertable collective dose from relocation is calculated for the whole period of relocation, and the length of this period is affected by RL.

In fact, as shown **Fig.3**, the periods of relocation depend upon both IL and RL.

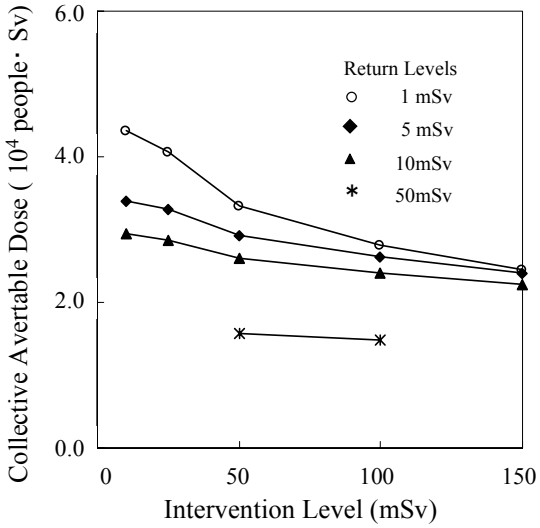

Fig.2 Expectation values of Avertable Collective Dose from relocation for intervention level.

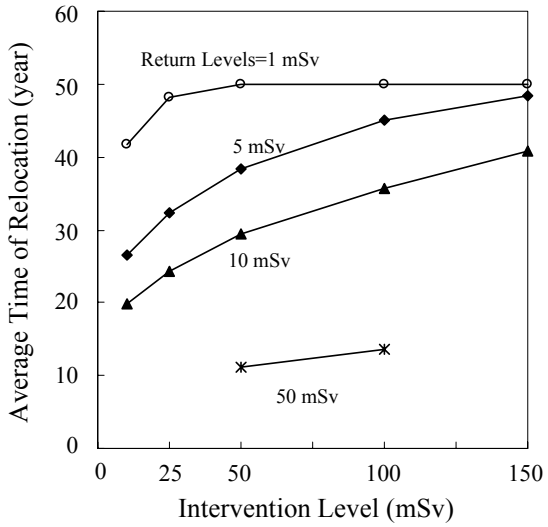

Fig.3 Expectation values of period of relocation.

The avertable per caput dose per year, which is calculated by averaging for the whole period of relocation, is shown in **Fig. 4**. These values depend on both IL and RL, and it is less sensitive to IL chosen but quite sensitive to a specific RL.

As explained in the introduction, the avertable per caput dose of about 10 mSv per month may serve as an optimized level for relocation. ICRP also concludes that relocation is

Table 1 Release fraction for TQUV-DWF

	Xe	I	Cs-Rb	Te-Sb	Sr-Ba	Ru	La
Fraction	9.50E-01	3.26E-02	2.80E-02	2.90E-04	1.60E-08	3.80E-11	6.40E-12

going to be justified for continuing dose of the order of 10 mSv per month[2]. From this value, we can assume that around 100 mSv per year will be adopted for the criteria for relocation. However, note that this value does not take into account the aspect of (c). From **Fig. 4**, if we judge the strategies of relocation by only this value, some strategies using RL to achieve the purpose (c) would not be justified.

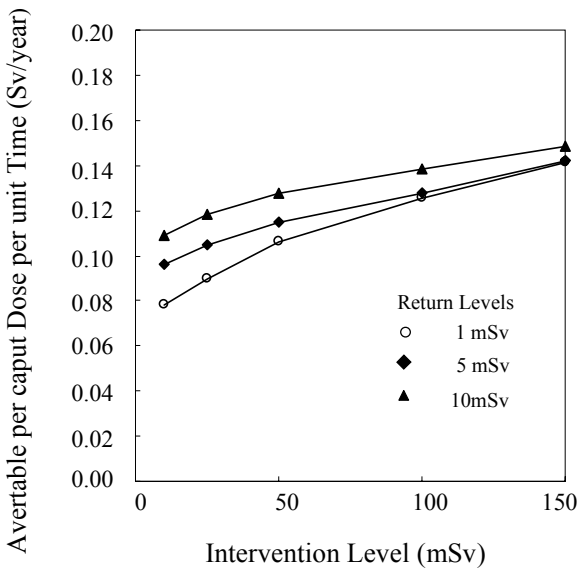

Fig.4 Expectation values of avertable per caput dose as a function of intervention level.

2. Time Dependence of the Quantities Associated with Relocation

Fig. 5 shows the time dependence of the number of people to be relocated. It indicates the sensitivity of the number of people to be relocated to IL at a constant RL of 10 mSv per year. In **Fig. 5**, the variations of the number of people to be relocated can be divided into the two stages. In the first stage, the number of people to be relocated is constant for a certain time, and only depends on the IL. The length of this stage is corresponding to the decay time of dose rates from IL to RL. Therefore, the length can be determined by the relationship between IL and RL.

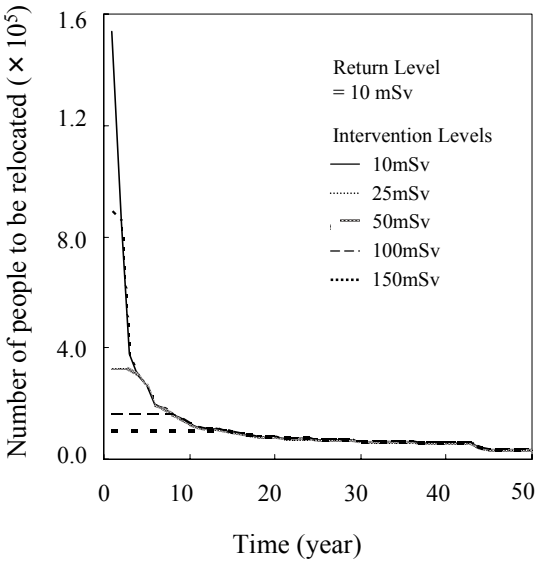

Fig.5 Time dependence of the number of relocated people.

Table 2 shows the variation of the time dependence of avertable per caput dose for IL, RL, and the length of first stage, t_{min}, which are obtained from **Fig.5**. The time dependence of avertable per caput dose has the same tendency as the case of number of people to be relocated. The avertable dose depends on IL in the first stage, and depends on RL in the second stage. However, the number of people to be relocated depends more strongly on time than avertable per caput dose.

In addition, this table indicates the length of the first stage can be determined by the ratio of IL to RL. For example, in the ratio of 10, the strategies have 8 years as the length of the first stage.

Moreover, from this result, the avertable per caput dose per year decreases with time, and become the unjustified level in the late-phase of the accident. The intervention level is optimized as to achieve the purpose (a) and (b). If these purposes are ensured, the third purpose (c) should be achieved. In fact, in Chernobyl accident, the criteria of decision making for implementation of protective actions had been gradually decreasing with time[8]. In the late-phase of accident, these decisions under the pressure of social, psychological and political factors, and led to a negative value of net benefit with optimization in radiation protection.

Table 2 Time dependence of Avertable per caput dose per year

t_{min}**	RL (mSv)	IL (mSv)	Avertable per caput dose per year (Sv)*				
			1-10 year	11-20 year	21-30 year	31-40 year	41-50 year
1	10	10	2.172E-01	1.101E-01	8.753E-02	7.228E-02	5.903E-02
4	10	50	3.082E-01	1.101E-01	8.753E-02	7.228E-02	5.903E-02
8	10	100	3.619E-01	1.101E-01	8.753E-02	7.228E-02	5.903E-02
8	5	50	3.062E-01	9.114E-02	7.102E-02	5.755E-02	4.628E-02
22	5	100	3.617E-01	1.016E-01	7.175E-02	5.755E-02	4.628E-02
8	1	10	2.123E-01	6.245E-02	4.815E-02	3.795E-02	2.991E-02
50	1	100	3.617E-01	1.016E-01	7.171E-02	5.270E-02	3.875E-02

*Avertable per caput dose are represented as average values over every 10 year.
**Length of first stage gained by Fig.5
***Shaded region is represented the first stage.

As mentioned in some studies from Chernobyl experience, not only the radiological protection attributes but also all relevant protection attributes should be taken into account in the decision-making process in the late phase of an accident[9]. It is necessary that we clarify the concepts of "safe living condition" and "return to normality", and achieve the purpose (c) in situations of prolonged radiation exposure.

III. Summary

In generic studies, the continuing relocation cost will be proportional to the number of people to be relocated and period of relocation, and the benefit equivalent of avertable healthy detriments attributed to implement relocation will be proportional to the avertable collective dose[7]. This study indicates that the average cost rather than the average benefit is strongly dependent upon IL in a probabilistic accident consequence assessment.

The time dependence of the quantities associated with relocation can be divided into two stages. The turning point of time dependence can be determined by the relationship between IL and RL.

On the basis of optimization using a simple cost-benefit analysis, the strategy of relocation using a RL to achieve the purpose (c) would not be able to justify. However, as this judgment is only based upon a simple cost-benefit analysis and radiological protection aspects, we should take into account non-radiological aspects such as the psychological stress, individual anxiety and disruption of normally life-style caused by the protective action.

Reference

1) D. J. Beninson, A. J. Gonzalez, "Optimization in Relocation Decisions," Optimization of Radiation Protection, Proceedings of symposium, Vienna, 10-14 March 1986, jointly organized by IAEA and NEA (OECD), International Atomic Energy Agency, Vienna, Austria.
2) ICRP, "Principle for Intervention for Protection of the Public in a Radiological Emergency," ICRP Publication 63, Annals of the ICRP, 22, No.4, 1991.
3) IAEA, "Intervention Criteria in a Nuclear or Radiation Emergency," Safety Series No. 109, International Atomic Energy Agency, Vienna, 1994.
4) IAEA, "International Basic Safety Standards for Protection against Ionizing Radiation and for the Safety of Radiation Sources," Safety Series No. 115, International Atomic Energy Agency, Vienna, 1996.
5) Hedemann Jensen, P., "ICRP publication 82 on protection against prolonged exposure –application in accident situations," RADIOLOGICAL PROTECTION IN THE 2000s-THEORY AND PRACTICE, Nordic Society for Radiation Protection, 13th Ordinary Meeting, Turku, Finland, 25-29 August 2002.
6) J. Ishikawa, K. Muramatsu, T. Sakamoto, "Systematic Source Term Analysis for Level 3 PSA of a BWR with Mark-Ⅱ Type Containment with THALES-2 Code," JAERI-Research 2005-021, Japan Atomic Energy Research Institute, 2005.
7) ICRP, "Cost-Benefit Analysis in the Optimization of Radiation Protection," ICRP publication 37, Annals of the ICRP, 10, No.2/3, 1983.
8) Yu. O. Konstantinov, "Decision making on population protection in a large-scale radioactive contamination following a nuclear reactor accident," Proceedings of the Russian-Hungarian seminar on radiation protection, 11-13 march, Research Institute of Radiation Hygiene Saint Petersburg, Russian Federation, (1991).
9) Hedemann Jensen, P., "Protective Actions in the Late Phase intervention criteria and Decision Making," Radiation Protection Dosimetry, 109 (1-2), p.45-51.

Journal of NUCLEAR SCIENCE and TECHNOLOGY, Supplement 5, p. 718–722 (June 2008)

A Probability Safety Assessment of MACSTOR/KN-400 during The Air Inlet Blockage

Kyung Min KANG and Moosung JAE*

Department of Nuclear Engineering Hanyang University
17 Haengdang-Dong, Sungdong-Gu, Seoul, Korea

A framework for assessing the safety of an interim spent fuel storage facility in Korea has been developed and applied in the air inlet blockage accident. It uses the PSA technology to be classified into three phases, which involve first the failure probability assessment phase for a basket and a cylinder. And secondly the possible accident scenarios in the spent fuel dry storage facility are identified. Lastly the accident consequence analysis has been done by the MACCS code. The phase of the analysis includes the quantitative assessment for the failure probability by modeling of the basket and the cylinder, which is the major element of containing radioactive substances. It also evaluates the probability that radioactive substances are released to outside when the initial event happens by applying the construction of the event tree methods. It describes a various heading elements that affect the air inlet blockage accident mitigation. And also using the released radioactive substances, the radiation damage to affect neighborhood and workers, is quantitatively evaluated. It is shown that this framework developed in this study can be applied to assess the synthetic safety for any other dry storage facilities.

KEYWORDS: probabilistic safety assessment, MACSTOR/KN-400, basket failure, radiation release frequency, CDF

I. Introduction

Since the launch of commercial operation of Kori unit 1 in 1978, now 20 nuclear power plants in total have been under operation now. The capacity of the spent fuel storage pool which each power plant possesses will soon arrive at the maximum capacity. Therefore, a long-term storage facility for the spent fuel management is now required. The interim spent fuel storage facility is necessary to store and manage the spent fuel continuously discharged from the ongoing power plant operations.

Currently, several types of the storage facilities are under design, construction, and operation internationally now. Although the design concept of these facilities is different, all systems are designed to ensure the safety limits.

For the initial process such that spent fuels are transferred to the facility in the reactor building, the radionuclide quantity and radioactive decay heat are decreased gradually. In the mean time, the condition which can cause an accident may occur and it may take the sufficient time reaching the management until it arrives to a limit condition. Therefore, the appropriate treatment can make the spent fuel storage facility preserve the safe conditions without a complex, automatic, and defensive system.

There are many possible stages, such as nuclear criticality, removal of radioactive decay heat, shielding of radiation, and sealing up the design function during lifetime. The evaluation of these elements is known as major issues for a safety assessment of spent fuel storage facility [1]. There are two way of safety assessment such as deterministic and probabilistic approach.

*Corresponding Author, Tel. +81-2-2290-1346, Fax. +81-2-2293-7014, jae@hanyang.ac.kr

The deterministic approach checks whether the safety parameters meet the corresponding safety limits with sufficient margins for the design basis accidents, while the probabilistic one evaluates allowable risk or frequencies of Core Damage Frequency (CDF) / Large Early Release Frequency (LERF). The deterministic safety analysis for the storage facility has been performed traditionally. However, nowadays the stochastic approach for design and operation of the facility is required more rigorously. The reference storage system, MACSTOR/KN-400, to be constructed at the Wolsung plant, is used as an example for applying the developed framework [2].

II. A framework

The framework introduced in this study is classified into three phases as shown in **Fig. 1**. In first phase, the failure probability of both a basket and a cylinder, which is the major element of containing radioactive substances, is modeled. In second phase, the accidents of spent fuel dry storage facility are modeled using the ETA (event tree analysis). Finally, accident consequence analysis modeling circumference areas is performed using the MACCS code. PSA (probabilistic safety assessment) is defined as a methodology development and its application. It may quantitatively assess the risk of nuclear power plant by obtaining both probability and consequence. In this study the safety analysis of spent fuel dry storage facility through an analogous method of the level 1, 2, and 3 PSA has been performed [3].

At the first phase the destruction probability of a basket and a cylinder is calculated by applying reliability physics model for the basket and cylinder materials. The second

phase includes the accident sequence generation for the spent fuel dry storage facility. In this phase, the quantitative internal and the external event that may occur in the dry storage facility are physically modeled. Then, the probability that each scenario can occur is calculated. The third phase involves the consequence analysis after the occurrence of any types of accidents. The important input used for this phase are circumference area, population, level of evacuation, and meteorological data.

Fig. 1 A framework for assessing the safety of spent fuel dry storage facility.

III. Methods

The first phase of the framework includes the analysis of a basket and cylinder which are an inner barrio of containing radioactive substances. The destruction probability for a basket and a cylinder failure is incorporated to the input for the next phase. The survey on this area shows that there had not existed the accepted method to assess the safety of the dry storage facility [4]. In this study, the destruction probability has been quantified by applying the reliability physics model. It is a method called by stress-strength analysis. This method may produce a failure probability quantitatively by obtaining the overlapped area that a random variable for stress exceeds another random variable[5]. This approach is applied to the system, MACSTOR/KN-400, which is a reference facility this study.

The stress considered in the air inlet blockage accident is a load stress and a thermal stress. Occurring at relatively lower temperature, it is assumed that total stress is a linear combination of the load stress and the thermal stress. Hence, total stress can be shown in the following Eq. (1). The load stress and thermal stress are respectively shown in Eq. (2) and Eq. (3) [6].

$$\delta_{total} = \delta_{load} + \delta_{thermal} \tag{1}$$

$$\delta_{load} = \frac{pR}{2t} \tag{2}$$

p : *pressure* $[MPa]$
R : *radius of basket* $[m]$
t : *thickness of basket* $[m]$

$$\delta_z = \frac{\upsilon E\alpha q'''}{8(1-\upsilon)k} R^2 - E\alpha\left[\Delta T - \frac{q'''R^2}{4k}\right] \tag{3}$$

R : *radius of basket* $[m]$
υ : *poisson ratio*
E : *modulus of elasticity* $[MPa]$
α : *coefficient of thermal expansion* $[\mu m/mK]$
q''' : *volumetric heat generation rate* $[W/m^3]$
k : *thermal conductivity* $[W/mK]$

Therefore, the total stress can be obtained from the following Eqs. (4).

$$\delta_{total} = \frac{pR}{2t} + \frac{\upsilon E\alpha q'''}{8(1-\upsilon)k} R^2 - E\alpha\left[\Delta T - \frac{q'''R^2}{4k}\right] \tag{4}$$

In this calculation, the distribution of total stress with increased pressure and temperature is obtained as shown in **Fig. 2**. As a result the distribution of the total stress turns out to be a normal distribution with a value of 50.49 MPa in mean value and in a standard deviation, 7.97 MPa. The distribution of allowable yield stress is cited from ASME code which is a normal distribution with a mean of 85 MPa and a standard deviation of 8.5 MPa [7].

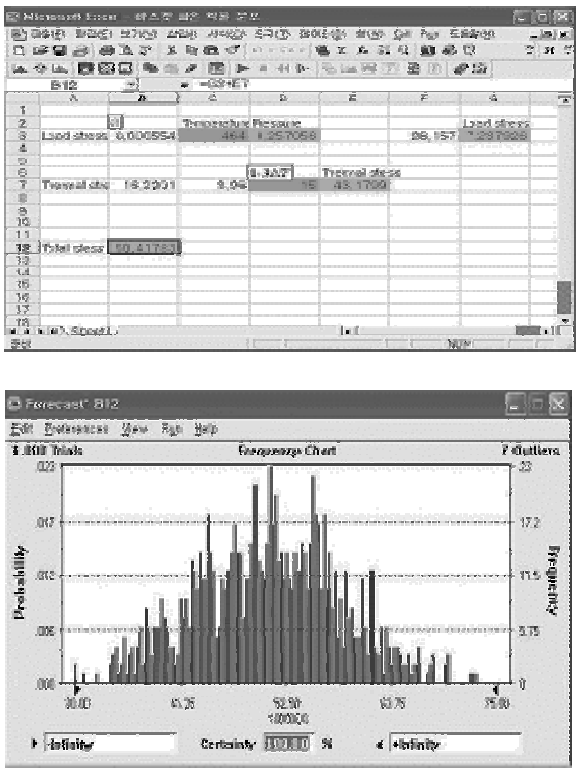

Fig. 2 Uncertainty analysis for stress.

The accident scenarios have been developed. The elements consisting of the scenarios include a cask drop, a flood, a fire and an explosion, a lightning, an earthquake, a loss of shielding, an adiabatic heat-up, a tornado and a missile attack, which are described in detail in NUREG-1567. In this study the air inlet blockage accident is used because of dominance in occurrence frequency. A various existing methods are surveyed for finding the most optimum tool

720modeling the accident scenarios appearing in this study. Each methodology can have advantages and weak points. It is concluded that ETA (event tree analysis) and FTA (fault tree analysis) method are enough for the simple accident progression. Therefore, in this study the ETA has been used for the quantitative analysis against the air inlet blockage accident, while the FTA for identifying the probability of radiation detection failure.

The initial incidents in the air inlet blockage accident may be caused by an earthquake, a flood, and a tornado. Given the occurrence of initial recovery failure, degree of blockage, duration time, destruction of a basket and a cylinder are used as heading events. The probability data used for this study is cited from PSA reports and IEEE data handbook [3]. The failure probability of a basket and a cylinder which is one of key elements has been obtained from the application of the reliability physics model.

Table 1 Data for the air inlet blockage accident

Heading	Mean	Standard Deviation
Initial accident frequency	1/year	
Initial recovery failure	3.0×10^{-1}	1.0×10^{-2}
Degree of blockage	2.0×10^{-1}	10×10^{-2}
	3.0×10^{-1}	
	5.0×10^{-1}	
Duration time	8.0×10^{-1}	1.0×10^{-2}

The MACCS 2 code (MELCOR Accident Consequence Code System) for consequence analysis is used. It is an accident consequence analysis code, which evaluate the effects caused by radioisotope released to environment. It has been developed by the SNL (Sandia National Laboratory) to assess severe accident risk for the nuclear power plants. The input data of MACCS2 code include circumference area data, meteorological data, population data around the system, and release fraction, and source term inventories of radioisotopes. In this study the values, such as CCDF, average individual risk, and whole body dose, are evaluated quantitatively. It is assumed that the burnup of the spent fuel in the MACSTOR/KN-400 is 7,800 MWD/MTU and has been cooled in the pool for six years. The source term amounts of each radiaoactive nuclide have been calculated by the ORIGEN-2 code.

Given the occurrence of leak in the system, inert gas, Kr-85 and H-3 are expected to release to the environment. The fuel temperature during the accident is assumed to be lower than 200℃. The STC number 3 for the SLOCA accident sequence shown in Level 2 PSA is chosen as the similar source term characteristics to this air inlet blockage accident in the system considered in this study. Table 2 shows release fractions used in this study [8].

Table 2 Release fractions of each group in a Small LOCA sequence

	Xe/Kr	I	Cs	Te
Release Frequency	1.0	7.7×10^{-3}	8.5×10^{-3}	5.2×10^{-3}

Sr	Ru	La	Ce	Ba
2.6×10^{-4}	1.2×10^{-6}	4.7×10^{-6}	2.5×10^{-8}	1.3×10^{-4}

IV. Results

It is assumed that a random variable, X, denotes the stress variable while a random variable, Y, represents strength. The random variable, Z, is defined as shown in Eq. (5). The mean and standard deviation value for the variable Z is also shown respectively in Eq. (6) and (7).

$$Z = X - Y \tag{5}$$

$$E[Z] = \mu_x - \mu_y \tag{6}$$

$$\delta_z = \sqrt{\delta_x^{\,2} + \delta_y^{\,2}} \tag{7}$$

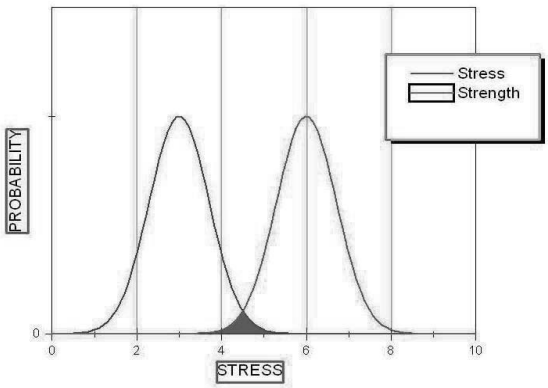

Fig. 3 Reliability physic model used in this study.

The intersected area in which we are concerned now can be calculated using the following Eq. (8). As shown in Eq. (9), the basket failure probability has been then obtained as a value of 1.12×10^{-3}.

$$R=\Pr(Z>0)=\int_0^{\infty}\frac{1}{\delta_h\sqrt{2\pi}}\exp\left[\frac{-(x-E(z))^2}{2\delta_x^2}\right]dx=\Phi\left(\frac{\mu_x-\mu_y}{\sqrt{\delta_x^2+\delta_y^2}}\right) \tag{8}$$

$$P(Y>X)=P\left(Z>\frac{\mu_x-\mu_y}{\sqrt{\delta_x^{\,2}+\delta_y^{\,2}}}\right)=1.12\times10^{-3} \tag{9}$$

The event tree for the inlet blockage accident sequence accident is shown in **Fig. 4**. It has nine head events. The code, RISKMAN is used for calculations. The code uses 1500 sampling data by Monte Carlo method with the average and standard variation described above. The total frequency for the occurrence of radioactive material releases results in a value of 1.46×10^{-7}, which means the system, MACSTOR/KN-400, can be considered to be very safe.

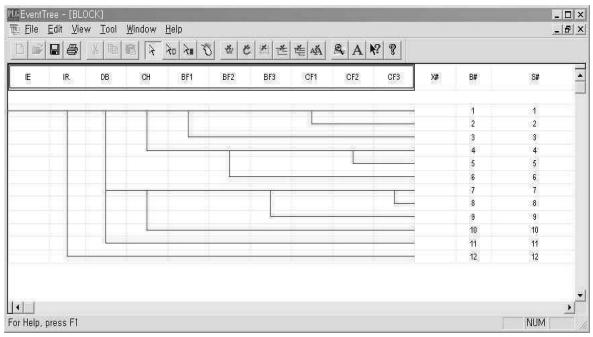

Fig. 4 A event tree for the air inlet blockage accident.

The MACCS2 code is used for assessing the fatality assessment. The latent cancer fatality in the form of the CCDF for both the average individual risk and whole body dose with respect to the distance from the location of the system has been obtained by the use of The MACCS2 code as shown in **Fig. 5** and **6**, respectively. It is also shown that the risk of the MACSTOR/KN-400 is much less than that of Wolsong plant. As shown **Fig. 6**, the average individual risk shows the similar trend to the whole body dose, which shows lower values than that of Wolsung plant.

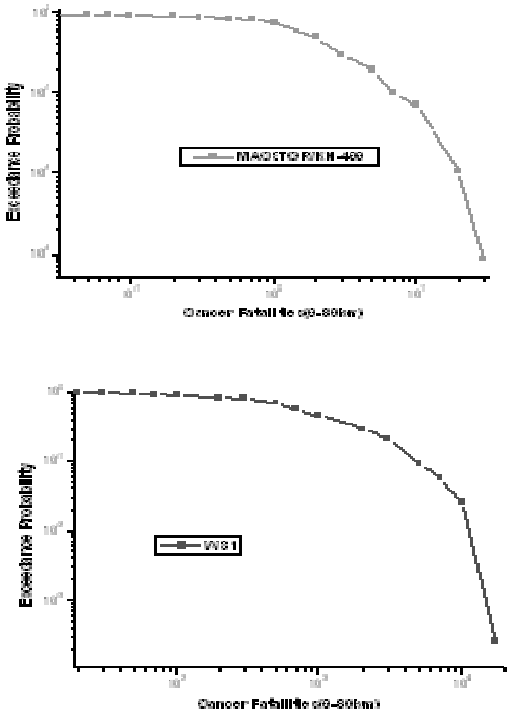

Fig. 5 The CCDF for the MACSTOR/KN-400 and the Wolsung unit 2 plant (0~80km).

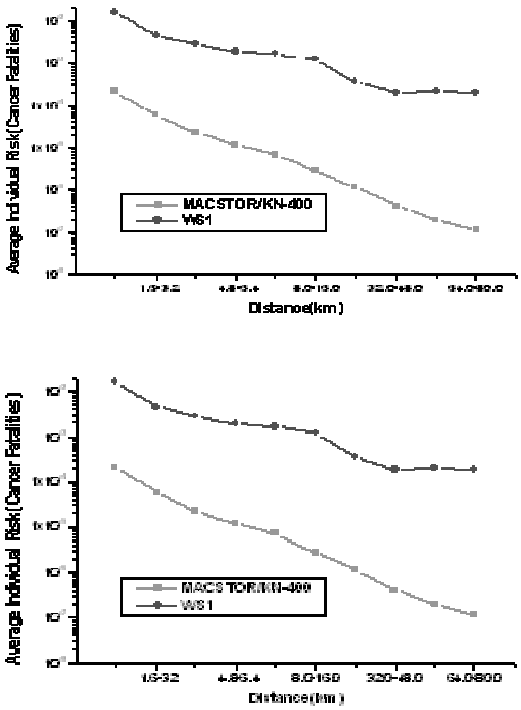

Fig. 6 Average individual risk and whole body dose (0~80km).

V. Conclusions

A framework for assessing the safety of an interim spent fuel storage facility in Korea has been developed and applied for the air inlet blockage accident sequence. It consists of three steps which are the basket / cylinder failure quantification step, the accident scenarios identification step, and the accident consequence analysis step. It is shown that this framework developed in this study can be applied to assess the safety for any other similar spent fuel storage facilities. The result might contribute to helping to improve the system design in advance as well as to obtaining public acceptance for the interim storage facility to be constructed. This framework has been demonstrated that it is systematically applicable and flexible in that it can be applied to any type of MACSTOR/KN-400. The results of this study can contribute to producing risk DB (data base) as well as to establishing accident management plans, Korea.

Acknowledgements

This work was supported by KINS (Korea Institute for Nuclear Safety) and partly by the Korean Science and Engineering Foundation (KOSEF) through iTRS, Seoul, Korea.

References

1) International Atomic Energy Agency, Safety Assessment for Spent Fuel Storage Facilities, Safety Series No. 118, p.5, 1994
2) Nuclear Environment Technology Institute, Development for Consolidated Dry Storage system for CANDU Spent Fuel (2nd Annual Report), p.3, 2003.
3) U. S. Nuclear Regulatory Commission, Standard Review Plan

for Spent Fuel Dry Storage Facilities,, NUREG-1567 (2000).
4) Cayetano Santos, Douglas Kalinousky, Christopher Ryder, Lee Abramson, Syed Shaukat, Jason Schaperow, and Alan Rubin, “A Probabilistic Failure Assessment of a Dry Cask Storage System”, Transactions of the 17th International Conference on Structural Mechanics in Reactor Technology (SMiRT 17) (2003).
5) James H. Rust, Nuclear Power Plant Engineering, Haralson Pub Co, p.357-403, 1979.
6) Donald M. Fryer, John F. Harvey, High Pressure Vessels, Chapman & Hall, p.23-24, 1998.
7) Mohammad Modarres, Mark Kaminskiy and Vasiliy Krivtsov, Reliability Engineering and Risk Analysis, MARCEL DEKKER, (1999).
8) Seok Won Hwang and Moosung Jae, "A Study on Risk Assessment Using the MACCS Code During Severe Accident in a Nuclear Power Plant (2003).

Journal of NUCLEAR SCIENCE and TECHNOLOGY, Supplement 5, p. 723–727 (June 2008)

Development of Health Effect Assessment Software Using MACCS2 Code

Seok-Won Hwang[1], Kyung Min KANG[2], Jong-Woon Park[1], Moosung JAE[2*]

1. Korea Hydro & Power Co.,Ltd, 25-1, Jang-Dong, Yuseong-Gu, Daejeon, Korea
2. Department of Nuclear Engineering Hanyang University
17 Haengdang-Dong, Sungdong-Gu, Seoul, Korea

The extended regulatory interests in severe accidents management and enhanced safety regulatory requirements raise a need of more accurate analysis of the effect to the public health by users with diverse disciplines. This facilitates this work to develop web-based radiation health effect assessment software, RASUM, by using the MACCS2 code and HTML language to provide diverse users (regulators, operators, and public) with easy understanding, modeling, calculating, analyzing, documenting and reporting of the radiation health effect under hypothetical severe accidents. The engine of the web-based RASUM uses the MACCS2 as a base code developed by NRC and is composed of five modules such as development module, PSA training module, output module, input data module (source term, population distribution, meteorological data, etc.), and MACCS2 run module. For verification and demonstration of the RASUM, the offsite consequence analysis using the RASUM frame is performed for such as early fatality risk, organ does, and whole body does for two selected scenarios. Moreover, CCDF results from the RASUM for KSNP and CANDU type reactors are presented and compared.

KEYWORDS: Accident Management, Severe Accident Phenomena, MACCS2, Level 3 PSA

I. Introduction

In case a hypothetical severe accident condition occurs at a nuclear power plant, radioactive materials could be released and transported through atmosphere and this may contaminate the environment and affect public health. The extended regulatory interest in severe accidents and enhanced safety requirements in regulations raise a need of more accurate analysis of the effect to the public health. The analysis generally called health effect analysis (HEA).

This effect can be evaluated deterministically or probabilistically. In comparison to the deterministic method which estimates the dose to the public conservatively for a limiting scenario, a probabilistic method can realistically treat diverse scenarios by integrating fatalities for many scenarios weighed by each frequency. This method is called Level 3 probabilistic safety assessment (PSA). This probabilistic health effect assessment (HEA) considers such factors as source terms, weather conditions, emergency plan, plant specific conditions (topography or community), definition plant damage states and frequency data.

The calculation of the factors mainly needs calculations of airborne and ground concentrations of each radionuclide and dispersion of the radioactive materials through atmosphere for various scenarios. Therefore, current HEA uses a computer program MACCS2 (MELCOR accident consequence code system) for this purpose. However this kind of computer code is very complicated to understand and thus for an analysis it needs an expertise in the severe accident phenomena, probabilities, radioactive materials transport, effect to the public organ, and so on. This prevents extended users (plant operators, regulators, engineers, doctors, general public) from easy access and analysis and moreover, this hinders HEA from evolution.

For easy access and analysis for the diverse users, health effect assessment software, RASUM, is developed in this work based on MACCS2 code by incorporating HTML[1] (hypertext markup language). The RASUM is a software where user-friendly functions are implemented such as images, tables, tags, and style-texts. Figure 1 shows the overall outline of the RASUM.

This paper is to address the overview of the base code MACCS2, development method of the software RASUM, verification of the RASUM. Finally as a demonstration, early fatalities, organ dose, whole-body dose, and CCDF (Complementary Cumulative Distribution Function) are analyzed by using the RASUM.

II. Overview of the MACCS2 Code

The environment would be contaminated by radioactive nuclide deposited from the plume and the population would be exposed to radiation. Estimation of the range and probability of the health effects induced by the radiation exposures not avoided by protective measure actions and the economic costs and losses that would result from the contamination of the environment is the object of the MACCS2 calculation[2].

*Corresponding Author, Tel No: +81-2-2290-1346, Fax No: +81-2-2293-7014, E-mail: jae@hanyang.ac.kr

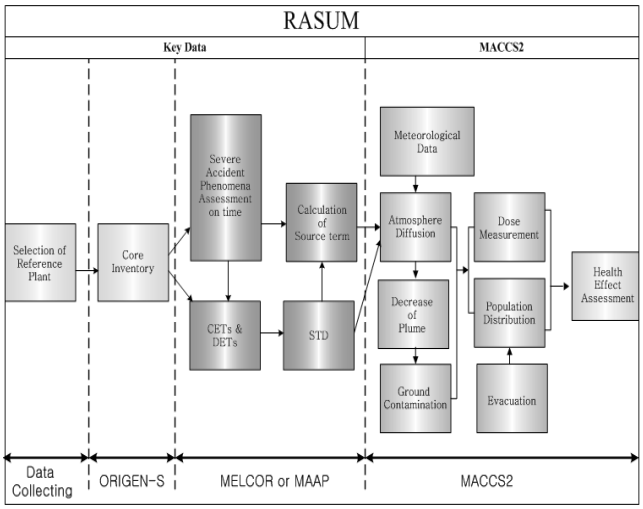

Fig. 1 Overall outline of the RASUM software

There are two aspects of the organization of MACCS2 which are basic to its understanding: The time scale after the accident is divided into various "phases", and the region surrounding the reactor is divided into polar-coordinate grid. The time scale after the accident is divided into three phases: emergency phase, intermediate phase, and long-term phase. Of the three time phases, the only one that must be defined by the user, is the emergency phase, the other two are optional.

The spatial grid used to represent the region is centered on the reactor itself. That is, the reactor is located at the point ($r=0$, $\theta=0$). The user specifies the number of radial divisions as well as their endpoint distances. Up to 35 of these divisions may be defined extending out to a maximum distance of 9999 km. The angular divisions, θ, used to define the spatial grid correspond to the sixteen directions of the compass.

All of the calculations of MACCS2 are stored on the basis of this polar-coordinate spatial grid. Since the emergency phase calculations utilize dose-response models for early fatality and early injury that are highly non-linear, it is necessary for those calculations to be performed on a finer grid than the calculations of the intermediate and long-term phases. For this reason, the sixteen compass sectors are subdivided into 3, 5, or 7 user-specified subdivisions in the calculations of the emergency phase.

In MACCS2, the dispersion and deposition of radionuclide released from the reactor containment to the atmosphere were modeled with a Gaussian plume model. Radiation doses to the population were calculated based on the radionuclide concentration that is predicted by the dispersion models. The exposure pathways considered in the evaluation of health effects are: (1) exposure to the passing plume, (2) exposure to radioactive materials deposited on the ground, (3) exposures to deposits on skin, (4) inhalation of radioactive materials directly from the passing plume, (5) inhalation of radioactive materials resuspended from the ground by natural and mechanical processes, (6) ingestion of contaminated foodstuffs, and (7) ingestion of contaminated water.

MACCS2 code used in this study is composed of 3 modules, which are processing the input data with verifying the efficiency, modeling the condition and treating the output data. It is composed of 3 main input data and the others needed to run the code. Especially, in this study, the emergency phase is only considered. During this time, other different methods as sheltering and shield by dose and evacuation can be suggested considering all the radioactive plume and exposure from ground contamination.

Intermediate and long term phase are calculated by CHRONIC module of MACCS2 code. During this period, radioactive plume disappears and only the exposure by ground contamination is considered. Then the defensive means such as temporary sheltering, decontamination and setting the restricted area are dealt. In this study, CHRONIC module is not used since it is not focused on evaluating the radiation effect. DOSDATA input data including conversion factor, meteorological data including wind direction, wind velocity, atmosphere stability and cumulative precipitation, etc. by each hour in a year, population distribution and data of the site near nuclear plant providing information about land fraction are used.

III. Method of RASUM Development

The RASUM, written in HTML, can provide awareness training to the operators whose work has a significant impact upon safe operation of nuclear power plants during an accident. It may be basically used for fundamental training in the severe accident assessment and response strategies, instrument degradation under severe accident conditions, and alternative instrumentation to verify instrument reading necessary for the implementation of severe accident strategies.

The initiation point of the RASUM and the scopes of EOPs (Emergency Operating Procedures) and severe accident management strategy are shown in Fig. 2. It is basically developed to help the control room operators and staffs to answer questions such as the following:

- What are the possible accidents sequences under given conditions?
- What is the expected physical accident status after some evident symptoms?
- What are the minimum consequences if some of actions are initiated prematurely?

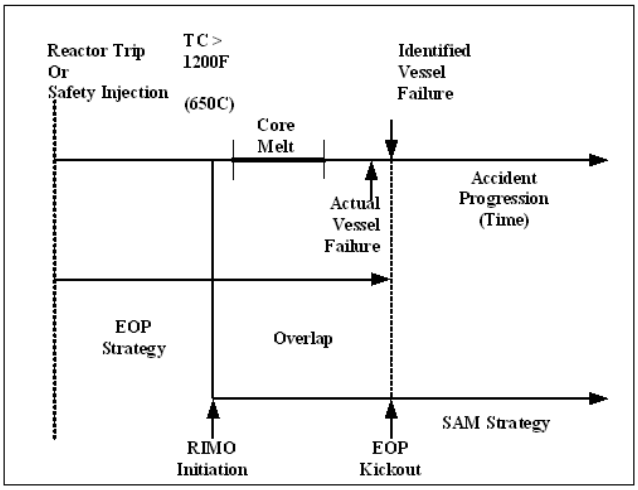

Fig. 2 The Initiation Timing for RASUM

User can see the result graphically, which is the output by running actual MACCS2 code and creating database for off-site health effect assessment. And most users can understand and access the general concepts and methodology of PSA. Created RASUM can be used for risk informed regulation and application, accident management plan, public acceptance, etc.

Web-based RASUM consist of 5 modules as below;

① Development Module
② PSA Training Module
③ Health Effect Assessments Output Module
④ Input Data Module
⑤ MACCS2 Run Module

Background of developing web-based RASUM is written in the first module. The second module consists of PSA contents addresses the overall methodology of PSA[3]. The third module t uses KSNP as a Reference plant for users to graphically confirm the results of an off-site health effect assessment such as an average individual risk, early and latent cancer fatalities, etc, which is divided into 10 different sections in the radius of 80 km in map for KSNP. In the fourth module, source term data on 19 release groups (Table 1) of KSNP, meteorological data throughout the year, population distribution data[4] and ground data around reference part are established as key data to perform the MACCS2 calculation. In the last module, users can link the web to perform the MACCS2 code written in ANSI Standard FORTRAN 77, modify and save the input data.

IV. Verification and Demonstration of the RASUM

1. Verification

In order to verify the function of the RASUM by evaluating offsite health effect, source term input, meteorological data, ground data and population distribution data, etc of KSNP for STC15 (LLOCA, large loss of coolant accident) & STC4 (LOFW, loss of feedwater flow) are used as shown in table 1.

Table 1 Characteristics and Frequency of STC15 & STC4 n Key Data (Sample)

Source Term	Containment Failure Mode	Initial Event	Frequency
STC 15	• Early Containment Failure: - SIT Injection Success - HPSIS Injection Success - Recirculation Cooling using CSS Success without CTMNT Heat Removal Sys.	Large LOCA	4.91E-07
STC 4	• Early Containment Failure(Rupture): - Reactor Trip Success - AFW Fail - Bleed RCS Fail - LPSI Injection Fail - LPSI Recirculation Success - CTMNT Spray Injection Success - Recirculation Cooling using CSS Success	Loss of Feed-water	1.80E-08

To illustrate the verification, the following calculations are made:

1. Complementary Cumulative Distribution Frequency(CCDF) for early fatalities and latent cancer fatalities
2. Early cancer fatalities within the radius of 80 km
3. Early fatalities risk, organ dose and whole-body dose

2. Demonstration

The main results of health effects are stochastically calculated by RASUM for KSNP as shown in Figure 3. Early fatalities, latent cancer fatalities, organ dose, whole-body dose and CCDF are calculated within the radius of 80km. Also, If the straight-line plume model was chosen (IPLUME=1) in MACCS2 code input data, the code can keep track of the centerline dose (whole-body, acute and life time dose) for possible contamination pathway.

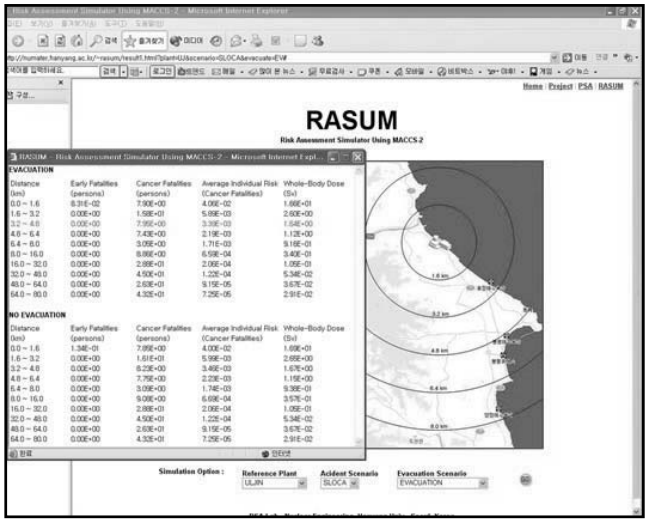

Fig. 3 Sample Results of STC15 and STC4 in KSNP using RASUM

Table 2 and **3** present the mean and 95 percentile value of the early fatalities risk of STC15 & STC4.

Table 2 Mean and 95 Percentile of Early Fatalities (0~32km)

STC	Early Fatalities		E/F×Frequency(Risk)	
	Mean	95 Percentile	Mean	95 Percentile
STC 15	6.21E-01	2.06E+00	3.06E-07	1.01E-06
STC 4	3.33E+01	7.02E+01	5.99E-07	1.26E-06

Table 3 Mean and 95 Percentile of Early Fatalities (0~80km)

STC	Early Fatalities		E/F×Frequency(Risk)	
	Mean	95 Percentile	Mean	95 Percentile
STC 15	6.21E-01	2.06E+00	3.06E-07	1.01E-06
STC 4	3.33E+01	7.02E+01	5.99E-07	1.26E-06

The actual MACCS2 calculations present consequences of early and latent cancer fatalities for 19 STC scenarios and frequencies. Current RASUM is developed for a test version, and thus it does not take into account all the parameters that related to atmospheric dispersion model in original MACCS2.

In addition, RASUM present results of respective organ dose depending on distance as shown in figure 4 and 5. The result of STC 15 shows that thyroid has the largest dose and stomach has the lowest value since the release fraction of iodine is the largest compared with another radionuclide out of the noble gases. The result of STC 4 shows that lung, bone and thyroid have similar values. For the case of stomach, the amount of dose shows the smallest value since stomach has a long contamination path way.

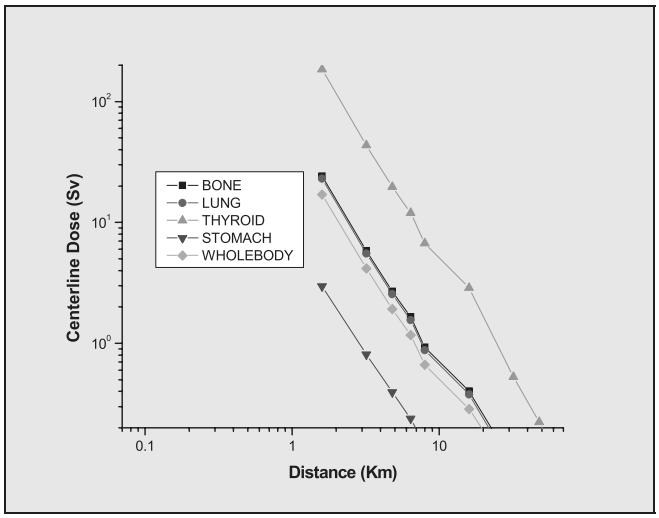

Fig. 4 Organ Doses on the distance (STC15: LLOCA)

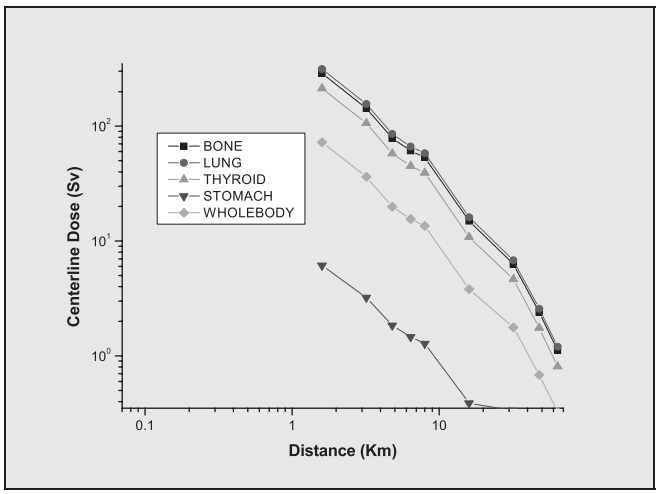

Fig. 5 Organ Doses on the distance (STC4: LOFW)

Figure 6 shows CCDF results for KSNP and CANDU type reactor using developed RASUM. The CCDF presents an estimation of the consequence magnitude distribution and the result of CCDF for early fatalities and latent cancer fatalities is strongly influenced by local meteorological state and population distribution. UCN34 has lower population density than WS1 and YGN34. In addition, the main wind direction of UCN34 east towered.

It is thus found that the RASUM developed in this paper is effective in understanding, modeling, calculating, analyzing, documenting and reporting of the radiation health effect under hypothetical severe accidents.

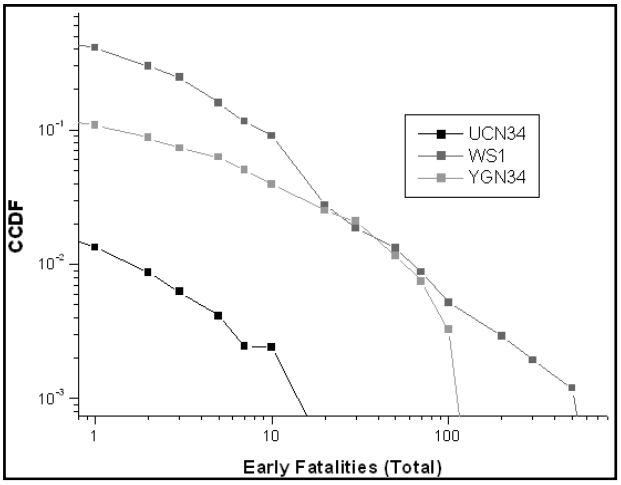

Fig. 6 CCDF for two **PWRs** and a CANDU type plant

IV. Conclusions

The extended regulatory interest in severe accidents and enhanced safety requirements in regulations raise a need of more accurate analysis of the effect to the public health. However, the traditional code for the HEA (MACCS2) requires an expertise in establishing input formation and running the code. Thus the RASUM software is developed to provide not only user-friendly input environment but also visualizations of HEA results such as dispersion of radioactive materials.

For verification and demonstration of the RASUM, the offsite consequence analysis using the RASUM frame is performed for such as early fatality risk, organ does, and whole body does for two selected scenarios. Moreover, CCDF results from the RASUM for KSNP and CANDU type reactors are presented and compared.

It can be concluded that the RASUM will contribute to implementation Accident Management Plan (AMP), Integration Leak Rate Test (ILRT) extension, and Risk Informed Regulation & Application (RIR&A) in Korea.

Acknowledgement

This work was supported by the Korean Science and Engineering Foundation (KOSEF) through the Innovative Technology Center for Radiation Safety (iTRS), Seoul, Korea.

References

1) Ho Seong Son, “DREAMWEAVER MX What’s up?,” Vivicom, August, 2002.
2) David I. Chanin, Mary L. Young, "Code Manual for MACCS 2, Volume 1, User's Guide," SAND97-0594, March, 1997.
3) Park Chang-Kyu, and Ha Jaejoo, “Probabilistic Safety Assessment,” Brain Korea, August, 2003
4) "Final Probabilistic Safety Assessment Report for Ulchins 3 & 4", Korea Electric Power Corporation, Seoul, Korea, 1997.

Journal of NUCLEAR SCIENCE and TECHNOLOGY, Supplement 5, p. 728–731 (June 2008)

Development of radiation risk assessment simulator using system dynamics methodology

Kyung Min KANG and Moosung JAE*

Department of Nuclear Engineering Hanyang University
17 Haengdang-Dong, Sungdong-Gu, Seoul, Korea

The potential magnitudes of radionuclide releases under severe accident loadings and offsite consequences as well as the overall risk (the product of accident frequencies and consequences) are analyzed and evaluated quantitatively in this study. The system dynamics methodology has been applied to predict the time-dependent behaviors such as feedback and dependency as well as to model uncertain behavior of complex physical system. It is used to construct the transfer mechanisms of time dependent radioactivity concentration and to evaluate them. Dynamic variations of radio activities are simulated by considering several effects such as deposition, weathering, washout, re-suspension, root uptake, translocation, leaching, senescence, intake, and excretion of soil. The time-dependent radio-ecological model applicable to Korean specific environment has been developed in order to assess the radiological consequences following the short-term deposition of radio-nuclides during severe accidents nuclear power plant. An ingestion food chain model can estimate time dependent radioactivity concentrations in foodstuffs. And it is also shown that the system dynamics approach is useful for analyzing the phenomenon of the complex system as well as the behavior of structure values with respect to time. The output of this model (Bq ingested per Bq m^{-2} deposited) may be multiplied by the deposition and a dose conversion factor (Gy Bq^{-1}) to yield organ-specific doses. The model may be run deterministically to yield a single estimate or stochastic distributions by "Monte-Carlo" calculation that reflects uncertainty of parameter and model uncertainties. The results of this study may contribute to identifying the relative importance of various parameters occurred in consequence analysis, as well as to assessing risk reduction effects in accident management.

KEYWORDS: ingestion chain model, dynamic, radioecology, system dynamics

I. Introduction

The offsite consequence analysis has been performed using a tool of system dynamics. The methodology to analyze accident consequence dynamically needs to be developed. A radiation assessment framework to assess the effects on health and the environment is required to establish. The risk from a severe accident for a reference plant used to be assessed by performing level 3 probabilistic safety assessment. The potential magnitude of radionuclide releases under severe accident loadings and offsite consequences as well as the overall risk are quantitatively evaluated in this study [1-3].

II. System Dynamics

System dynamics is a method to give comprehensive analysis which verifies changes in the variables of the structure with graphical and quantitative output as a progressive and useful analysis tool. This study uses a simulation language called VENSIM (Ventana Simulation Environment) to solve homogeneous differential equations. The VENSIM is a representative computer simulation language, which easily solves variable relationships and the structural elements of a model diagram with a model equation. It provides a mutual relation software environment for development, exploration, analysis, and optimization for simulation models. Also, it is dynamic simulation language that analyzes the time interval (Δt) in the concept of time flow. It is an advantage to analyze the variable of the model with a time interval. Especially, VENSIM presents a visible output where a figure represents a graph with a value of system behavior and system status. It is useful to model comparative analysis for the complicated systems [4].

III. Modeling

The Gaussian plume model for a continuous source originates is obtained by applying Fick's law for constant diffusivity coefficient and uniform wind speed. The steady state solution of the basic transport model can be derived. The assumption of constant diffusivity is valid only for that the size of the plume is greater than the size of the dominant turbulent eddies, so that all turbulence implicit in this parameter takes part in the diffusion. The meteorological conditions are assumed to have constant values during the travel of the plume limits of short time periods and small distances. These limitations should be taken into account when applying this model. Even though these conditions are exactly met practically, the Gaussian plume model has been widely used. The mathematical description of the Gaussian model is given as follows. The basic equation for an elevated release is as follows.

‡ Corresponding Author, Tel. +81-2-2290-1346,
Fax. +81-2-2293-7014, E-mail: jae@hanyang.ac.kr

$$C(x,y,z)=\frac{Q}{2\pi u_{10}\sigma_z\sigma_y}\exp\left[-0.5\left(\frac{y^2}{\sigma_y^2}+\frac{(z-h)^2}{\sigma_z^2}\right)\right] \quad (1)$$

,where C is air concentration (g s m^{-3}); Q is the release rate (g s^{-1}) or total amount released (g); u_{10} is the wind speed at 10 m above the ground (m s^{-1}); σ_z is the standard deviation of the vertical Gaussian distribution (m); σ_y is the standard deviation of the horizontal Gaussian distribution (m); x is the rectilinear co-ordinate along the wind direction (m); y is the rectilinear co-ordinate for cross-wind (m); z is the rectilinear co-ordinate above the ground (m); and h is the effective release height (m).

The origin of the co-ordinate system is considered to be at ground level beneath the discharge point. The atmospheric dispersion and its transfer mechanisms are modeled as **Fig. 1**.

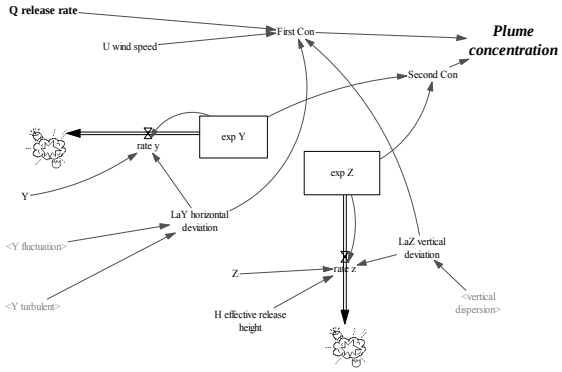

Fig. 1 Gaussian plume model using system dynamics

The transfer kinetic processes for radionuclides can be described by a set of linear first-order differential equations. Each equation corresponding to each compartment, which represents an environment element, is obtained from the change of the radioactivity concentration with respect to time based on the mass balance. The system dynamics is advantageous to model the changes over time for radionuclides process behaviors. The radionuclide concentrations in foodstuffs are then evaluated by calculating time dependent inventory. A set of differential equations are constructed for all the compartments. The coupled differential equation for each compartment is then solved numerically on daily time steps using an algorithm to yield the time-dependent inventories. And in the **Fig. 2** shows the diagram to describe the dynamic behaviors for several effects such as deposition, weathering and washout, resuspension, root uptake, translocation, leaching, senescence, intake and excretion of soil, intake and excretion of feedstuffs by animals.

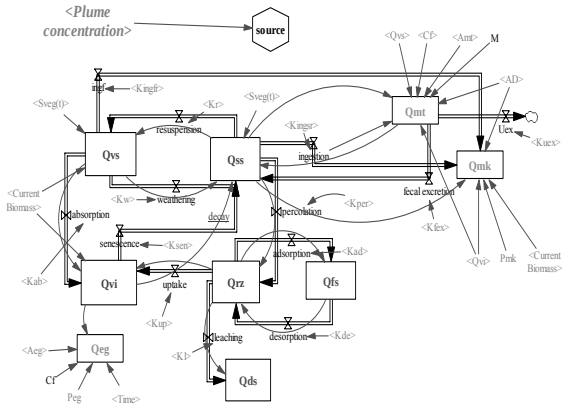

Fig. 2 Dynamic ingestion model using system dynamics

The food-chain model simultaneously simulates the flow of radionuclides through three land-management units: rangeland-grazing, human-food crops, and pasture/hay systems. Each land-management unit is represented by six state variables as shown in Fig. 3. The state variables denote the quantity of radionuclide in specific compartments. These transport process quantities, which is to be obtained from time dependent equations, include vegetation surfaces (Q_{vs}); vegetation internal tissues (Q_{vi}); soil surface, 0 - 0.1 cm (Q_{ss}); root zone, 0.1 - 25 cm (Q_{rz}); fixed soil, 0.1 - 25 cm (Q_{fs}); and deep soil, > 25 cm (Q_{ds}). In addition, land management units may have compartments with the quantities or concentrations of radioactivity in products such as fruits, vegetables(leafy, other), grains, grain plants for silage, grass and meats (beef, poultry), milk, milk products, and eggs. Other specific food sources are excluded because of either very minor effective sources to man or insufficient data [5-6].

The risk, R_i for early health effect is modeled in the accident consequence code as follows [7].

$$R_i = 1 - e^{-H_i} \quad (2)$$

,where H_i represents the cumulative hazard of early health effect. It can be modeled by a weibull function as follows.

$$H_i = \ln(2)\left(\frac{LD}{LD_{50,i}}\right)^{v_i} \quad (3)$$

for $LD>LD_{thr,I}$

where LD is the lethal dose.

$LD_{50,i}$ denotes the dose which causes 50% fatality of the exposed population due to early health effect i, v_i represents the shape parameter, and $LD_{thr,I}$ shows the dose threshold of early health. It is modeled as a function of the dose rate(DR) as follows.

$$LD_{50,i} = \frac{D_{0,i}}{DR} + D_{\infty,i} \quad (4)$$

where $D_{0,I}$(in Gy^2/h) and $D_{\infty,I}$ approximates the $LD_{50,I}$.

The dynamic early fatality can be modeled as shown in **Fig. 3**.

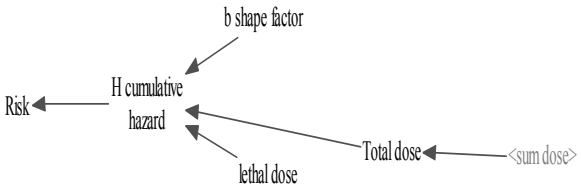

Fig. 3 Early fatality model using system dynamics

IV. Results

The food-chain model for rice after deposition in unit, Becquerel per area, has been evaluated quantitatively by system dynamics calculation algorithm. The system dynamics models the transfer of radionuclides efficiently. The values of the input parameters to the dynamic ingestion pathway model are equivalent to the values of both the site-specific environment and the agriculture data-base in the Kori area. The January data is used for the deposition times as a typical winter whether. The example radionuclides, Cs-137 is chosen in this study because it is one of significant nuclides to the ingestion doses exposed during severe accidents. The radioactivity concentration, Cs-137 deposition, might be very pronounced with deposition time. The direct deposition onto plant leaves or grains results in an important contamination due to high translocation. The time-specific and time-integrated concentrations of radionuclides for foods per unit fallout deposition are shown to vary dramatically by radionuclide as shown in **Fig. 4**. The parameter uncertainty existing in this approach may result from natural variability associated with a lack of knowledge about the actual value.

The uncertainty analysis using the Monte Carlo method has been performed in this study. The uncertainty of the median value for time-integrated concentrations of Cs-137 radionuclides has been surveyed to allow confidence intervals to be assigned as shown. The uncertainty may come from unavoidable errors in structure and various parameter uncertainties. Those are propagated through the developed model to result in **Fig. 5**.

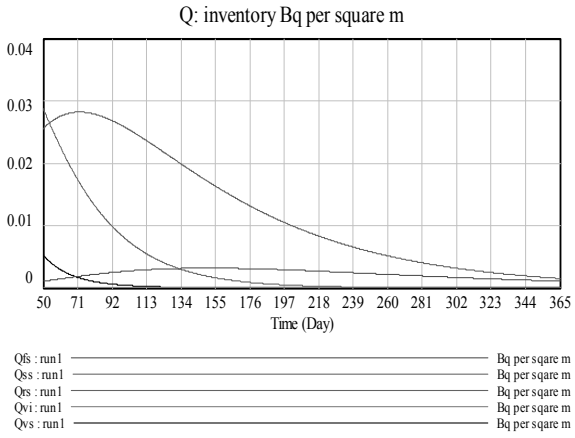

Fig. 4 Time-integrated concentrations of radionuclides in foodstuffs, inventory of compartment.

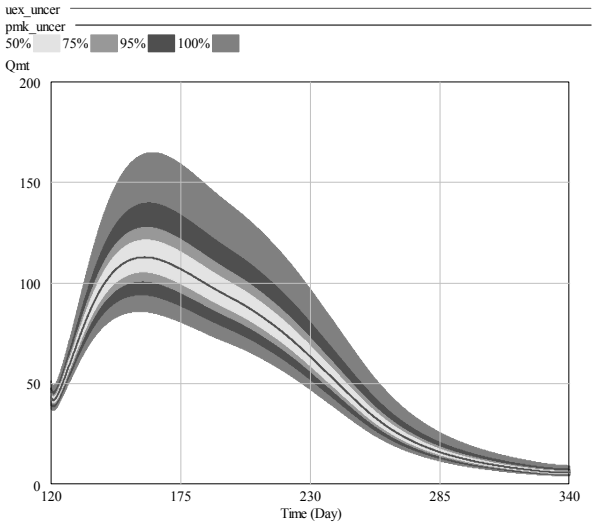

Fig. 5 Uncertainty analysis for concentrations of radionuclides in meat (Unit: 10^{-8}Bq kg^{-1})

V. Conclusions

A dynamic model for ingestion pathway has been developed and evaluated quantitatively by applying system dynamics to consequence analysis. The radioactivity concentration in foodstuffs is chosen as an example parameter for validating this dynamic approach. It is also shown that the system dynamics approach is efficient in modeling and evaluation for analyzing the phenomenon of the complex system as well as the behavior of structure values with respect to time. The major merit of this model include its ability to dynamically simulate important vegetation, soil transport processes, account for seasonal changes in these transport processes, evaluate discrete fall-out dates, and agricultural events such as tillage and harvests. It provides individual food product concentrations and contributions from specific feed sources. The uncertainty analysis using the Monte Carlo method has been performed as well. The uncertainty of the median value for time-integrated concentrations of Cs-137 radionuclides has been analyzed to allow confidence intervals. It might contribute to identifying the relative importance of various parameters occurred in consequence analysis, as well as to assessing risk reduction effects in accident management.

Acknowledgements

This work was supported by the Korean Science and Engineering Foundation (KOSEF) through the Innovative Technology Center for Radiation Safety (iTRS) and Hanyang University, Seoul, Korea.

References

1) W. T. Hwang. al., “Development of a Dynamic Ingestion Pathway Model, Applicable to Korean Environment”, The Korean Association for Radiation Protection, 18(1), p. 9-24, 1993
2) Breshears, David D.; Kirchner, Thomas B.; Otis, Mark D.; Whicker, F. Ward, “Uncertainty in Predictions of Fallout Radionuclides in Foods and of Subsequent Ingestion.”, Health

Physics. 57(6):943-953, December 1989.
3) Son, T. W., and Chung, H. K., "System Dynamics Approach for Analyzing Dynamic Motivation Model Using VENSIM," Korean System Dynamics Society, pp.61-86. 1999.
4) VENSIM reference manual version 4, Ventana System, Inc; 1999.
5) Whicker, F. Ward; Kirchner, T. B, Pathway: "A Dynamic Food-chain Model to Predict Radionuclide Ingestion After Fallout Deposition," Health Physics, 52(6), p. 717-737, 1987.
6) Abbott, Michael L.; Rood, Arthur S, Comida: "A Radionuclide Food Chain Model for Acute Fallout Deposition", Health Physics, 66(1), p. 17-29, 1994.
7) C. H. Lee, et al., " A development of Computer Code for Evaluating Internal Radiation Dose through Ingestion and Inhalation Pathway", KEAR/RR-998/90, 1991.

Journal of NUCLEAR SCIENCE and TECHNOLOGY, Supplement 5, p. 732–735 (June 2008)

Mitigation of Radiation Load by Trapping of Tritium in Off-gas during Dry-processes

In-Ha JUNG*, Joung-Ick CHUN, Jang-Jin PARK, Kee-Chan SONG, and Myung-Seung YANG.

Korea Atomic Energy Research Institute,150 Deokjin-dong, Yuseong-gu, Daejeon, Korea

Although tritium gas is produced a small amount comparing to the other fission products, it should be controlled for long half-life, high residence time, high isotopic exchange rate and ease of assimilation into living matter. A demand for lengthening the life time of disposal site needs treatment of spent nuclear fuel to reduce the volume of high level radwaste. This study is for trapping the tritium gas during dry processes carried out in oxygen condition, having a potential of exposure into operators and environment. The experiments were performed into two different hydrogen concentration ranges, i.e. 1000 ~ 9000 ppm of high range of hydrogen concentration and 25 ~ 100 ppm of low range of hydrogen concentration. At high range of hydrogen concentration, H_2O conversion ratio at 400℃ indicated above 98 % up to 7000 ppm, and 100 % at 450 ℃. All the results of H_2O conversion ratio at the low range of hydrogen concentration are represented close to 99%. Converted H_2O vapor was adsorbed at the Molecular sieve close to 100 %. More than 98% of H2O conversion ratio was attained up to 4 cm/s of linear gas velocity, whereas over 99% for the low range of hydrogen concentration. Some catalytic effect of ability of conversion hydrogen into H_2O on stainless steel was studied.

KEYWORDS: tritium, trapping, cuperic oxide, dry process, spent fuel, treatment, DUPIC, voloxidation, advanced voloxidation

I. Introduction

Tritium, a weak beta emitter, is produced in nuclear power reactors during the fission of heavy nuclei and by neutron interaction with coolants, moderators and some light elements, such as lithium, beryllium and boron. It is necessary to be controlled its production at nuclear facilities owing to its relatively long half-life, high residence time in the environment, high isotopic exchange rate and ease of assimilation into living matter.

The amount of tritium produced through neutron reactions in the coolant and moderator is so small that the tritiated effluents from them can be released directly to the environment without additional processing, while the portion of tritium produced in the fuel element is typically ~60 %. About 50 % of the tritium produced in the fuel element reacts with the zircaloy cladding to form a hydride.

In the LWR fuel reprocessing plant, most of the tritium arrested in the fuel and cladding appears in the liquid waste streams in the form of HTO during dissolution in nitric acid, finding 0.5% of them in the dissolver off-gas stream[1]. Otherwise, during dry processes such as Pyrochemical processing and DUPIC (Direct Use of PWR fuel in CANDU Reactors)[2] fuel fabrication process, possibility to be released to environment in the form of HT or T_2 [3, 4]. These spent nuclear fuel treatment processes are gradually spotlighted recently for extending the operation of disposal site.

The prior subject in the wet processes relating the tritium is treatment of HTO in liquid state. But no appropriate technique is developed for dry processes.

ORNL (Oak Ridge National Laboratory) developed a Voloxidation process for pre-treatment of the nuclear spent fuel, which is to oxidize spent oxide fuel at low temperatures (~500°C) for removal of tritium and increasing the dissolution rate during aqueous processing [5,6].

Recently, KAERI (Korea Atomic Energy Research Institute) and INL (Idaho National Laboratory) are developing with collaboration a new process of Advanced voloxidation process. Advanced voloxidation not only performs existing functions but also removes and collects gaseous, volatile and semi-volatile fission products. These fission products are removed following an oxidation cycle at ~500 ℃ by higher temperatures and possibly vacuum conditions[7].

It is known that there are two processes for capturing the tritium gas, one is removal of HT in gaseous state, and the other is removal of HTO in liquid or vapor state[8]. The removal of HT gas has been employed with hydrogen getters, but this technique is normally selected for non-oxidative processes[8]. Few papers are reported on the trapping of tritium during the dry processes except design criteria of the reprocessing plant in JAERI[9].

This study aims removal of HTO by molecular sieve followed by converting HT in the cupric oxide to mitigate radiation load during dry-processes carried out in oxidation condition.

II. Experimental

The experiment was carried out in non-radiation conditions.

*Corresponding Author, Tel No: +82-42-868-8965 Fax No: +82-42-868-2403 E-mail: nihjung@kaeri.re.kr

99.9% purity of cupric oxide catalyst powder (Pure chemical Co. Japan, particle size 2~5mm, granule type) was used to convert H_2 gas to H_2O vapor. This powder was charged into the H_2O conversion tower of stainless steel of 20 mm I.D. (Internal Diameter) and 300 mm height. Converting tower was equipped with heater to increase temperature up to 550 ℃.

Simulating the tritium gas release during spent fuel cutting and/or voloxidation process, 10,000 ppm of hydrogen gas mixed with high purity nitrogen gas was used as a feed gas. Voloxidation process is carried out in air condition, mixed hydrogen gas was supplied with compressed air to adjust concentrations of hydrogen. All gases were supplied into the H_2O converting tower through mass flow controller.

H_2 gas is converted into H_2O vapor after passing the converting tower. Molecular sieve was used to remove H_2O vapor from the process. The specifications of H_2O vapor and/or condensed H_2O removal tower (dehumidifier) are as follows.

- Size and material of the tower : 32 mm I.D. × 320 mm length (250 ㎖), visible Acryl
- Content : molecular sieve 13X (60 %) + 4A (40 %, indicator)
- Particle size and type : 8-12 mesh (1.68 ~ 2.38 mm), granule type
- Absorption capacity: 25 mL of water in 160 g of material

The concentrations of un-reacted residual hydrogen and of H_2O vapor were measured by two Gas Chromatographies (Multi-GC 2000, Donam Instrument Co. Korea) each. **Table 1** shows the specifications of GC columns used for measurement of H_2 and H_2O concentrations.

Table 1 Specifications of GC columns used for measurement of H_2 and H_2O concentrations

	Column for H2 gas	Column for H2O vapor
Column	Helifelx AT-Mole Sieve 30m x 0.53mm	Econo-CapTM ECTM-1000 Capillary Columns 30m x 0.53mm, ID 1.2㎛
Temp. Range	-60 ~ 300℃	40 ~ 250℃
Carrier Gas	Helium	Helium
Detector type	TCD	FID at 250℃

The layout of hydrogen trapping experimental apparatus is shown in **Fig. 1.** This apparatus has two dehumidifiers; one is for removal of converted H_2O escaped from the H_2O convert tower and the other is for removal H_2O for measurement of H_2 residual gas to eliminate the interference from decomposed hydrogen from H_2O. Each dehumidifier has a valve and it is closed not to use. For calibration of the H_2O concentration at the gas chromatography, a standard mixture gas of 30 ppm water balanced argon gas (Scott Specialty Gases) was used.

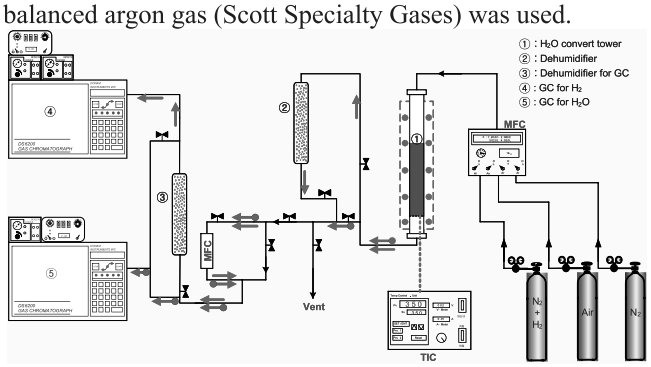

Fig. 1 Layout of hydrogen trapping experimental apparatus.

The flow rate of hydrogen and compressed air supplied into the H_2O converting tower was fixed to 1 L/min during observing the H_2O conversion ratio and varied for the H_2O conversion ratio according to the gas linear velocity. The height of cupric oxide in the H_2O conversion tower was fixed to 100 mm (about 280 g in weight) for all the experiments. The temperature of the conversion tower was varied in the range of 100 ~ 400 ℃. The experiments were performed in two different hydrogen concentration ranges, i.e. 1000 ~ 9000 ppm of high range of hydrogen concentration and 25 ~ 100 ppm of low range of hydrogen concentration. H_2O conversion ratio was also observed according to the gas linear velocity. The effect of H_2O conversion at the surface of stainless steel was also observed with evacuating the CuO catalyst from the H_2O conversion tower.

III. Results and Discussion

Fig. 2 and **3** are the results of H_2O conversion ratio according to the hydrogen concentrations at the experimental range of temperatures. H_2O conversion experiments are executed from 100℃ to 450℃ with 50℃ increment for higher range of hydrogen concentration as shown in Fig. 2, and a part of those experiments was performed for lower range of hydrogen concentration as shown in Fig. 3.

As a whole, H_2O conversion ratios according to the hydrogen concentration were decreased identically with increasing the hydrogen concentration at the same temperature. At high range of hydrogen concentration, H_2O conversion ratio at 400℃ indicated above 98 % up to 7000 ppm of hydrogen concentrations, and 100 % at the temperature of 450 ℃. At low range of hydrogen concentration, H_2O conversion ratio showed higher than that of high range of hydrogen concentration at the corresponding temperature. This is obviously related to the conversion rate of the cupric oxide according to the hydrogen concentration. However, all the results at the low range of hydrogen concentration represented above 98% of H_2O conversion ratio regardless of the reaction temperatures in the experimental ranges. On the other hand, converted H_2O was adsorbed at the dehumidifier close to 100 % although the results are not presented here.

H_2O conversion ratio according to the gas linear velocity

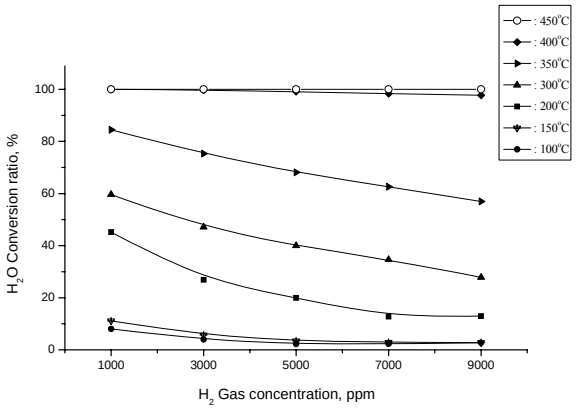

Fig. 2 H_2O conversion ratio at high range of hydrogen concentration according to temperature and H_2 concentration

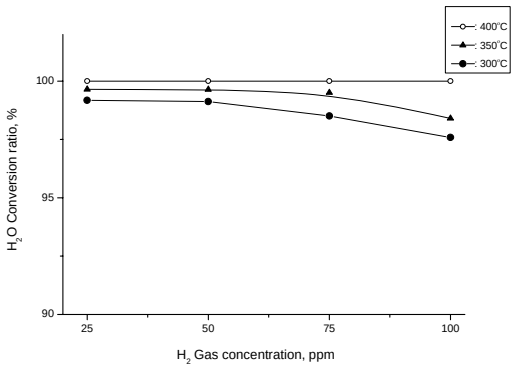

Fig. 3 H_2O conversion ratio at low range of hydrogen concentration according to temperature and H2 concentration.

at the conversion tower for both high and low range of hydrogen gas concentrations of 3000 ppm and 100 ppm were observed at 400℃. Those results are represented in **Fig**. **4** and **5**. They show H_2O conversion ratios in % according to the gas linear velocities through the H_2O conversion tower in the range of 1 cm/s ~ 6 cm/s at 400 ℃ and 100 mm height of cupric oxide. The gas linear velocity indicated in these figures are corresponded to 0.4 L/min ~ 2.5 L/min flow rate at the room temperature.

For high range of hydrogen concentration, above 98% of H_2O conversion ratio was attained up to 4 cm/s of gas linear velocity, whereas over 99% for the low range of hydrogen concentration.

It is known that stainless steel has conversion ability hydrogen to H_2O at some temperature ranges. Even though the results do not show any tendency in spite of several repetitions of experiments, somewhat extent of hydrogen was converted at the surface of stainless steel metal at high temperature. During the experiments of catalytic effect of stainless steel, the conversion column was cleaned after evacuating the cupric oxide. **Fig. 6** and **7** show this phenomenon. Although stainless steel has a ability to convert hydrogen into H_2O, the results showed a irregular tendency.

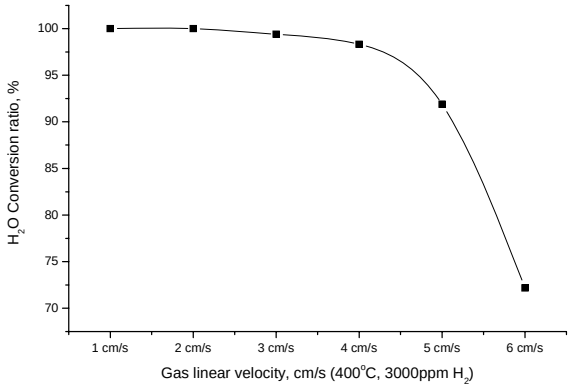

Fig. 4 H_2O conversion ratio according to the gas linear velocity at 400℃ and 3000 ppm of H_2 gas concentration.

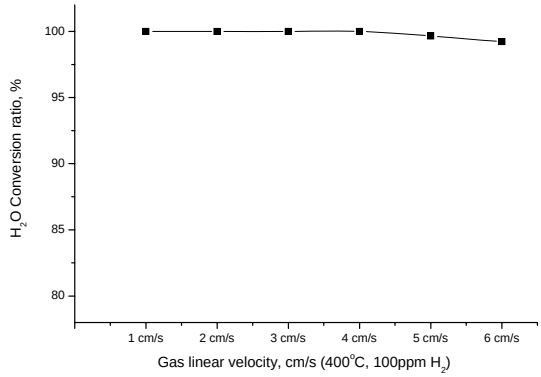

Fig. 5 H_2O conversion ratio according to the gas linear velocity at 400℃ and 100 ppm of H_2 gas concentration.

This effect might not give any helps, when the material is used for a long time at an oxygen condition.

IV. Conclusions

This study aimed removal of HTO by molecular sieve followed by converting HT in the cupric oxide to mitigate radiation load during dry-processes carried out in oxidation condition. The experiments were performed into two different hydrogen concentration ranges, i.e. 1000 ~ 9000 ppm of high range of hydrogen concentration and 25 ~ 100 ppm of low range of hydrogen concentration. At high range of hydrogen concentration, H_2O conversion ratio at 400℃ indicated above 98 % up to 7000 ppm of hydrogen concentration, and 100 % at the temperature of 450 ℃. At low range of hydrogen concentration, H_2O conversion ratio showed higher than that of high range of hydrogen concentration at each corresponding temperature. All the results of H_2O conversion ratio at the low range of hydrogen concentration represented above 98%. For high range of hydrogen concentration, above 98% of H_2O conversion ratio was attained up to 4 cm/s of gas linear velocity, whereas over 99% for the low range of hydrogen concentration. The results confirmed that stainless steel can convert hydrogen

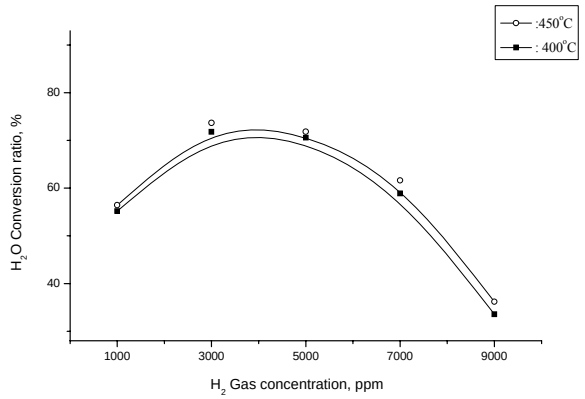

Fig. 6 Catalytic effect of H_2O conversion at stainless steel metal surface at high range of hydrogen concentration.

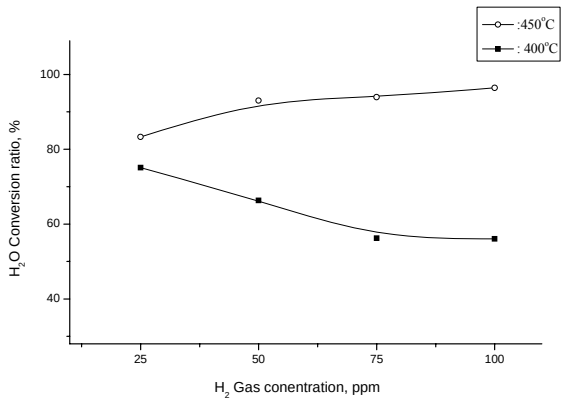

Fig. 7 Catalytic effect of H_2O conversion at stainless steel metal surface at low range of hydrogen concentration.

into H_2O at some temperature ranges, but showed an irregular tendency. This effect might not give any helps, when the material is used for a long time at an oxygen condition. In summary, tritium gas in dry processes can be trapped with cupric oxide and removed with Molecular sieve.

Acknowledgement

This project has been carried out under the Nuclear Research and Development program by Korea Ministry of Science and Technology.

References

1) Management of waste containing tritium and carbon-14, Vienna: International Atomic Energy Agency, Technical reports series, ISSN 0074–1914; no. 421, pp 33 (2004).
2) M. S. YANG *et al*., "THE STATUS AND PROSPECT OF DUPIC FUEL", *NUCLEAR ENGINEERING AND TECHNOLOGY*, **38**, 4, pp 359, (2006).
3) DOE, "Tritium Handling and Safe Storage," DOE-HDBK-1129-99 (1999).
4) IAEA-INTERNATIONAL ATOMIC ENERGY AGENCY, Handling of Tritium-Bearing Wastes, Technical Reports Series No. 203, IAEA, Vienna (1981).
5) G. E. Brand, E. W. Murbach, "Pyrochemical Reprocessing of UO_2 by AIROX: Summary Report," NAA-SR-11389 (1965).
6) J. H. Goode, R. G. Stacy, V. C. A. Vaughen, "Head-End Processing Studies with (U, Pu)O_2 Reactor Fuels from the PNL-3 Irradiation Experiments," ORNL/TM-7498 (1982).
7) B. R. Westphal, K. J. Bateman, C. D. Morgan, J. F. Berg, P. J. Crane, D. G. Cummings, J. J. Giglio, M. W. Huntley, R .P. Lind, and D. A. Sell, "Effect of Process Variables During the Head-End Treatment of Spent Oxide Fuel", *Nuclear Technology*, (in publication).
8) Management of waste containing tritium and carbon-14, Vienna: International Atomic Energy Agency, Technical reports series, ISSN 0074–1914; no. 421, pp 52 (2004).
9) Gunzo Uchiyama *et al*., Development of Voloxidation Process for Tritium Control in Reprocessing, JAERI-M91-199, (1991)